Aus der Klinischen Kooperationseinheit Neuroimmunologie und Hirntumorimmunologie,
Universitätsmedizin Mannheim und DKFZ

Prof. Dr. med. Michael Platten

Development and microenvironment guided optimization of personalized immunotherapeutic strategies in brain tumors

Inauguraldissertation zur Erlangung des medizinischen Doktorgrades an der Medizinischen Fakultät Mannheim der Ruprecht-Karls-Universität zu Heidelberg

vorgelegt von
Christopher Krämer

aus
Mainz
2023

Dekan: Herr Prof. Dr. med. Sergij Goerdt

Referent: Herr Prof. Dr. med. Michael Platten

Teilergebnisse der vorliegenden Arbeit wurden zur Veröffentlichung angenommen: **Krämer C***, Kilian M*, Chih YC, Kourtesakis A, Hoffmann DC, Boschert T, Koopmann P, Sanghvi K, Roia Ad, Jung S, Jähne K, Shultz LD, Ratliff M, Harbottle R, Green EW, Will R, Wick W, Platten M and Bunse L. NLGN4X TCR transgenic T cells to treat gliomas. Neuro-Oncology 2023 Sep 06

Teilergebnisse der vorliegenden Arbeit wurden veröffentlicht in: Kilian M, Sheinin R, Tan CL, Friedrich M, **Krämer C**, Kaminitz A, Sanghvi K, Lindner K, Chih YC, Cichon F, Richter B, Jung S, Jähne K, Ratliff M, Prins RM, Etminan N, von Deimling A, Wick W, Madi A, Bunse L, Platten M. MHC class II-restricted antigen presentation is required to prevent dysfunction of cytotoxic T cells by blood-borne myeloids in brain tumors. Cancer Cell. 2023 Feb 13;41(2):235-251.e9. doi: 10.1016/j.ccell.2022.12.007. Epub 2023 Jan 12. PMID: 36638785.

Contents

1 Abbreviations

Abbreviation	Meaning
ANOVA	ANOVA analysis of variance
APC	APC Antigen-presenting cell
BOLETH	B-lymphoblastoid cell line
BL/6J	immunocompetent black 6 mice
CAR	Chimeric antigen receptor
CCL	CC chemokine ligand
CCR	C-C Motif Chemokine Receptor
CD3/CD28	postive TCR stimulation control with CD3/CD28 beads
CD	Cluster of differentiation
cDNA	complementary DNA
CG	congenic
CI	confidence interval
CNS	Central nervous system
Cre	Cyclization recombination
CRISPR	Clustered Regularly Interspaced Short Palindromic Repeats
CTFR	Cell Trace Far Red
CTLA-4	Cytotoxic T-lymphocyte-associated protein 4
CXCL	Chemokine (C-X-C motif) ligand
da	disease asscociated
DAPI	4,6-Diamidin-2-phenylindol
DC	Dendritic cell
DMEM	Dulbecco's modified eagle medium
DMSO	Dimethyl sulfoxide
DNA	Deoxyribonucleic acid
EAE	experimental autoimmune encephalomyelitis
EGFR	Epidermal growth factor receptor
EF-1 alpha	Elongationfactor 1 alpha
ERT2	Estrogen receptor 2
FACS	Fluorescence-activated cell sorting
FBS	Fetal bovine serum
FOX-P3	Forkhead-Box-Protein 3
ft	frequent type
Flox	Locus of X-over P1
Flu	Influenza virus epitope
FMO	Fluorescence minus one: antibody staining mix for FACS lacking one fluorochrome-labeled antibody
Gapdh	Glyceraldehyde-3-phosphate dehydrogenase
GFP	Green fluorescent protein
GFAP	Glial fibrillary acidic protein

GL261	Glioma 261
Grz	Granzyme
GTEX	Genotype-Tissue Expression
h	homoestatic
H2-D1	H-2 class I histocompatibility antigen, D-K alpha chain
H2-Ab1	H-2 class II histocompatibility antigen
H2-K1	H-2 class I histocompatibility antigen
H3.3K27M	Histon H3.3 substitution on amino acid 27: lysine to methionin
HER2	human epidermal receptor 2
HLA	Human major histocompatibility complex
HSC	hematopoietic stem cells
ICB	Immune checkpoint blockade
ICAM-1	Intercellular adhesion molecule
ICOS	Inducible T-cell Co-Stimulator
IDH1	Isocitrate dehydrogenase 1
IFN-γ	Interferon-gamma
IL2rg	Interleukin 2 receptor subunit gamma
IL	Interleukin
i.c.	Intracranial
i.p.	intraperitoneal
IRES	internal ribosomal entry site
Irf	Interferon regulatory factor
ISO	Isotype
Klf2	Kruppel-like factor 2
K562	chronic myelogenous leukemia cell line
KO	Knock-out
Ki67	Marker Of Proliferation
LAG-3	Lymphocyte-activation gene-3
LDH	Lactate dehydrogenase
LN	lymph node
Ly6	Lymphocyte antigen 6
Ma	Macrophages
MACS	Magnetic-activated cell sorting
Mart-1	Melanom antigen recognized by T cells-1
Mcm3	Minichromosome Maintenance Complex Component 3
MC	Monocytes
MFI	Median fluorescence intensity
MG	Microglia
MHC	Major histocompatibility complex
Mock	Mock transduced T cells: no TCR delivery
MOG	Myelin Oligodendrozyten Glykoprotein

MRI	Magnetic resonance imaging
NFAT	Nuclear factor of activated T-cells
NLGN4X	Neuroligin 4, X-linked
NK cells	Natural killer cells
NOD	Non-obese diabetic
NSG	immunodeficient non-obese diabetic scid gamma
OD	optical density
OVA	Ovalbumin
OVA I	Ovalbumin MHC class I
OVA II	Ovalbumin MHC class II
OT-1	Ovalbumin T cell receptor
P	Peptide
PBMC	Peripheral blood mononuclear cells
PD-L1	Programmed death ligand 1
PD-1	Programmed death protein 1
PCR	Polymerase chain reaction
PBS	Phosphate-buffered saline
Perf	Perforin
pLEX307	lentiviral expression vector under the EF-1-alpha promoter
pSMARTer VX	S/MAR vector Version X
PRKDC	protein kinase, DNA-activated, catalytic subunit
RLU	relative luminescence units
RNA	Ribonucleic acid
RT	Room temperature
RT-qPCR	Real-Time quantitative PCR
scid	Severe combined immunodeficiency
s.c.	Subcutaneously
SEM	Standard error the mean
SFG	Retroviral expression vector
S/MAR	Scaffold/matrix attachment region
TCF1	T cell factor 1
TCR	T cell receptor
TCGA	TCGA The Cancer Genome Atlas
Tet	Tetramer
TIGIT	T Cell Immunoreceptor With Ig And ITIM Domains
TIL	Tumor infiltrating lymphocyte
TIM-3	T-cell immunoglobulin and mucin-domain containing-3
TME	tumor microenvironment
TNF-α	Tumor necrosis factor alpha
TOX	Thymocyte Selection Associated High Mobility Group Box

Treg	Regulatory T cell
t-SNE	t-distributed Stochastic Neighbor Embedding
UMAP	Uniform Manifold Approximation and Projection
U87	U87 glioma cell, wild-type
U87 NLGN4X	U87 glioma cell with overexpression of the NLGN4X protein
U87 TMG	U87 glioma cell line with expression of a tandem minigene containing the NLGN4X antigen
VEGF	Vascular Endothelial Growth Factor
WHO	World health organization
WT	Wildtype

2 Introduction

Gliomas are the most common primary brain tumors with an annual incidence of 6.6 per 100.000 in the USA. [Reifenberger et al., 2017] Despite emerging advances in the field of immunotherapy gliomas are still characterized by a poor clinical prognosis. Under maximal standard therapy the current median overall survival in patients with glioblastomas is limited to 32 months [Lim et al., 2022]. Furthermore, especially due to immunosuppressive effects on the tumor microenvironment [Bunse et al., 2018] [Quail and Joyce, 2017] and the immune privileged nature of the central nervous system there is still a lack of understanding of the underlying mechanisms that drive endogenous and induced immune responses in brain tumors.

Advances in the molecular profiling of gliomas in particular and numerous other tumor entities in general challenged the established classifications systems employing histopathological features. As a consequence, the WHO published the new Classification of Tumours of the CNS in 2021. [Louis et al., 2021] Previously, gliomas were termed as grade I if they were associated with a slow growing phenotype and favorable clinical prognosis, while grade IV gliomas depicted highly malignant tumors. The latter account for half of all gliomas.

The WHO 2016 classification already respected the impact of the presence of several molecular markers for the clinical outcome. Thus, the existence of an IDH-1 mutation distinguishes between two biological different tumors with a distinct course of disease. IDH-1 mutant gliomas are thought to occur upon several serial mutations most commonly within the TP53 and ATRX genes. Another important classification pattern utilizes the whole arm 1p/19q codeletion for differentiation between IDH-mutant astrocytoma and oligodendrogliomas. [Reifenberger et al., 2017]

The new WHO classification introduces an unified nomenclature for CNS tumors respecting the molecular features of tumors rather than specific locations or histo-morphological features. The grading of brain tumors is now performed within a specific tumor type and not across tumor subtypes meaning that for example IDH-mutant astrocytomas are graded from 2-4 according to an integrated molecular and histopathological diagnostic. [Louis et al., 2021]

Current standard therapeutic schemes are selected with respect to the histopathological classification and grading according to the WHO scheme. Post-surgical radiotherapy promotes local control and prolongs the survival of patients with diffuse WHO grade III or IV gliomas. Polychemotherapy using a combination of procarbazine, lomustine and vincristine as well as Temozolomide complement standard therapeutic schemes and are chosen referring to the presence of molecular markers. [Reifenberger et al., 2017]

Irrespective of the described aggressive therapeutic approaches the clinical prognosis of brain tumors often remains poor. Thus, immunotherapeutic concepts are emerging and gain increasing importance for treatment. However, these approaches are hampered by the low immunogenicity of gliomas. [Reifenberger et al., 2017]

2.1 Immunotherapeutic concepts for treatment of brain tumors

Diverse immunotherapies have emerged in the recent years and can be distinguished into three categories. First, cellular concepts using adoptive transfer of diverse cell products, second approaches utilizing vaccination against either neoepitopes or tumor associated antigens and third immune checkpoint blockade targeting different receptors with an inhibitory function on the immune response.

2.1.1 Vaccination as an immunotherapeutic approach

The principle of vaccination in tumor therapy is to induce an endogenous immune response to unmutated tumor associated antigens or neoepitopes arising from mutations within in the tumor cells by presenting the immunogenic epitope sequences to the immune system. Different approaches either apply a single peptide encoding the immunogenic sequence of the antigen or a mixture of peptides representing different individually expressed antigens. Different antigen presenting cell types are resonsible for the priming of CD4+ and CD8+ T cells against specific target sequences recognized by their T cell receptors. Antigen presenting cells are therefore a relevant target of vaccination therapies.
The application of vaccines has shown to induce specific immune responses in patients with newly diagnosed glioblastomas in a clinical phase I trial. [Hilf et al., 2019] A small population of patients has been treated with an individually manufactured vaccine derived from immunopeptidome and transcriptome analysis of both unmutated antigens and neoepitopes. Immunopeptidome analysis thereby investigates peptide sequences that are bound to MHC molecules. Common unmutated antigens were identified out of previously generated glioma specimens. Subsequently, the relevance of the previously found antigens was tested for each patient using mass spectrometry to characterize the present antigens and immunopeptidome analysis to address binding to the HLA-A system. Relevant neoepitopes were selected according to the following scheme: They had been confirmed by mass spectrometric analysis as HLA ligands or they had a high binding likelihood to the patient's HLA class I molecules. [Hilf et al., 2019] The described approach resulted in a median overall survival of 29 months [Hilf et al., 2019] that did not show improvements compared to the standard therapeutic regimen in glioblastomas [Lim et al., 2022] that is currently 32 months.
As a result a vaccination induced response of CD8 T cells was observed in a vast majority of treated patients. T cells directed against the tumor associated antigens NGLN4X and PTP-013 have been identified to have functional anti-tumor properties in ex vivo cytotoxicity assays. However, since the described study is limited by only minor rates of either complete or partial response, there is still much to be explored to optimize treatment success and to transfer these results to broader clinical application. [Hilf et al., 2019]
IDH-1 mutant gliomas have shown to be accessible to vaccination in a preclinical model. Peptides derived from the mutated region in the IDH-1 gene in IDH-1 mutant gliomas bind to MHC class II and induce a mutation specific CD4 T cell response. Peptide vaccination of HLA humanized mice, which are deficient for the murine MHC and transgenic for the human HLA-A2 and HLA-DR1 gene, can result in reasonable anti-tumor responses against an experimental tumor model overexpressing IDH-1. [Schumacher et al., 2014]

These findings were transferred to a first clinical phase 1 trial (NOA-16 trial) with 33 patients with newly diagnosed IDH1 mutant astrocytomas included. Treatment with an IDH1 specific vaccine resulted in about 90 percent of the patients showing an immune response to the IDH-1 vaccine. In case of a reaction of the immune system about 80 percent of those patients depicted a progression free survival for a least two years. Pseudoprogression as an indicator of an inflammatory response at the tumor site was observed at high frequencies and might be driven by IDH-1 specific CD4 T cells clones as depicted by exemplary analysis of one sample from a patient with pseudoprogression. The NOA-16 trial demonstrates, that the antigen specific vaccination might be beneficial for patients suffering from these types of tumors. [Platten et al., 2021]

2.1.2 Immune Checkpoint blockade - Releasing the break of the immune system for cancer therapy

Immune checkpoint blockade is most commonly known to target either the PD-1-PD-L1 axis or the CTLA-4 receptor. After TCR activation in T cells CTLA-4 is upregulated and competitively inhibits the binding of CD28 to the B7 ligands B7-1 (CD80) and B7-2 (CD86) and thereby hampers the costimulation of activated T cells [Wei et al., 2018] (comp. Fig. 1). In 1996 the group of James P. Allison discovered that the administration of an antibody directed against CTLA-4 mediated potent tumor control of a subcutaneously implanted colon carcinoma [Leach et al., 1996]. Amongst others, these findings initiated the application of immune checkpoint therapy in the treatment of cancer and were rewarded with the Nobel prize of medicine in 2018.
On the other hand T cell activation simultaneously leads to upregulated expression of PD-1 on the surface of B cells and T cells [Agata et al., 1996] and thereby peripheral tolerance of T cells due to the endogenous expression of PD-1 ligands in the periphery. [Keir et al., 2006] In the same manner PD-L1 mediates immune evasion of tumor cells by promoting the apoptosis of antigen-specific T cells in vivo and in vitro [Dong et al., 2002]. In chronically stimulated T cells impaired methylation of the PDCD1 DNA locus results in prolonged expression of PD-1. [Youngblood et al., 2011]
Until now there is multiple evidence for the therapeutic potential of immune checkpoint blockade in different solid cancer entities such as melanoma [Topalian et al., 2012], non-small-cell-lung cancer [Brahmer et al., 2015] and metastatic urothelial bladder cancer [Powles et al., 2014].
However, the application of immune checkpoint blockade in brain tumors has long been questioned due to their low immunogenicity. The observed clinical response of ICB treated hypermutated glioblastoma [Bouffet et al., 2016] indicated the potential of ICB in the context of brain tumors and paved the way for diverse investigations in the role of immune checkpoint treatment in brain cancer therapy. *Cloughesy et al.* showed that neoadjuvant immune checkpoint blockade with pembrolizumab targeting PD-1 induced a prolonged survival in patients with recurrent glioblastoma highlighting the therapeutic potential of this treatment. [Cloughesy et al., 2019]
Interestingly, the success of immune checkpoint therapy (ICT) requires both the presentation of MHC class I and MHC class II restricted neoantigens on tumor cells in preclinical tumor models. [Alspach et al., 2019] Previously, several publications have

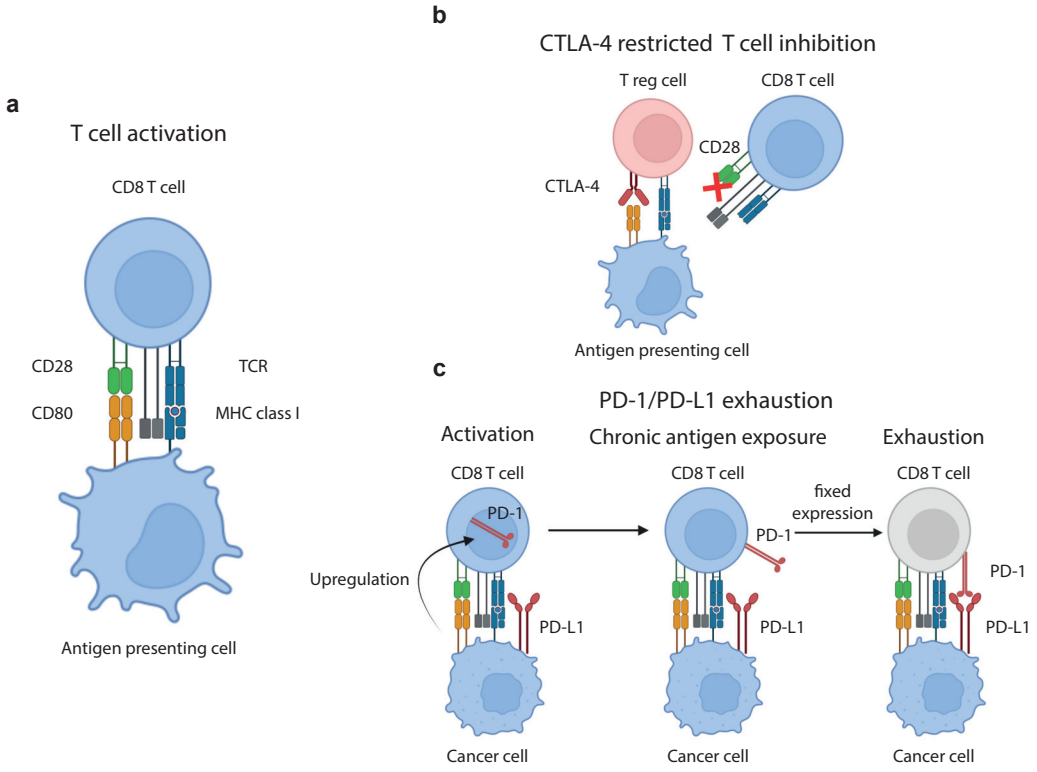

Figure 1: **Mechanisms of T cell activation and regulation**
Antigens are presented on MHC molecules on the surface of antigen presenting cells or cancer cells binding to the T cell receptor complex on naive T cells. Inhibitory signals are presented by CTLA-4 on regulatory T cells and by PD-L1 on APCs and cancer cells. Chronic antigen exposure leads to fixed expression of PD-1 binding to PD-L1 on cancer cells resulting in T cell exhaustion.

highlighted the relevance of CD4 positive T Helper (TH) cells for tumor regression [Kreiter et al., 2015] by enhancing the response of cytotoxic T lymphocytes via activation of antigen-presenting cells through the CD40-CD40L interaction [Schoenberger et al., 1998]. In an approach to evaluate a potential benefits of combination therapy with different immunotherapeutic agents targeting both CTLA-4 and the PD-1/PD-L1 axis robust responses in a subset of patients were observed. The advantage of the combination treatment is based on the different molecular pathways of action utilized by anti-CTLA-4 and anti-PD-1/PD-L1 antibodies: Exhausted-like CD8 T cells are targeted by both anti-CTLA-4 and anti-PD, whereas specific Th1-like CD4 subsets are primary regulated through anti-CTLA-4 blockade [Wei et al., 2017].
Treatment success of ICB can be evaluated by the means of serial magnet resonance imaging after tumor cell inoculation. In a preclinical study MRI evaluation of mice treated with anti-PD-1 and anti-CTLA-4 showed dichotomic response patterns. According to the response assessment in neuro-oncology (RANO) criteria ICB treated mice are classified as responders if they depict either stable disease or a regression of the tumor volume between defined MRI time points. In contrast, non-responder mice show a progressive disease characterised by substantial ongoing tumor growth. ICB non-responders exhibited a decrease in immune cell infiltration and higher amounts of regulatory T cells, while the clonality of the TCR repertoire is impaired by failed proliferation of antigen specific T cells. Surprisingly, the anti-tumor immunity was mainly driven by CD4 T cells and not CD8 T cells. Response to ICB was further hampered by the presence of immunosuppressive myeloid cells with an M2-like phenotype including the upregulation of PD-L1. The latter was strongly expressed on intratumoral macrophages and thus targeting of this subset with additional PD-L1 can further positively affect the immunogenicity of the TME. [Aslan et al., 2020] Furthermore the relevance of myeloid cells for the success of ICB has been strengthened, as MHC class II is upregulated in myeloid cell subsets of ICB responder mice this suggests enhanced antigen presentation in successful immune checkpoint therapy. [Aslan et al., 2020]
Thus, the possible impact of myeloid cell infiltration and antigen presentation via MHC class II in the context of immune-checkpoint blockade in general and with a focus on specific subsets of T effector cells proves to be worth further investigation.
Despite some advances in the application of immune checkpoint therapy there is still a reasonable proportion of brain tumor patients without a clinical response to treatment with ICB. Initially, hypermutated gliomas were thought to be similar to other mismatch repair (MMR) deficient cancer entities, however, recent findings challenged this perspective. Hypermutation in gliomas either occurs spontaneously and is associated with defects in the DNA mismatch repair systems or is observed after treatment with temozolomide (TMZ) upon recurrence of the tumor. The latter are caused by a selection pressure induced by temozolomide favouring tumor cells with an acquired MMR deficiency which alters the cells to be resistant to treatment with temozolomide. Thereby the defects in DNA mismatch repair systems are also induced by exposure of the tumor cells to temozolomide.[Yip et al., 2009] [Touat et al., 2020] Hypermutation in colo-rectal carcinoma causes an increased number of neoantigens modifying the immunogenicity of the tumor and enhancing immune cell infiltration. [Ganesh et al., 2019] However, despite a high mutational burden in hypermutated gliomas they do not depict a high number of so called

indel homopolymers that arise from small insertions or deletions causing frameshift mutations with an increased immunogenicity. This might explain the lack of responses in anti-PD-1 treated patients who showed worse survival rates compared to those patients having received other systemic drugs. [Touat et al., 2020]

2.1.3 Adoptive cell transfer

Adoptive cell transfer comprises the infusion of diverse cellular products into a patient such as autologous tumor infiltrating lymphocytes (TILs), T cell receptor engineered T cells or CAR T cells. Autologous TILs have demonstrated to be effective in patients with metastatic melanoma using tumor reactive T cells after ex vivo rapid expansion. Treatment with immunodepleting chemotherapy prior to the treatment resulted in a regression in nearly half of the patients. [Dudley et al., 2002]. For gliomas this approach has yet not gained increasing importance with only a single clinical study on the adoptive transfer of autologous tumor infiltrating lymphocytes in glioblastoma patients. [Quattrocchi et al., 1999]
A key development promoting the invention of further therapies in brain tumors has been the introduction of chimeric antigen receptor (CAR) T cells. [Kilian et al., 2021] CAR T cells are composed of an extracellular antigen recognition domain combined with a hinging transmembrane domain and an intracellular signaling domain for downstream signaling. These genetically engineered T cells promise to efficiently and specifically target cancer antigens, however binding of CARs is restricted to surface antigens that are often not completely tumor specific. Especially in patients with lymphomas CAR T cells are auspicious approaches. The CD19 antigen is expressed by more than 90 % of all B cell malignancies and on B cells during distinct differentiation stages. CAR T cells redirected to the CD19 antigen have shown reasonable results in several clinical trials. The binding to the antigen is usually mediated by variable regions derived from a monoclonal antibody in the extracellular domain of the receptor. CAR T cells are further characterised by a CD3 domain enabling intracellular signaling in accordance to normal T cell activation. [Rosenberg and Restifo, 2015]
A mutation within the epidermal growth factor receptor variant III (EGFRvIII) is present in approximately 30 % of all newly diagnosed glioblastomas and can be targeted by both vaccination [Schuster et al., 2015] and CAR T cells [O'Rourke et al., 2017]. Treatment with EGFRvIII specific CAR T cells resulted in stable disease in one of the treated patients for 18 months. Expansion of infused cells in the peripheral blood was observed in all patients in this study and post-infusion specimens of 5 patients showed infiltration of CAR T cells into the tumor. However, decreasing antigen expression on tumor cells due to interaction with the specific T cells and an upregulation of immunosuppressive mechanisms limited the efficiency. [O'Rourke et al., 2017]
CAR T cells have also been employed in other brain malignancies such as diffuse midline gliomas that feature a mutation in the H3K27M gene and show an upregualtion of the disialoganglioside GD2 on the cell surface that can be targeted by CAR T cells [Majzner et al., 2022]. Treatment of four patients with an H3K27M mutated tumors with GD-2 recognizing CAR T cells resulted in clinical and radiographic improvements with limited off-target cytotoxicity demonstrating the feasibility of this approach. Extensive single cell

analysis of the delivered cellular products and CSF samples from treated patients showed correlative differences fitting to the clinical response patterns. [Majzner et al., 2022]
The administration of CAR T cells through intracranial and not systemic delivery routes is in principal capable of inducing potent anti-tumor responses in brain tumors, as it has been used in a preclinical model of atypical theratoid/ rhaboid tumors (ATRT). [Theruvath et al., 2020] ATRTs occur mainly in young children under 3 years with a median survival limited to 17 months under optimal standard therapy. These specific tumor cells show a constant high expression of the immune checkpoint molecule B7-H3 due to a mutation resulting in a residual activity of an embryonic pathway. As B7-H3 is consequently only highly expressed in the prenatal brain and in ATRTs, B7-H3 was identified as potent target for cellular immunotherapy in this special tumor entity. [Theruvath et al., 2020] B7-H3 reactive CAR T cells have been described to be able to generate potent anti-tumor responses in vitro and in preclinical xenograft models targeting pancreatic ductal adenocarcinoma, ovarian cancer and neuroblastoma. [Du et al., 2019] Comparisons of different delivery routes for brain tumors in a preclinical model of B7-H3 expressing ATRT xenografts favored intraventricular administration of CAR T cells over intravenous infusion. Intraventricular delivered CAR T cells were able to cure all mice applying 0,5 x 10^6 T cells while for intravenous injection a fivefold higher dose was required. Immunofluorescence microscopy of ATRTs 48 hours after infusion of CAR T cells showed an enrichment of B7-H3 reactive CAR T cells in the tumor when T cells were applied intratumorally or intraventricularly while in intravenously treated mice no CAR T cells were detectable suggesting an increased infiltration in case of local administration. B7-H3 CAR T cells persisted after a tenfold lower dose of cells when infused via the ventricular system. [Theruvath et al., 2020] These data suggest, that intraventricular delivery leads to an earlier and more effective infiltration of tumor reactive CAR T cells. Previously, a clinical case report had shown that chimeric antigen receptor cells targeting the IL13R2 receptor can result in transient complete regression of intracranial tumor lesion after infusion in both the tumor cavity and the ventricular system. Thus, targeting of glioma specific antigens via intracranial administration of genetically modified T cells is in prinicple feasible and able to induce clinical responses. [Brown et al., 2016]
In addition to the delivery of CAR constructs to T cells, transduction with reactive T cell receptors is another possibility to generate genetically engineered T cells. The MHC class I restricted MART-1 epitope present in most of the patients with melanomas can be targeted by MART-1 TCR transgenic T cells resulting in anti-tumor immunity. [Chodon et al., 2014] MART-1 TCR transgenic T cells administered to 15 patients showed persistence of transferred autologous T cells for up to 1 year. Even more than 10 percent of circulating cells for at least two months were engineered T cells. Two patients experienced clinical tumor regression correlating with a persistence of TCR engineered T cells for more than 1 year demonstrating the principal capability of those cells to mediate potent tumor control in a clinical context. [Morgan et al., 2006] As preclinical data suggests an improvement of therapeutic success of ACT in combination with an in vivo antigen stimulation [Lou et al., 2004], infusion of MART-1 TCR transgenic T cells was combined with a dendritic cell vaccination with the MART-1 peptide in a clinical phase I study. Nine of thirteen treated patients showed tumor regression. Transgenic T cells persisted at levels of up to 20 % of peripheral T lymphocytes for more than two months. No serious toxicity was reported.

[Chodon et al., 2014] Until now the only study investigating the therapeutic capacity of TCR transgenic CD8 T cells in gliomas focuses on the H3.3K27M mutation present in diffuse midline gliomas. [Chheda et al., 2018] The respective TCR recognizing the H3.3K27M mutation was isolated from healthy donor T cells *in vitro* stimulated with the H3.3K27M peptide. Adoptive cell transfer of H3.3K27M specific TCR transgenic T cells resulted in decreased tumor growth in a preclinical mouse model. [Chheda et al., 2018] Yet, the mechanisms that drives the resistance to adoptive cell therapy in the subset of patients without clinical responses are poorly understand. Preclinical studies aiming to investigate the influence of different factors such as cell dose, cytokine treatment or in vivo antigen stimulation on the tumor control in the setting of adoptive cell therapy in a B16 melanoma model depicted different determinants for therapeutic success. The cell dose administered to tumor bearing mice strongly correlated with tumor growth and a survival benefit was observed with increasing numbers of infiltrated T cells. Interestingly, T cell differentiation negatively correlated with ACT efficiency favoring memory T cells over effector T cells. A combination therapy with a viral vaccine further increased survival in dependency of the applied titer of viral vaccine. Finally, infusion of Interleukin-2 improved therapeutic results, however, the number of doses did not correlate with tumor regression. [Klebanoff et al., 2011]
To sum up screening for reactive T cell receptors and subsequent delivery of T cells transgenic for the found TCR would be a promising approach in patients with gliomas. But the current status of research is rare for both preclinical and clinical studies investigating the effects of TCR transgenic T cells. Furthermore, the effect of antigen presentation in the presence of specific tumor-directed lymphocytes has not been investigated yet and might have an impact on our current understanding of cellular therapeutic concepts.

2.2 Implications of the immune privileged nature of the brain for immunotherapeutic interventions

For a sufficient immune response antigen presentation to T helper and effector cells is a key mechanism in driving the tumor rejection by the endogenous immune system, however, the exact mechanisms of antigen spreading from the brain to peripheral immune system has long remained unclear. But very recently new evidence partly deciphered the function of the meningeal lymphatic system and the location of antigen presentation outside of the CNS. The meningeal lymphatic vessels play a key role in this context, as they enable the drainage of the cerebrospinal fluid and secondly promote the travelling of immune cells to the draining lymph nodes. In a multiple sclerosis model the response of T cells was drastically reduced after ablation of the meningeal lymphatics. [Louveau et al., 2018] Consequently, the role of the lymphatic system has been investigated in the context of CNS malignancies. Overexpression of VEGF-C in a mouse model bearing syngeneic GL261 gliomas using either a viral vector or a mRNA vector led to increased lymphangionesis. Prophylactic treatment with the VEGF-C encoding vector resulted in long-term survival after challenge with an intracranial tumor and enhanced travelling of antigen-specific T cells to the deep cervical lymph nodes. Therefore, trafficking of immune cells via the meningeal lymphatics to the deep cervical lymph nodes as the location of antigen

presentation in the immune response to brain tumors has demonstrated its relevance. Furthermore, treatment with the VEGF-C vector was able to improve the effect immune checkpoint therapy. [Song et al., 2020]

2.3 The immune cell landscape in brain tumors

The landscape of myeloid cells in brain malignancies composes a heterogenous population of cell. [Klemm et al., 2020] microglia as the antigen presenting cells of the central nervous system derive from erythromyeloid precursors in the embryonal yolk sac. [Kierdorf et al., 2013] The *Flt3:Cre;Rosa26:mTmG* mouse model is a lineage tracing model used to determine that all hematopoietic cells except for microglia originate from hematopoietic stem cells expressing the tyrosine kinase FLT3 and are therefore marked with a specific reporter. [Boyer et al., 2011] Using this lineage tracking model the dichotomy of the myeloid cell compartment in brain tumors became obvious, as both local brain resident microglia and hematopoietic stem cell derived monocytes and macrophages are present in the micromilieu of brain tumors. [Bowman et al., 2016] Therefore the myeloid cell compartment in CNS malignancies is composed of a heterogenous population of both local embryonic precursor derived cells and myeloid cells developed from peripheral hematopoietic cells. In deciphering the properties of the diverse cell compartment in tumors the development of RNA single sequencing has dramatically shaped our understanding of the complexity of different immune cell subsets present in different cancer entities and inflammation.

A comprehensive study characterized the myeloid cell landscape in the inflamed brain using a model of neuroinflammation during different disease stages. Single-Cell analysis of CD45+ cells from naïve and MOG35-55 immunized mice revealed CNS associated macrophages (CAMs), microglial cells and HSC (hematopoietic stem cell)-derived myeloid cells as the different types of myeloid cell subsets. MOG35-55 is thereby used to generate autoreactive T cells which are the key driver of the MS pathogenesis. Neuroinflammation is associated with an upregulation of MHC class II associated genes in both microglial cells and CAM in several CNS compartments highlighting its relevance for the onset of an autoimmune reaction. Further investigation on which specific cell type is responsible for antigen presentation revealed that antigen presentation associated gene signatures can be detected in specific subsets of microglia, CAM and HSC derived myeloid cells respectively. microglia specific deletion of MHC class II does not alter the infiltration of several immune cell subsets, whereas deletion of MHC II in in a specific population of dendritic cells which are CD11c+ Cx3cr1+ positive hampered the onset of neuroinflammation as an indicator of reduced antigen presentation in these knock-out mice. [Jordao et al., 2019] These results indicate that the antigen presentation via MHC class II might be restricted to a specific cell type.

As for myeloid cell the landscape of T cells in tumors is composed of heterogenous populations of CD4+ and CD8+ T lymphocytes accompanied by CD4+ Treg cells, as depicted by single cell profiling in non-small-cell lung cancer samples. T lymphocytes were characterized by different gene signature ranging from a naïve status to a genotype associated with effector function. Exhausted like phenotypes associated with high expression of immune inhibitory molecules can be identified in CD4+ Treg cells as well as

in CD8+ and CD4+ T cells. [Guo et al., 2018]
The impact of genetic alterations and the origin of different tumors can further shape the local microenvironment and immunogenicity resulting in an even more complex intratumoral immune cell compartment. [Klemm et al., 2020] [Friebel et al., 2020] One way by which tumors influence the compostion of the microenvironment are specific tumor metabolites such as 2-Hydroxyglutarat (2-HG) that is present in IDH-1 mutant tumors. [Bunse et al., 2018] In the context of brain tumors single cell sequencing and mass cytometry revealed these fundamental differences between IDH-1 mutant and wildtype gliomas and also between primary brain malignancies and metastasis in the CNS. [Friebel et al., 2020][Klemm et al., 2020].
Brain metastasis are characterised by an increased infiltration of T cells than gliomas and in particular in IDH-1 mutant gliomas the rates of tumor associated macrophages and microglia cells are increased in primary brain tumors compared to secondary malignancies. [Klemm et al., 2020] Interestingly the myeloid cell compartment is fundamentally different in IDH-1 mutant gliomas. In contrast IDH-1 wildtype tumors showed an increased amount of microglia cells and reduced numbers of tumor associated macrophages. [Klemm et al., 2020] Moreover, both cell types are characterized by a rather immunosuppressive phenotype in IDH-1 mutant tumors. [Klemm et al., 2020] Mechanistically the changes in the myeloid cell phenotype in IDH-1 mutant tumors is driven by changes in the tryptophan metabolism. [Friedrich et al., 2021] Thus, the tumor directs the development of tumor exclusive and specific subsets of tumor associated macrophages. [Friebel et al., 2020] Consequently, these results highlight the low levels of T lymphocytes in primary brain tumors and thereby emphasize the relevance of the delivery of antigen reactive T cells to the tumor microenvironment.
The investigation of the tumor educated differences of the local microenviroment even resulted in clinical translation of these results: For example the increased immunogenicity of the local tumor mircoenviroment in secondary brain malignancies suggested that treatment with immune checkpoint therapy might be beneficial for these patients. A clinical phase 2 trial investigating the anti-tumor effect of Pembrolizumab as an PD-1 inhibitor in patients with either melanoma or non-small-cell lung cancer brain metastasis confirmed this hypothesis with durable responses in about 20-30 % of the participants. [Goldberg et al., 2016]

2.4 Mechanisms of T cell exhaustion

The functional status of intratumoral T cells is a key determinant of tumor responses. Consequently, a main focus has been on exhausted T cells as one therapeutically relevant cell population. Detailed analysis of this subset of CD8 T cells allows discrimination into two subpopulations representing a progenitor exhausted subtype characterized by flowcytometry as TIM3- and TCF1+ and a terminally exhausted subtype described as TIM3+ and TCF1-. After TCR stimulation through antigen presentation progenitor exhausted T cells differentiate into terminally exhausted CD8 T cells. This subset shows greater ability of IFN-y production and an increased cytotoxicity while they lack polyfunctionality in terms of cytokine production. Since antigen presentation drives the differentiation into a terminally exhausted phenotype, these cells exhibit higher clonality

while progenitor exhausted CD8 T cells possess superior ability for proliferation. As a consequence, they show significantly improved tumor control and higher expansion rate in response to ICB with anti-PD-1. [Miller et al., 2019]
Consistent with their reduced capacity to diminish tumor growth PD-1^{high} CD8 T cells are characterized by upregulation of inhibitory gene signatures. Nevertheless, PD-1^{high} CD8 T cells show significant upregulation of genes associated with chemotaxis such as chemokine CXC motif ligand 13 (CXCL13) and might be involved in the recruitment of several immune cell types to the TME through chemotaxis. [Thommen et al., 2018]
In line with these results the meaning of TCF1 as a central regulator of the stem cell like properties of PD-1 expressing CD8 T cells has been further demonstrated in the context of antigen vaccination and immune checkpoint blockade. TCF1+ PD-1+ CD8 T cells mediated tumor control as demonstrated by increased tumor growth upon ablation of this cell population and thereby highlighted the therapeutic potential of this progenitor exhausted cell population. TCF1 + cells were characterized by their ability to expand and showed transcriptional profiles with similarities to hematopoietic stem cells. [Siddiqui et al., 2019]
Interestingly, these TCF1+ CD8+ T cells are localized in an intratumoral niche with a high abundance of antigen presenting cells and expression of MHC class II. These zones functionally mirror the T cell zone in lymphoid tissue. Interestingly, these MHC class II positive and APC dense regions were decreased in patients bearing kidney, prostate or bladder tumors with a progressive disease. [Jansen et al., 2019] Thus, antigen presentation using MHC class II seems to be a substantial component to maintain the functional properties of antigen specific CD8 T cells.
In IDH-1 mutant and wildtype gliomas the composition of the T cell compartment shows some similarities compared to those findings generated in non-small cell lung cancer. As previously described CD4 and CD8 T cells with an effector signature are also found in both IDH-1 mutant and wildtype gliomas. Effector cells were accompanied by cells showing an effector memory program. One of these clusters showed high expression of NK cell like genes and simultaneously performed analysis of the T cell receptor sequences revealed a similar gene expression with high levels of NK cell receptors for clonally expanded and highly cytotoxic CD8 T cells. Interestingly CD161 as one of these NK cell receptors emerged as an inhibitory receptor on antigen specific T cells and was accessible to inactivation with the result of enhanced anti-tumor reactivity. [Mathewson et al., 2021]

2.5 A mouse model to study the impact of MHC class II related antigen presentation in the tumor microenvironment

As indicated earlier, microglia derive from myeloid precursor cells in the extra-embryonic yolk sac. Consequently, there is no regeneration of microglial cells from hematopoietic stem cells during live time [Ransohoff and Cardona, 2010]. Therefore, microglial proliferation results from local expansion of cells rather than from invasion and differentiation of precursor cells.
The chemokine receptor *Cx3cr1* is broadly expressed on myeloid derived blood cells and on microglial cells [Jung et al., 2000]. Expressing the Cre recombinase fused to an Estrogen ligand binding domain under the *Cx3cr1* promoter and considering the lack of renewal of microglia during live time this technique enables microglia specific targeting of a gene of interest [Goldmann et al., 2013]. The combination of $Cx3cr1^{CreER}$ transgenic mice with MHC class II flox mice allows either general deletion of MHC class II in all myeloid cells expressing *Cx3cr1* or specifically in microglia [Wolf et al., 2018]. In line with the $Cx3cr1^{CreER}$ model MHC II expression on myeloid cells except for microglia is restored 6 weeks after the initial Tamoxifen (TAM) treatment [Goldmann et al., 2013] allowing distinction between MHC II deletion on all myeloid cells by the use of continuous TAM treatment or on microglial cells only after initial TAM-treatment.
Therefore, this mouse models enables specific studies of the impact of antigen presentation on the local tumor microenvironment.

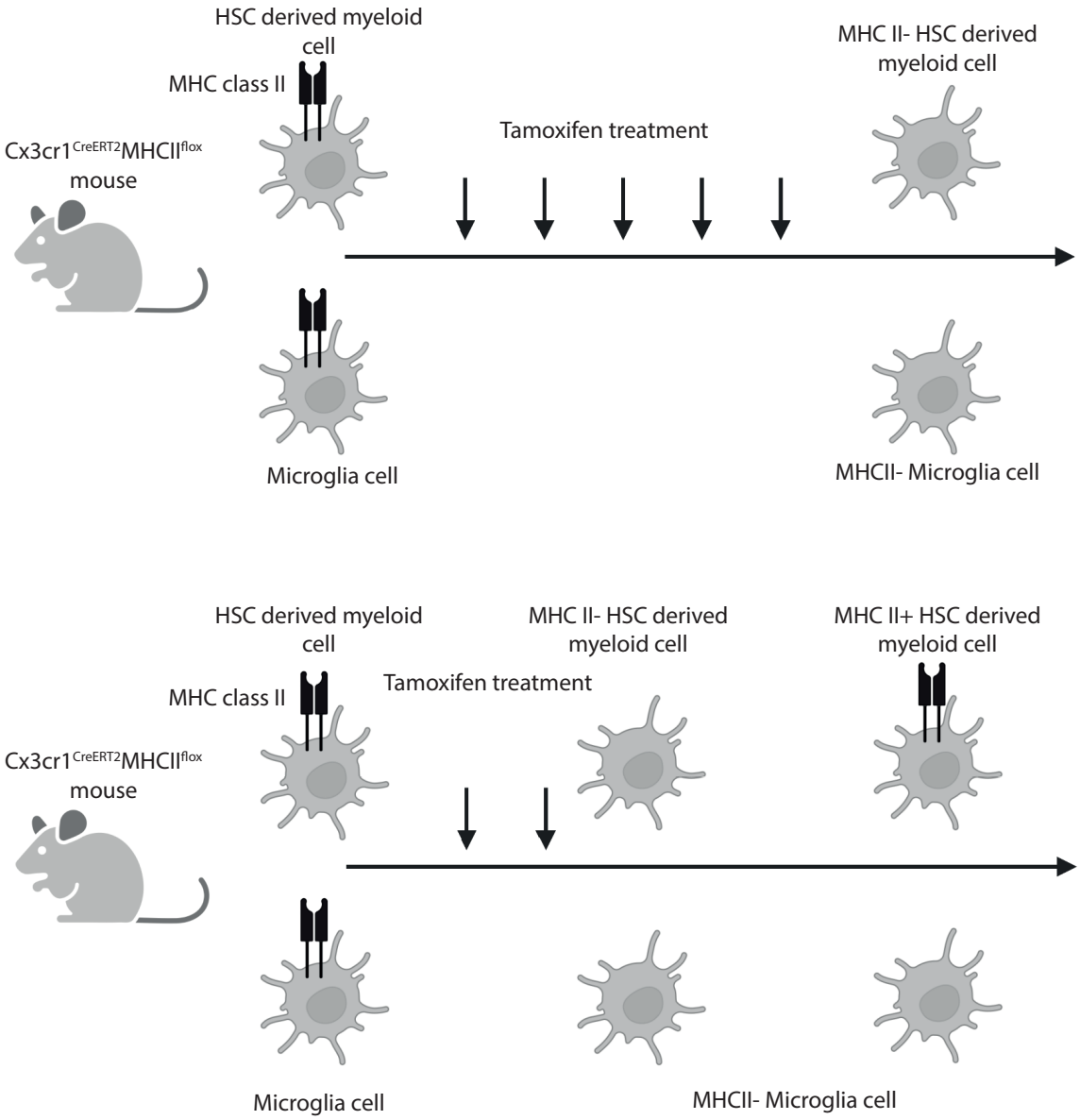

Figure 2: **The Cx3cr$^{\mathbf{CreERT2}}$MHCII$^{\mathbf{flox}}$ mouse model enables specific targeting of MHC class II on myeloid cells and exclusively on microglia cells**
Cx3cr$^{\mathrm{CreERT2}}$MHCII$^{\mathrm{flox}}$ mice are either treated with continuous or only initial tamoxifen. Continuously treated mice feature a MHC class II deficient phenotype in all myeloid cells. Short term initial treatment results in MHC II deletion that is only present in microglia cells after several weeks, as new HSC derived myeloid cells that are MHC class II proficient replace the MHC II deleted HSC derived myeloid cells.

2.6 Brain tumor models

One of the most commonly used syngeneic murine glioma models is the GL261 cell line initially generated by intracranial injection of 3-methylcholantrene into the brain of C57BL/6 mice. [Ausman et al., 1970] These tumor cells typically feature point mutations in the p53 and K-ras gene while missing defined driver mutations. [Szatmari et al., 2006] GL261 glioma are further characterized by an aggressive in vivo tumor growth depending on the implanted number of cells and moderate immunogenicity. [Szatmari et al., 2006] Without stimulation GL261 cells show MHC class I restriced antigen presentation, however, MHC class II expression is only present after induction with interferon-γ [Szatmari et al., 2006]
For research on human glioblastomas the U87MG glioblastoma cell line is widely used. Introduced by J Ponten et al. in 1968 [Ponten and Macintyre, 1968] U87MG were subjected to multiple characterisations [Olopade et al., 1992] [Clark et al., 2010] revealing a complex mutational landscape of the tumor. For in vivo growth these cells have to be administered to immunodeficient mice [Fogh et al., 1977] restricting the studies of the interactions of the immune system. However, by injection of human stem cells into immunodeficient mice this approach allows characterization of immune cell reactions within the tumor microenvironment.

2.7 The NLGN4X antigen in healthy brain and CNS malignancies

The GAPVAC study [Hilf et al., 2019] has discovered the NLGN4X antigen as a possible antigen for immunotherapy of brain tumors. The NLGN4X antigen is localized within the protein sequence of the Neuroligin 4 protein linked to the X-chromosome that is also expressed in healthy brain tissue.
Neuroligins are synaptic cell adhesion molecules localized on the postsynaptic membrane. NLGN4 is encoded on the X chromosome [Sudhof, 2008] and in contrast to most of the Neuroligins and Neurexins NLGN4 is not evolutionary constricted. [Bolliger et al., 2008] Neuroligins endogenously bind to Neurexin, which are also cell adhesion molecules localized at the presynaptic membrane. [Ichtchenko et al., 1995]
Neuroligins and Neurexin typically form a complex between the synaptic membrane. Neuroligins were initially thought to promote presynaptic specialization [Scheiffele et al., 2000], however, later evidence suggested that Neuroligins are essential for synaptic function but not formation. [Varoqueaux et al., 2006] Neuroligin is predominantly localized at excitatory neuron in the cerebral cortex and seems to be involved in the regulation of excitatory synaptic transmission. [Marro et al., 2019] Overexpression of NLGN4 in human Neurons resulted in an increased number of Synapsin-1 positive densities localized at dendrites. This suggests an increased general number of synapsis but did not increase the number of functional excitatory synapsis. [Marro et al., 2019] NLGN3 – another member of the family of Neuroligins – is described to promote tumor growth of gliomas in a paracrine fashion through the numerous phosphorylation pathways leading to enhanced expression of genes involved in cell proliferation and interestingly in synaptic function. [Venkatesh et al., 2017]

In 2019 *Venkataramani et al.* described the existence of neurogliomal synpasis between tumor cells and neurons in human gliomas. Neurons and tumor microtubes form synaptic structures promoting glioma growth through glutamergic excitatory signalling. [Venkataramani et al., 2019] *Osswald et al.* showed that functional networks formed by tumor microtubes could drive resistance to therapeutic strategies, while disruption of these networks through knock-down of the growth-associated protein 43 (GAP-43) resulted in controlled tumor growth. [Osswald et al., 2015]
The NLGN4X protein it is mainly expressed in the brain. Apart from the central nervous system there is protein expression in smooth muscle cells and in the breast and placenta. NLGN4X is known to be overexpressed in human gliomas (comp. Fig. 3 3 a and b).
Due to the low expression pattern apart from the brain and the typical overexpression in human gliomas NLGN4X might be a suitable target for a T cell therapy using adoptive transfer of T cell receptor engineered T cells.

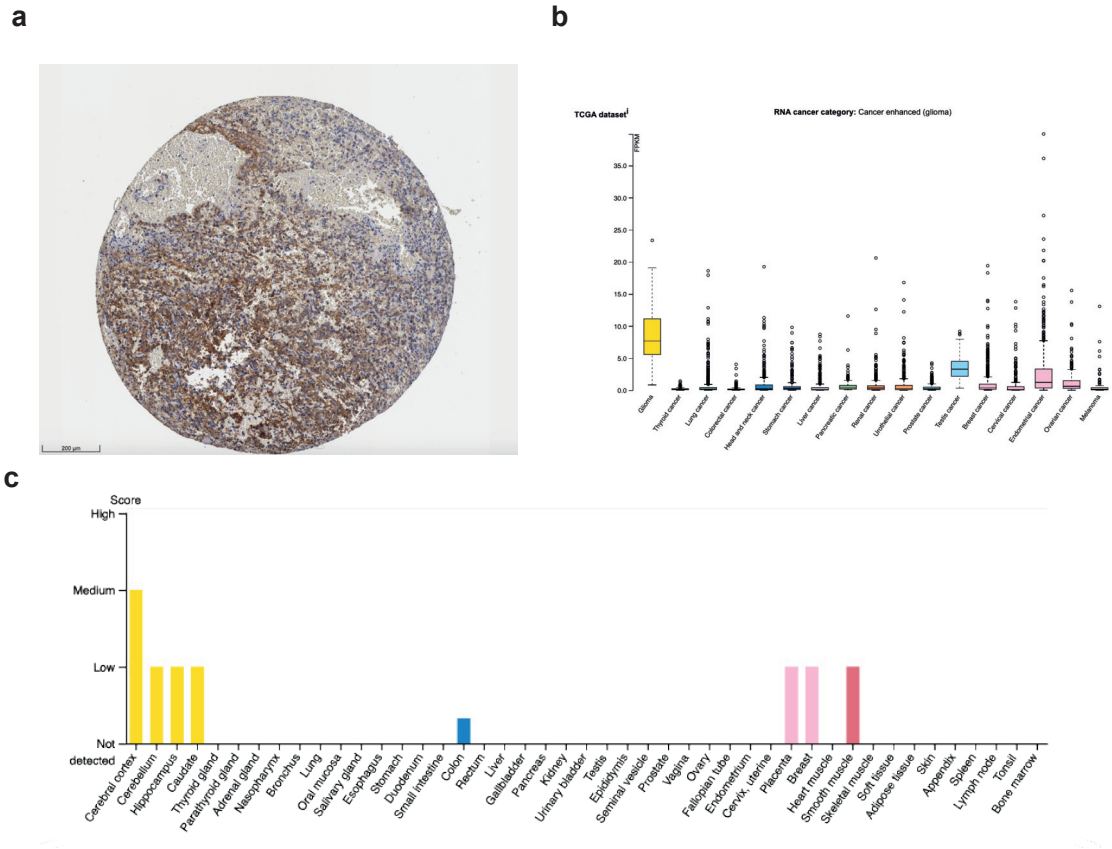

Figure 3: **NLGN4X in healthy human tissue and malignant gliomas**
Data from the Human Protein Atlas available from http://www.proteinatlas.org. a. Exemplary image of a malignant glioma, high grade, from a 56 year old patient, available under: HPA001651 https://www.proteinatlas.org/ENSG00000146938-NLGN4X/pathology/glioma b. RNA expression overview of NLGN4X in human cancer. Data from the TCGA generated by The Cancer Genome Atlas presented by the Human Protein Atlas: https://www.proteinatlas.org/ENSG00000146938-NLGN4X/pathology c. Protein expression in healthy human tissue data from the Human Protein atlas at: https://www.proteinatlas.org/ENSG00000146938-NLGN4X/tissue

2.8 Hypothesis

Despite the current advancements in the therapy of malignancies of the central nervous system the prognosis of glioblastomas is still extremely limited and the mechanisms of cancer regression in response to different therapeutic concepts remain unclear. Therefore, there is an urgent need for the development of new highly specific therapies.
The first part of this thesis will thus focus on generating a preclinical model to study the efficiency of T cell receptor engineered T cells directed against a glioma associated antigen derived from an highly individualized immunotherapy. Therefore, the Neuroligin 4, X-linked antigen will be investigated as a potential target for a cellular immunotherapeutic approach. This thesis will assess if human T cells engineered to express a NLGN4X-specific T cell receptor are capable of mediating a therapeutic anti-tumor response in a preclinical setting.
Secondly, according to the presented state of current research a functional T cell response is dependent on both MHC class I and MHC class II restricted antigen presentation. However, the nature of the underlying mechanisms lacks profound understanding. Since successful immunotherapeutic approaches require robust knowledge of the processes resulting in effector cell activation and infiltration, a detailed understanding of MHC class II restricted antigen presentation and downstream processes might have a wide impact on this field of research. In order to assess the functional role of MHC class II on myeloid cells, the described $Cx3cr1^{CreERT2}$-$MHCII^{flox}$ mouse model will be utilized to prove if MHC class II plays a crucial role in initiating and maintaining a functional immune response of both the T helper and T effector cell compartment. Therefore, I will investigate the impact of a genetic deletion of MHC class II on different subsets of immune cell populations and their interactions. Furthermore, I will study the effect of the altered microenvironment on the success of an immunotherapeutic therapy.
The first part of this thesis was part of a larger research project, all shown results were generated by myself if not stated differently. The second part of this thesis was part of a larger research project together with Michael Kilian. The presented results in this thesis were generated by myself, if not stated differently in the respective parts of the results section.
The aim of this thesis is to develop a therapeutic concept to deliver individualized T cell receptor engineered T cells targeting a glioma associated antigen and to understand the mechanisms that shape the T cell effector responses.

3 Material and Methods

3.1 Reagents

3.1.1 Chemicals

Item	Manufacturer
4-(2-hydroxyethμl)-1-piperazineethanesulfonic acid (HEPES)	Invitrogen
123count eBeads Counting Beads	Invitrogen
Accutase	Gibco Life Technologies
ACK Lysing Buffer	Gibco Life Technologies
Albumin Fraktion V	Carl Roth
Ampicillin	Carl Roth
Benzonase	Santa Cruz Biotechnology
Bepanthen	Bayer
Blasticidin	Sigma-Aldrich
Carprofen	Pfizer
CloneAmp HiFi PCR Premix	CloneAmp HiFi PCR Premix Takara
Click's Medium	Fujifilm
Dimethμl sulfoxide (DMSO)	Carl Roth
Donkey Serum	
DMEM	DMEM
Enhanced chemoluminescence (ECL) solution Amersham	Cytiva
Ethμlenediaminetetraacetic acid (EDTA)	Sigma Aldrich
FACS flow	BD Biosciences
Fetal bovine serum (FBS)	Sigma-Aldrich
Fixable viability dye eFluor780	eBioscience
FuGene HD transfaction reagent	Promega
Gateway™ BP Clonase™ II Enzyme mix	Thermo Fisher
Gateway™ LR Clonase™ II Enzyme mix	Thermo Fisher
Hank's Buffered Salt Solution (HBSS) Sigma-Aldrich	Hank's Buffered Salt Solution (HBSS) Sigma-Aldrich
Human serum AB	Sigma-Aldrich
Ionomycin	Sigma-Aldrich
Kanamycin	Carl Roth
Ketamine	Zoetis
L-Glutamine	Sigma-Aldrich
Lipopolysaccharides (E. coli)	Sigma-Aldrich
Low-melting agarose	Sigma-Aldrich
Lympho-Paque solution	Genaxxon

Matrigel	Gibco Life Technologies
Methanol	ThermoScientific
Normal goat serum (NGS)	Cell Signaling Technology
Non-essential amino acids (NEAA)	Gibco Life Technologies
Phosphate Buffered Saline (PBS)	Sigma-Aldrich
Penicillin	Invitrogen
Percoll	GE Healthcare
Phorbol 12-myristate 13-acetate (PMA)	Sigma-Aldrich
Propanol	Sigma-Aldrich
Puromycin	Applichem
Ready-to-Use Lentiviral Packaging Plasmid Mix	Cellecta
Retronektin	Takara
RPMI-1640	Pan Biotech
Sodium chloride	Carl Roth
Sodium pyruvate	Sigma-Aldrich
Streptomycin	Invitrogen
SYBR Green qPCR master mix (ROX)	Applied Biosystems
T Cell TransAct™, human	Miltenyi
Tamoxifen	Sigma-Aldrich
TexMACS medium	Miltenyi
Tris hydrochloride	Carl Roth
Trypan blue Gibco Life Technologies	Trypan blue Gibco Life Technologies
Tween	MP Biomedicals
Vectashield HardSet Antifade Mounting medium with DAPI	Vector Laboratories
Xvivo15 Medium	Lonza

3.1.2 Kits

Item	**Manufacturer**
CD4 T Cell Isolation Kit Miltenyi	Miltenyi
CD8a T Cell Isolation Kit Miltenyi	Miltenyi
Chromium Single Cell 5' Reagent Kit	10x Genomics
Cytofix/ Cytoperm Fixation/ Permeabilization Kit	BD
CytoTox 96 Non-Radioactive Cytotoxicity Assay	Promega
High-Capacity cDNA Reverse Transcription Kit	Applied Biosystems
Intracellular Fixation & Permeabilization Buffer Set Thermo Fisher	Thermo Fisher

MagniSort™ Mouse T cell Enrichment Kit	Thermo Fisher
MagniSort™ Human T cell Enrichment Kit	Thermo Fisher
Nano-Glo Luciferase assay reagents	Promega
Neon™ Transfection System 100 µL Kit	Thermo Fisher
NEB Golden Gate Assembly Kit	New England BioLabs
NucleoBond Xtra Maxi kit	Macherey-Nagel
RNeasy Mini Kit	Qiagen

3.1.3 Cytokines

Item	**Manufacturer**
rh-IL2	Novartis
h-IL7	Miltenyi
h-IL15	Miltenyi
IFN-y	Peprotech

3.1.4 Primary antibodies, unconjugated

Antigen	**Host**	**Clone**	**Manufacturer**	**Method**
Murine CD28	mouse	polyclonal	eBioscience	In vitro
Murine CD3	mouse	polyclonal	BioLegend	In vitro
Murine CD16/32	mouse	polyclonal	BioLegend	FC
Murine MHC II	rat	M5/114.15.2	eBioscience	IF
Human CD3	rabbit	SP7	GeneTex	IF
Murine CD4	rat	GK1.5	Thermo Fisher	IF
Murine CD8	rat	4SM15	Thermo Fisher	IF
Murine CD11b	rabbit	M1/70	Novus Biologicals	IF
Murine GFAP	rabbit	Polyclonal	abcam	IF
Murine Iba-1	rabbit	Polyclonal	abcam	IF
TotalSeqC Hashtag 1-10	Rat	M1/42; 30-F11	BioLegend	10X

3.1.5 Secondary antibodies

Antigen	**Host**	**Conjugate**	**Manufacturer**	**Method**
Rat IgG	Goat	Alexa Fluor 488	Invitrogen	IF
Rat IgG	Goat	Alexa Fluor 633	Invitrogen	IF
Rabbit IgG	Goat	Alexa Fluor 633	Invitrogen	IF

Rabbit IgG	Donkey	Alexa Fluor 546	Invitrogen	IF
Rabbit IgG	Donkey	Alexa Fluor 488	Invitrogen	IF
Mouse IgG	Donkey	Alexa Fluor 647	Invitrogen	IF

3.1.6 Primary antibodies, conjugated

Antigen	**Conjugate**	**Clone**	**Manufacturer**
hHLA-A2	APC	BB7.2	BioLegend
hCD3	BV510	UCHT1	BD-Horizon
hCD3	SuperBright702	OKT3	Thermo Fisher
hCD4	PE-Dazzle 594	A161A1	BioLegend
hCD8a	PE-Cy7	SK-1	BioLegend
hCD8a	PerCp-Cy5.5	53-6.7	BioLegend
hCD8a	AlexaFluor700	SK-1	BioLegend
hCD137	PE	17B5-1	BioLegend
hCD69	BV711	FN50	BioLegend
hGranzyme B	FITC	GB11	BioLegend
hGranzyme B	PerCp-Cy5.5	QA16A02	BioLegend
hIFN-gamma	BV421	4S.B3	BioLegend
hPerforin	PerCp-Efluor710	dG9	Thermo Fisher
hPerforin	AlexaFluor700	B-D48	Thermo Fisher
hTNF-alpha	BV605	MAb11	BioLegend
hTNF-alpha	APC	MPG6-XT22	BioLegend
hTNF-alpha	APC	MAb11	BioLegend
hCD45RA	PE-Dazzle	HI100	BioLegend
hCD45RO	BV605	UCHL1	BioLegend
hCCR7	BV510	G043H7	BioLegend
hPD-1	Pe-Cy7	EH12.2H7	BioLegend
hTim-3	BV421	RMT3-23	BioLegend
hLag-3	PerCP-Cy5.5	11C3C65	BioLegend
hCX3CR1	APC	2A9-1	BioLegend
m4.1BB	APC	4B4-1	BioLegend
mCD11b	PE/Cy-7	M1/70	BioLegend
mCD11b	PE-Dazzle	M1/70	BioLegend
mCD11c	PE	N418	BioLegend
mCD19	BV605	6D5	BioLegend
mCD3	BV711	17-A2	BioLegend
mCD3	FITC	17-A2	BioLegend
mCD4	PE-Cy7	GK1.5	BioLegend
mCD4	PE-TexasRed	RM4-5	BioLegend
mCD8	AF700	53-6.7	BioLegend
mCD8	PerCp-Cy5.5	53-6.7	BioLegend
mCD25	PE-Cy7	PC61	BioLegend

mCD31	APC	MEC13.3	BD Bioscience
mCD45	BV510	30-F11	BioLegend
mCD80	PerCp-Cy5.5	16-10A1	BioLegend
mF4/80	BV421	BM8	BioLegend
mF4/80	FITC	BM8	BioLegend
mFOXP3	APC	FJK-16s	BioLegend
mICAM	FITC	YN1/1.7.4	BioLegend
mIFN-gamma	PE	XMG1.2	BioLegend
mKi67	BV605	16A8	BioLegend
mLy6C	FITC	HK1.4	BioLegend
mLy6C	APC	HK1.4	BioLegend
mMHCII	APC	M5.114.15.2	BioLegend
mMHCII	AF700	M5.114.15.2	BioLegend
Nk1.1	FITC	PK136	BioLegend
mPD-L1	BV711	10F.9G2	BioLegend
mPD-1	PerCp-Cy5.5	J43	BioLegend
mPD-1	PE-Cy7	RMP1-30	BioLegend
mTCF-1	PE	7F11A10	BioLegend
mTCRbeta constant chain	PE	H57-597	BioLegend
mTCRbeta constant chain	APC	H57-597	BioLegend
mTGFb	PE	TW7-16B4	BioLegend
mTIM3	BV421	RMT3-23	BioLegend
mTNF-alpha	BV421	MP6-XT22	BioLegend

3.1.7 *in vivo* Antibodies

Item	**Clone**	**Manufacturer**
mPD-L1	10F.9G2	BioXCell
mPD-1	RMP1-14	BioXCell
mCTLA-4	9D9	BioXCell
InVivoMAb mouse IgG2b isotype control	MPC-11	BioXCell
InVivoMAb rat IgG2a isotype control	2A3	BioXCell
InVivoMAb rat IgG2b isotype control	LTF-2	BioXCell

3.1.8 Buffers

Buffer	**Ingredients**	**Manufacturer**
CellTrace FarRed staining buffer	1X PBS, 0,1 % BSA	Sigma-Aldrich, Roth
CellTrace Violet staining buffer	1X PBS, 0,1 % BSA	Sigma-Aldrich, Roth

FACS buffer	1X PBS , 3 % FBS, 2 mM EDTA	Sigma-Aldrich, Sigma-Aldrich, AppliChem
MACS buffer	1X PBS , 3 % FBS, 10 mM EDTA	Sigma-Aldrich, Sigma-Aldrich, AppliChem

3.1.9 Primer

Target	**Sequence**
OVA I epitope primer fwd	TGGAGCAGCTGGAGAGCATC
OVA I epitope primer rev	TGGTCCACTCGGTCAGCTTC
NLGN4X epitope fwd	CACCTGGATGAGAGATCCTTACTGC
NLGN4X epitope rev	CATGAATATCATCTTCCGTGGGCACG
NLGN4X epitope fwd 2	ATCCCACTTATGACGCCAAACACC
NLGN4X epitope rev 2	TGTTTTGTCCTCCACTGAAGGTGTTAAAAG

3.1.10 Peptides

Peptide	**Amino Acid Sequence**
Flu	Gly-Ile-Leu-Gly-Phe-Val-Phe-Thr-Leu
Mart-1	Ala-Ala-Gly-Ile-Gly-Ile-Leu-Thr-Val
MOG	Met-Glu-Val-Gly-Trp-Tyr-Arg-Pro-Pro-Phe-Ser-Arg-Val-Val-His-Leu-Tyr-Arg-Asn-Gly-Lys
NLGN4X	Asn-Leu-Asp-Thr-Leu-Met-Thr-Tyr-Val
OVA MHC I	Ser-Ile-Ile-Asn-Phe-Glu-Lys-Leu
OVA MHC II	Ile-Ser-Gln-Ala-Val-His-Ala-Ala-His-Ala-Glu-Ile-Asn-Glu-Ala-Gly-Arg

3.2 Plasmid maps

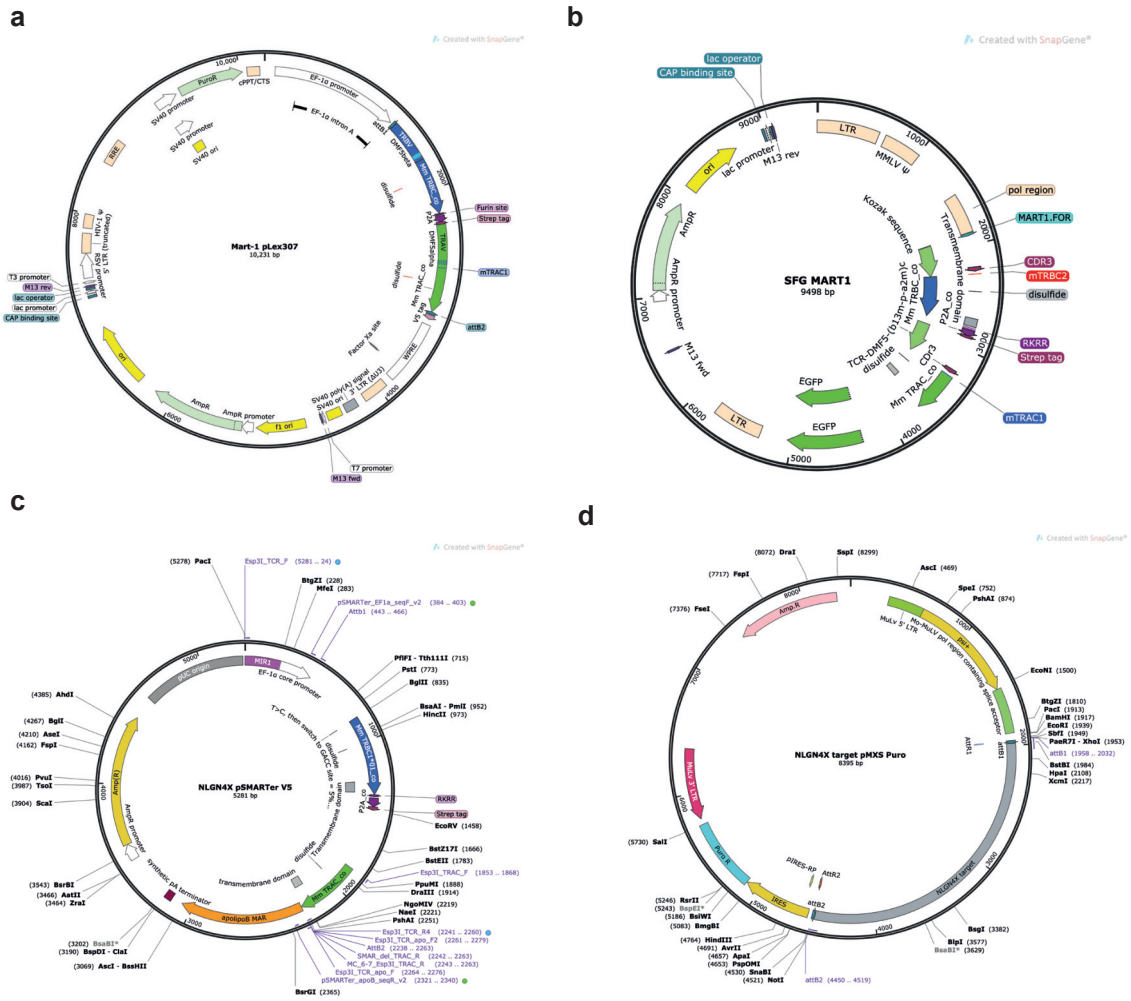

Figure 4: **Cloning strategy**
a Mart-1 TCR *pLEX307* lentiviral vector **b** Mart-1 TCR *SFG* retroviral vector **c** NLGN4X TCR *pSMARTer V5* vector **d** NLGN4X antigen *pMXS Puromycin* retroviral vector.

3.3 Methods

3.3.1 Mice

NOD.Cg-*Prkdc*^{scid}*Il2rg*^{tm1Wjl}/SzJ (NSG) mice came from the Jackson Laboratory and were bred at the DKFZ animal facility. NOD.Cg-*Prkdc*^{scid} *H2-K1*^{tm1Bpe} *H2-Ab1*^{em1Mvw} *H2-D1*^{tm1Bpe} *Il2rg*^{tm1Wjl}/SzJ (NSG MHCI/II KO) mice were purchased from the Jackson Laboratory and bred at the DKFZ animal facility. MHCII$^{flox/flox}$ mice were purchased from the Jackson Laboratory and bred at the DKFZ animal facility. Cx3Cr1^{CreERT2} mice were provided by Steffen Jung, Department of Immunology, The Weizmann Institute of Science, Rehovot, Israel. Cx3Cr1^{CreERT2}-MHCII$^{flox/flox}$ mice were generated by Michael Kilian,

German Cancer Research Centre Heidelberg, crossing both strains to achieve homozygous MHCII$^{flox/flox}$ and heterozygous Cx3Cr1^{CreERT2} mice that were then used for breeding. Cx3Cr1^{CreERT2}-MHCII$^{flox/flox}$ and MHCII$^{flox/flox}$ littermates were used for experiments. All animal procedures were performed following the institutional laboratory animal research guidelines and were approved by the governmental institutions (Regional Administrative Authority Karlsruhe, Germany). For experimental groups 6 to 16 weeks old mice were matched by age and sex.

3.3.2 Cell lines and modification of gene expression

The murine glioma cell line GL261 was purchased from the National Cancer Institute Tumor Repository. Adherent murine cell lines were cultured in DMEM supplemented with 10% FBS, 100 Units (U)/ ml Penicillin and 100 μg/ml Streptomycin at 37°C, 5% CO2 if not stated differently. HEK Phoenix Eco cells and HEK 293 T were also cultured in DMEM supplemented with 10% FBS, 100 Units (U)/ ml Penicillin and 100 μg/ml Streptomycin at 37°C, 5% CO2. U87 and Mewo cells were cultured in DMEM with FBS, Penicillin and Streptomycin as described above if not stated differently. U87 NLGN4X were generated by transfection with the NLGN4X protein in pMXs-IRES-PuroR using FuGene HD transfection reagent (Promega). Prior to transfection U87 cells were seeded at density of 100,000 cells per well in a six well plate and rested for 24 h. Cells were transfected with 2 μg of the respective plasmid DNA, rested for 48 h and then positively selected under application of 5 μg/ml Puromycin. U87 TMG were created by transfection with a tandem minigene containing the NLGN4X antigen sequence (section peptides) in pMXs-IRES-PuroR using FuGene HD transfection reagent (Promega) as described above. Primary glioblastoma cell lines were cultured in DMEM-F12 supplemented with B27 (Thermo-Fisher), 20 ng/ml epidermal growth factor, 20 ng/ml fibroblast growth factor (Thermo-Fisher) and 1% Penicillin/ Streptomycin (P/S) at 37°C, 5% CO2. PB-1 were transduced with a lentiviral vector encoding HLA-A*02 and selected using Puromycin at a concentration of 5 μg/ml. PB1 was provided by D.Hoffmann (German Cancer Research Centre). Jurkat TCR deficient T cells were cultured in RPMI-1640 supplemented with 10% FBS, 100 U/ml Penicillin, 100 μg/ml Streptomycin. Human T cells were cultured in Xvivo15 medium supplemented with 10% human serum, 100 U/ml Penicillin, 100 μg/ml Streptomycin and 2mM L-Glutamin (Thermo Fisher). For transduction and activation human T cells were incubated in complete T-Lymphozyte medium (CTL) containing 45% Click's medium, 45% RPMI medium and 10% fetal bovine serum supplemented with 10 ng/ml human IL-7 and 5 ng/ml human IL-15.
GL261-OVA cell lines were generated by transfection with OVA MHC I and II full length epitope, OVA MHC I and II minigene, OVA MHC I epitope, OVA MHC II epitope in pMXs-IRES-BsdR using FuGene HD transfection reagent (Promega). Prior to transfection GL261 cells were seeded at density of 100,000 cells per well in a six well plate and rested for 24 h. Cells were transfected with 2 μg of the respective plasmid DNA, rested for 48 h and then positively selected under application of 2μg/ml Blasticidin. The generated cell lines were evaluated functionally validated using in an overnight co-culture experiment using OT-1 reactive T cells from OT-1 transgenic mice. Expression of activation markers was assessed by flow cytometry and cytotoxicity assay as stated below.

U87 NLGN4X cells with overexpression of the NLGN4X antigen were generated as described previously using a pMXs-IRES-PuroR vector. After transfection cells were positively selected with 5 μg/ml Puromycin.

3.4 Assessment of NLGN4X expression in primary glioblastoma cell lines

Primary glioblastoma cell lines were cultured as described before and washed with ice-cold PBS. Afterwards, cells were resuspended in 1% β-mercaptoethanol (M3148-100ml, Sigma, part of Merck, Darmstadt, Germany)-supplemented RLT lysis buffer, integral part of the QIAGEN RNeasy Mini Kit (74004, Qiagen, Hilden, Germany). Lysate was homogenized with QiaShredder columns (79654, Qiagen, Hilden, Germany). RNA extraction was carried out with the QIAGEN RNeasy Mini Kit and all steps done according to the manufacturer´s instructions. On column, DNAse digestion was performed with the RNAse free DNAse set (79254, Qiagen, Hilden, Germany). RNA was eluted into RNAse-free water (4387936, ThermoFisherScientific, Waltham, Massachusetts, USA). Reverse transcription was performed according to the manufacturer´s recommendations using the High-Capacity cDNA Reverse Transcription Kit with RNase Inhibitor (4374967, Applied Biosciences Applied Biosciences, Foster City, California, USA) and 1 μg RNA per 20 μl reaction. For quantitative real-time PCR, Taqman Gene Expression Master Mix (4369016, ThermoFisherScientific, Waltham, Massachusetts, USA) and the respective TaqMan probes (Applied Biosystems, Foster City, California, USA) were used. The following probes were used: NLGN4X (Hs00535592-m1) and HPRT1 (Hs02800695-m1), GAPDH (Hs99999905-m1) and TBP (Hs99999910-m1) as housekeeping genes. All reactions were carried out in a 384-well reaction plate (4ti-0384/C, 4titude Ltd, Wotton, UK) covered with an optical adhesion film (4ti-0560, 4ti-tude Ltd, Wotton, UK). PCR reactions were checked by omission of templates in negative controls. Relative quantification of gene expression was determined by comparison of threshold values. All results were normalized to Bestkeeper (Pfaffl et al. 2004; PMID 15127793) as combined housekeeping genes.

3.4.1 Cloning of human transgenic and murine OVA reactive TCRs

To construct a lentiviral or retroviral vector containing a NLGN4X reactive TCR (Flu and Mart-1 TCRs were used either as positive or negative control TCRs), first the variable chains of the TCRs were synthesized by Eurofins and cloned into an *S/MAR vector* (*pSMARTer V5*) using the NEB Golden Gate assembly mix (New England Biolabs). The S/MAR vector contained the murine alpha and beta chains. This construct was used for electroporation. For generation of a lentiviral construct, the full length TCR was cloned into *pLEX307* (Addgene) via pDONR using the Gateway Cloning System (Thermo Fisher). For generation of a retroviral construct, human TCRs were cloned into a SFG (*addgene*) vector using In-Fusion cloning from Takara Bio Europe.

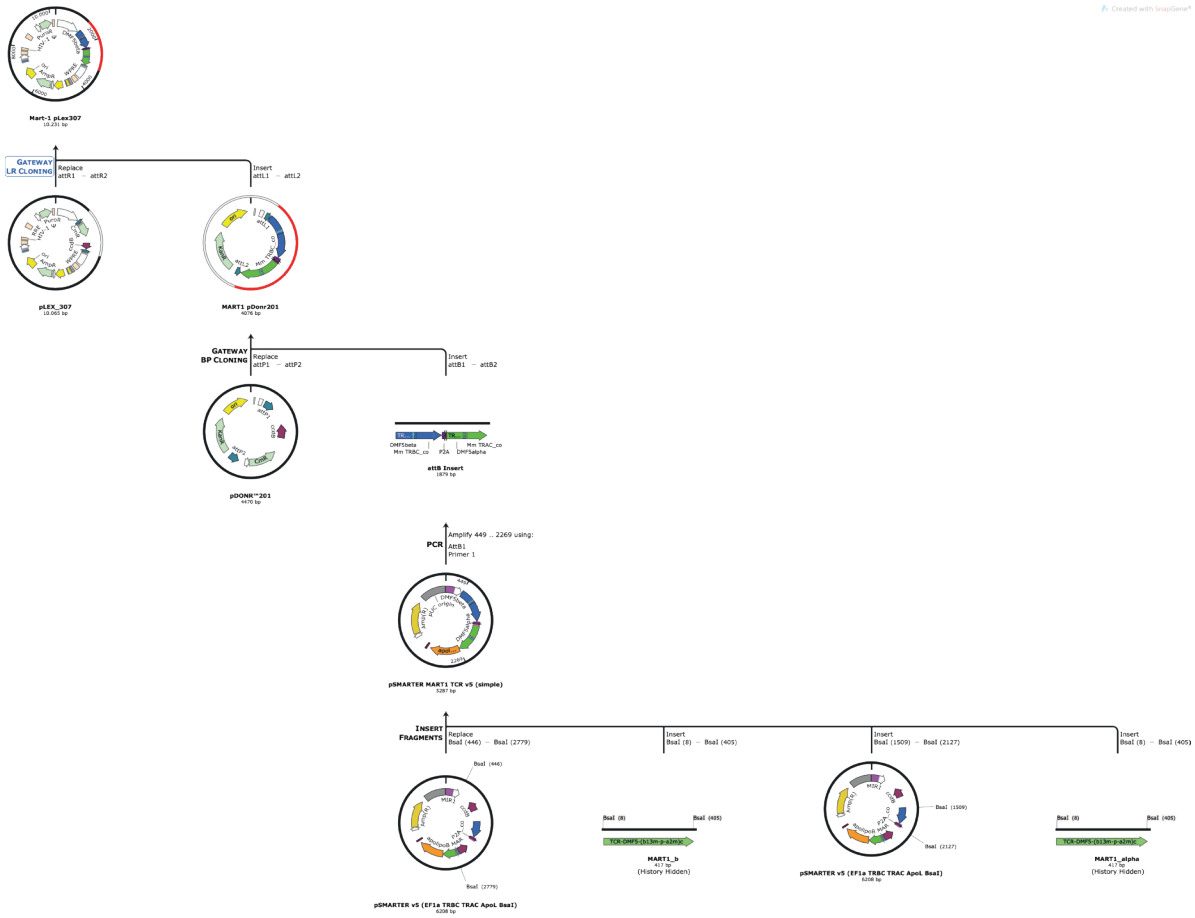

Figure 5: **Human plasmid maps**
The TCR variable chains were cloned into *pSMARTer V5* S/MAR vector. Using AttB PCR Att sites were added to the TCR sequence to enable gateway cloning. The TCR was then cloned into the destination Vector *pLEX307* using gateway cloning.

3.4.2 Isolation of Peripheral blood mononuclear cells (PBMCs)

Whole blood samples of healthy donors were obtained from the IKTZ Heidelberg and PBMCs were isolated by density gradient based centrifugation with Lympho-Paque solution (Genaxxon). Subsequently, obtained PBMCs were washed with PBS supplemented with 1 mM EDTA and finally frozen down for later downstream application.

3.4.3 Electroporation of Jurkat cells

2 Mio Jurkat CD8+ TCR deficient T cells cells per electroporation were used and 5 μg of each TCR and NFAT reporter encoding vectors were delivered (Neon electroporation system: settings: 1325 V, 3 pulses, 10 ms). After 24 h incubation TCR expression was determined by flow cytometric analysis of TCRbeta positive cells compared to untransduced T cells.

3.4.4 Viral Transduction of human T cells

pLEX307 lentiviral vector HEK 293 T cells were co-transfected with a TCR encoding lentiviral construct (pLEX307) if not stated differently and Ready-to-Use Lentiviral Packaging Plasmid Mix (Cellecta) using Fugene transfection reagent. Virus containing supernatant was harvested after 24 h, 48 h and 72 h. Human T cells were isolated andactivated in TexMACS Medium supplemented with human Interleukin 7 (0.2 IU/ml), human Interleukin 15 (290 IU/ml) and 10 μl per 1 million T cells human T Cell TransAct™ beads (Miltenyi). After 24 h T cells were washed and used for transduction. Upon transduction the lentiviral supernatant was added and spinloaded onto Retronectin coated 6 well-plates. Subsequently, up to 2 Mio. activated T cells/ well were transduced by spinoculation on virus loaded plates and incubated overnight and then subjected to a second transduction by spinoculation. TCR expression was assessed 24-48 h after the second transduction cycle.
For some experiments lentiviral supernatant was produced by the Core facility for Genomics and Proteomics (German Cancer Research Centre) and T cells were activated as above. After activation T cells were transduced by spinoculation and incubated for 48h prior to evaluation of TCR expression by flow cytometry.

SFG retroviral vector The SFG retroviral vector was a gift from Martin Pule (Addgene Nr. 22493) and the packaging plasmids RD-114 and PeqPam were kindly provided by Tim Sauer. In brief, T cells were directly activated after isolation from fresh peripheral blood mononuclear cells and activated for 48 h in CTL medium supplemented with 10 ng/ml hIL-7.5 ng/ml hIL-15 and Transact Beads (Miltenyi) according to manufacturer's instructions. HEK 293T cells were seeded at a density of 2.2 Mio cells per 10 cm dish and co-transfected with the TCR encoding SFG vector and RD-114 and PeqPam as helper plasmids using Fugene HD transfection reagent. Viral supernatant was harvested after 48 h, filtered and spinloaded onto Retronectin coated 24 well plates. Subsequently, viral supernatant was discarded and T cells were added in 1 ml of CTL medium and incubated for 4 days at 37°C, 5 % CO_2. TCR transduction efficiency was assessed by flowcytometric analysis of the GFP and TCRbeta expression in CD3+ T cells.

3.4.5 *in vitro* Expansion of human T cells

For expansion of human T cells the protocol for activation was used, cells were splitted every two days and fresh medium containing hIL-7 and hIL-15 was added.

3.4.6 Tumor cell inoculation

Murine tumor models 1 x 10^5 unmodified GL261 glioma cells or modified GL261 OVA cells were injected at a concentration of 50 x 10^6 cells per ml in 2 μl PBS into the right hemisphere of Cx3Cr1^{CreERT2}-MHCII$^{flox/flox}$, Ly5.1 or C57Bl/6J mice. The site of tumor cell injection was located 2 mm right lateral of the bregma and 1 mm anterior to the coronal suture and in 3 mm depth. 11 days after the operation tumor growth was assessed by weekly magnet resonance imaging if not stated differently.

Human tumor models Up to 1 x 10^6 unmodified or NLGN4X overexpressing U87 glioma cells or Mewo melanoma cells were resuspended in a solution of 100 μl Matrigel (Corning Life Science) and 100 μl PBS and 200 μl were injected into the right flank of NSG mice. For intracranial tumor experiments 1 x 10^5 U87 NLGN4X overexpressing expressing tumor cells were injected at a concentration of 50 x 10^6 cells per ml in 2 μl PBS into the right hemisphere 1 mm anterior to the coronal suture, 2 mm lateral to the bregma and in 3 mm depth. 15 days after the operation tumor growth was assessed by weekly magnet resonance imaging if not stated differently.

3.4.7 Intraventricular and intravenous adoptive transfer of human TCR transgenic T cells

Intravenous adoptive transfer NSG MHC I/II knockout mice received 1 Mio U87 NLGN4X overexpressing glioma cells in 200 μl of a 1:1 Matrigel and PBS solution as stated above. Prior to injection T cells were expanded for 7 days and transduction efficiency was assessed by flow cytometric analysis of murine constant TCRbeta chain positive T cells. On day 11 and day 17 and up to 3.5 Mio T cells in 200 μl were injected into the tail vene of tumor bearing mice. Tumor growth was monitored by investigator-blinded manual measurements every one to two days until the endpoint criterium of a maximum tumor diameter of 1 cm was reached.

Intraventricular adoptive transfer NSG MHC I/II knockout mice received 1 x 10^5 Mio U87 NLGN4X or U87 TMG glioma cells into the right hemisphere. Prior to injection T cells were expanded for up to 5 days and transduction efficiency was assessed by flow cytometric analysis of murine constant TCRbeta chain positive T cells. On day after randomization up to 5.0 Mio T cells were injected into the left ventricle at 0,5 mm lateral to the bregma and 2,2 mm depth. For all adoptive T cells transfers of human TCR transgenic T cells, recipient mice were treated with two i.p. injections of 50,000 IU hIL-2 on the day of and one day after the T cell injection.

3.4.8 *In vivo* antibodies

For immune checkpoint therapy 100 μg anti-CTLA-4 (9D9, BioXCell), 250 μg anti-PD-1 (RMP1-14, BioXCell) and 200 μg anti-PD-L1 (10 F.9G2, BioXCell) per mouse were administered by intraperitoneal (i.p.) injection in 200 μl PBS on days 13, 16, 19, 22 and 25 after tumor cell inoculation if not stated differently. Mice in the control group received equal amounts of the corresponding isotype controls for anti CTLA-4 MCP-11, for anti-PD-1 2A3 and for anti-PD-L1 LTF-2 by i.p. injection in 200 μl PBS at the same time points.

3.4.9 MRI imaging

MRI was carried out by the small animal imaging core facility at DKFZ using a Bruker BioSpec 3Tesla (Ettlingen, Germany) with ParaVision software 360 V1.1 or at the Radiology Department, University Clinic Heidelberg using a BioSpec 94/20 USR, Bruker

BioSpin GmbH. For imaging, mice were anesthetized with 3.5% sevoflurane in air. For lesion detection, T2 weighted imaging was performed using a T2 TurboRARE sequence: TE = 48 ms, TR = 3350 ms, FOV 20x20 mm, slice thickness 1,0mm, averages = 3, Scan Time 3m21s, echo spacing 12 ms, rare factor 8, slices 20, image size 192x192. Tumor volume was determined by manual segmentation using Bruker ParaVision software 6.0.1.

3.4.10 Survival Experiments

Murine Tumor Models $Cx3Cr1^{CreERT2}$-$MHCII^{flox/flox}$ mice with conditional deletion of MHC class II in all myeloid cells were challenged with injection of 1 x 10^5 GL261 glioma cells into the right hemisphere and tumor growth was assessed by magnet resonance imaging at days 13, 18, 25 and 28. Mice were randomized to receive either triple immune checkpoint blockade with anti-CTLA-4, anti-PD-1 and anti-PD-L1 or the corresponding isotype controls on day 13 after the first MRI according to equal tumor volume means among the different groups. $Cx3Cr1^{CreERT2}$-$MHCII^{flox/flox}$ mice with genetic deletion of MHC class II in microglia cells were equally challenged with 1 x 10^5 GL261 glioma cells into the right hemisphere. Tumor growth was assessed by MRI on days 12, 18 and 26. Mice received equivalent treatment as above on days 12, 15, 18, 21 and 24.

Human Tumor models For subcutaneous experiments NSG MHCI/II Knockout mice were challenged with 1 x 10^6 U87 NLGN4X glioma cells into the right flank and tumor growth was assessed by daily observer blinded measurements of the tumor starting at days 10. Mice were randomized to receive either NLGN4X TCR transgenic T cells or Mock transduced T cells or no cellular treatment. After intravenous adoptive transfer tumor growth was measured daily and mice were checked for any stop criteria frequently as stated above.
For intracranial experiments NSG MHCI/II knockout mice were challenged with injection of 1 x 10^5 U87 NLGN4X glioma cells or U87 TMG cells into the right hemisphere and tumor growth was assessed by magnet resonance imaging at days. Mice were randomized to receive a intraventricular adoptive transfer of either NLGN4X TCR transgenic T cells or negative control T cells (Flu TCR transgenic T cells or Mock transduced T cells) or no treatment.
For all intracranial animal experiments mice were checked daily for tumor-related symptoms or extracranial tumor growth and sacrificed if tumor burden or stop criteria were met or if the animals depicted neurological symptoms.

3.4.11 Processing of spleen, peripheral lymph nodes and tumor tissue

Spleens and peripheral lymph nodes were excised and meshed twice through a 70 μm cell strainer to generate a single cell suspension. Erythrocytes were lysed using ACK Lysis buffer containing 150mM NH_4Cl, 10 mM $KHCO_3$ and 100 μM Na_2EDTA. For processing of tumor tissue from GL261 glioma bearing mice the latter were cardially perfused under deep anesthesia. The right hemisphere was removed and mechanically dissected and subsequently digested in HBSS (Sigma Aldrich) supplemented with 50 μg per ml liberase under continuous rotation for 30 minutes at 37°C. Obtained tissue was meshed through a

100 μm and 70 μm cell strainer and cells were purified by density-gradient centrifugation with Percoll (GE Healthcare).

3.4.12 Immunofluorescence Staining

Brain tumor sections of murine gliomas After transcardial perfusion with PBS brains were embedded in Tissue-Tek and stored at -80°C prior to dissection. Cryosections were airdried for 15 minutes at room temperature and subsequently fixed with ice-cooled methanol for 10 minutes. After fixation slides were washed and permeabilized with PBS supplemented with 0.1 % Tween and unspecific binding was abolished by blocking with 4 % normal goat serum (NGS, Cell Signaling Technology) in 0.1 % Tween + PBS for 1h at room temperature. For IF staining using human anti-CD3, rat anti-mouse CD4, rat anti-mouse CD8a and FITC rat anti-mouse ICAM antibodies slides were blocked and stained with 5 % NGS + 0.1 % Tween + PBS instead. Primary antibodies were incubated overnight at 4°C at a dilution of 2.5 μg/ml for rat anti-mouse MHC II at a dilution of 1:150 and 1:250, for rabbit anti-mouse IBA-1 (Abcam), 1:300 for rabbit anti-human CD3 (GeneTex), 10 μg/ml for rat anti-mouse CD4 (ThermoFisher), 2.5 μg/ml for rat anti-mouse CD8a (ThermoFisher) if not stated differently, 2.5 μg/ml rabbit anti-mouse CD11b (Novus Biologicals), 1:200, 1:500 and 1:1000 for rabbit anti-mouse GFAP (Abcam). The following secondary antibodies were used with the described dilutions in blocking serum dilution for 1 hour at room temperature: Alexa Fluor 488 labeled goat anti-rat at 10 μg/ml and 4 μg/ml, Alexa Fluor 633 labeled goat anti-rat at 10 μg/ml, Alexa Fluor 633 labeled goat anti-rabbit at 10 μg/ml (Invitrogen). For subsequent staining with fluorochrome conjugated antibodies slides were washed as previously described and then incubated with FITC-conjugated rat anti-mouse F4/80 (BM8, BioLegend) at a dilution of 2.5 μg/ml, FITC-conjugated rat anti-mouse ICAM (YN1/1.7.4, BioLegend) at 5 μg/ml, APC-conjugated rat anti-mouse CD31 (MEC13.3, BD Bioscience) at 2 μg/ml for 2 h at 4°C. Finally, cryoslides were preserved with Vectashield HardSetMounting Medium with DAPI for counterstaining of nuclei. Widefield images were taken using Zeiss CellObserver with color and greyscale CCD cameras AxioCAM MRm/MRc. For confocal microscopy Zeiss LSM 700 was used. Images were processed and analyzed with Fiji software.

Immunofluorescence staining sections of human tumors and tumor cells After preparation of the cryosections as described above the following primary antibody conjugated to a fluorochrome was added at a dilution of 1:100: FITC-conjugated mouse anti-human CD3 (UCHT1, BioLegend) and incubated for 2 h at 4°C. Finally slides were preserved with Vectashield HardSetMounting Medium with DAPI for counterstaining of nuclei.

3.4.13 Flow cytometry

For intracellular staining cells were incubated with 5 μg per ml Brefeldin A (Sigma-Aldrich) for 5 h at 37°C, 5 % CO_2 to allow intracellular enrichment of targeted proteins. Primary murine cells were blocked with rat anti-mouse CD16/32 (clone 93, 1:100, eBioscience) and subsequently stained with the respective antibodies in PBS for 30 minutes

at 4°C for extracellular markers. For human T cells PBS supplemented with 10 % human serum was used for blocking and cells were subsequently stained as above. For intracellular staining of cytokines cells were fixed and permeabilized using IC fixation buffer and IC permeabilization buffer, respectively (both eBioscience) and then stained with the relevant dyes for 45 minutes at 4°C.
For analysis of MHC II expression on different immune cell subsets in GL261 glioma bearing Cx3Cr1^{CreERT2}-MHCII$^{flox/flox}$ mice cells were blocked, permeabilized and fixed as above and stained with eFluor780 conjugated fixable viability dye (1:1000 eBioscience), Brilliant Violet (BV) 510- conjugated rat anti-mouse CD45 (clone 30-F11, 1:150, BioLegend), AlexaFluor 700- conjugated rat anti-mouse MHC II (clone M5.114.15.2, 1:100, BioLegend), PE-Dazzle-conjugated rat anti-mouse CD11b (clone M1/70, 1:100, BioLegend), BV421-conjugated rat anti-mouse F4/80 (clone BM8, 1:100, BioLegend), PE-conjugated rat anti-mouse TGFß (clone TW7-16B4, 1:100 BioLegend), BV605-conjugated rat anti-mouse CD19 (clone 6D5, 1:100 BioLegend), BV711-conjugated rat anti-mouse PD-L1 (clone 10F.9G2, 1:100, BioLegend), FITC-conjugated rat anti-mouse Nk1.1 (clone PK136, 1:100, BioLegend), APC-conjugated rat anti-mouse Ly6C (clone HK1.4, 1:100 BioLegend), PE-Cy7-conjugated rat anti-mouse CD4 (clone GK1.5, 1:100, ThermoFisher) and PerCp-Cy5.5-conjugated rat anti-mouse CD80 (clone 16-10A1, 1:100, BioLegend). For analysis of the T cell compartment of the same GL261 glioma bearing mice cells were stained with eFluor780 conjugated fixable viability dye (1:1000 eBioscience), Brilliant Violet (BV) 510- conjugated rat anti-mouse CD45 (clone 30-F11, 1:150, BioLegend), PE-TexasRed-conjugated rat anti-mouse CD4 (clone RM4-5, 1:150, ThermoFisher), BV421-conjugated rat anti-mouse Tim3 (clone RMT3-23, 1:100, BioLegend), AlexaFluor 700-conjugated rat anti-mouse CD8 (clone 53-6.7, 1:100, BioLegend), APC-conjugated rat anti-mouse FoxP3 (clone FJK-16s, 1:100, ThermoFisher), PerCP-Cy5.5-conjugated rat anti-mouse PD-1 (clone J43, 1:100, ThermoFisher), BV711-conjugated rat anti-mouse CD3 (clone 17-A2, 1:100, BioLegend), FITC-conjugated rat anti-mouse Nk1.1 (clone PK136, 1:100, BioLegend), PE-Cy7 conjugated rat anti-mouse CD25 (clone PC61, 1:100, BioLegend), BV605-conjugated rat anti-mouse Ki67 (clone 16A8, 1:100, BioLegend) and PE-conjugated rat anti-mouse TCF1 (clone 7F11A10, 1:100, BioLegend). For analysis of tumoral MHC class II expression tumor cells and tumor infiltrating leucocytes were blocked and extracellular staining was performed with eFluor780 conjugated fixable viability dye (1:1000 eBioscience), Brilliant Violet (BV) 510-conjugated rat anti-mouse CD45 (clone 30-F11, 1:150, BioLegend), PE-Cy7-conjugated rat anti-mouse CD11b (clone M1/70, 1:100, BioLegend), APC-conjugated rat anti-mouse Ly6C (clone HK1.4, 1:100, Biolegend), perCP-Cy5.5-conjugated rat anti-mouse CD4 (clone RM4-5, 1:100, BioLegend), AlexaFluor 700- conjugated rat anti-mouse MHC II (clone M5.114.15.2, 1:100, BioLegend), BV421-conjugated rat anti-mouse F4/80 (clone BM8, 1:100, BioLegend), PE-conjugated rat anti-mouse CD11c (clone N418, 1:100, BioLegend) and tumor cells were detected in the FITC channel based on GFP expression.
TILs from GL261 OVA Full bearing Cx3cr1CreER-MHCII flox mice were stimulated with either SIINFEKL (MHC class I), the respective MHC class II or MOG peptide and Brefeldin A as above for 5 h at 37°C, 5 % CO_2 and then blocked, fixed and permeabilized as above and stained with eFluor780 conjugated fixable viability dye (1:1000 eBioscience), Brilliant Violet (BV) 510- conjugated rat anti-mouse CD45 (clone 30-F11, 1:150,

BioLegend), FITC-conjugated rat anti-mouse CD3 (clone 17A2, 1:150, BioLegend), perCP-Cy5.5-conjugated rat anti-mouse CD8 (clone 53-6.7, 1:100, BioLegend), PE-Cy7-conjugated rat anti-mouse PD-1 (clone RMP1-30, 1:100 BioLegend), APC-conjugated rat anti-mouse CD4 (clone RM4-5, 1:100, BioLegend), PE-conjugated rat anti-mouse IFN-gamma (clone XMG1.2, 1:100 ThermoFisher) and BV421-conjugated rat anti-mouse TNF-alpha (clone MP6-XT22, 1:100, ThermoFisher).
For evaluation of GL261 OVA cell lines T cells were blocked, fixed and permeabilized as above after 48 h of co-culture and 5 h stimulation with Brefeldin A at 5μg per ml and stained as follows: eFluor780 conjugated fixable viability dye (1:1000 eBioscience), Brilliant Violet (BV) 510- conjugated rat anti-mouse CD45 (clone 30-F11, 1:150, BioLegend), FITC-conjugated rat anti-mouse CD3 (clone 17A2, 1:150, BioLegend), perCP-Cy5.5-conjugated rat anti-mouse CD8 (clone 53-6.7, 1:100, BioLegend), PE-conjugated rat anti-mouse IFN-gamma (clone XMG1.2, 1:100 ThermoFisher) and BV421-conjugated rat anti-mouse TNF-alpha (clone MP6-XT22, 1:100, ThermoFisher).
For analysis of human T cells the latter were blocked in PBS supplemented with 10 % human serum and stained subsequently with eFluor780 conjugated fixable viability dye (1:1000 eBioscience), Brilliant Violet (BV) 510- conjugated mouse anti human CD3 (clone UCHT1, 1:50, BD Horizon), PE-conjugated Armenian Hamster anti-mouse TCR ß chain (clone H57-597, 1:50, BioLegend), PE-Cy7-conjugated mouse anti-human CD8a (clone SK1, 1:50, BioLegend), FITC or PerCP-Cy5.5 conjugated mouse anti-human Granzyme B (GB11, 1:50, BioLegend), BV421-conjugated mouse anti-human IFN-y (clone 4S.B3, 1:50, BioLegend), APC-conjugated mouse anti-human TNF alpha (clone MPG6-XT22, 1:50, BioLegend), PerCP-eFluor 710 conjugated mouse anti-human Perforin (clone dG9, 1:50, ThermoFisher). For HLA analysis of human PBMCs cells were blocked and stained as above using eFluor780 conjugated fixable viability dye (1:1000 eBioscience), Brilliant Violet (BV) 510- conjugated mouse anti human CD3 (clone UCHT1, 1:50, BD Horizon), PerCP-Cy5.5-conjugated mouse anti-human CD8a (clone SK1, 1:50, BioLegend) and APC-conjugated mouse anti-human HLA-A2 (clone BB7.2, 1:50, BioLegend). For phenotypic analysis human T cells were analyzed with the following antibodies as described above: eFluor780 conjugated fixable viability dye (1:1000 eBioscience), SuperBright702-conjugated anti-human-CD3 (1:50, comp. Table antibodies), AlexaFluor 700-conjugated anti-human-CD8 (1:50, comp. Table antibodies), PE-Dazzle-conjugated anti human CD45RA (1:50, comp. Table antibodies), BV605-conjugated anti-human CD45RO (1:50, comp. Table antibodies), BV510-conjugated anti-human CCR7 (1:50, comp. Table antibodies), PE-conjugated anti-mouse TCR ß chain (1:50, comp. Table antibodies), PE-Cy7-conjugated anti-human PD-1 (1:50, comp. Table antibodies), BV421-conjugated anti-human Tim3 (1:50, comp. Table antibodies), perCp-Cy5.5 conjugated anti-human Lag-3 (1:50, comp. Table antibodies) and APC-conjugated anti-human CX3CR1 (1:50, comp. Table antibodies).

3.4.14 T cell activation assays

NFAT reporter based activations assays Jurkat TCR deficient T cells were equipped with the respective TCR and NFAT reporter by electroporation as indicated previously. Healthy donor derived PBMCs, U87 glioma cells or K562 leukemia cells at a density of 3

Mio cells/ml were peptide pulsed for 1 hour or overnight at a final peptide concentration of 10 μg/ml in 96 well plates. After confirmation of TCR expression Jurkat cells at a density of 3 Mio cells/ml were cocultured with peptide loaded antigen presenting cells for 5 h. Subsequently, Nano-Glo Luciferase assay reagents (Promega) were diluted according to the manufacturer's instruction and added to the coculture. Luminescence was recorded on a PHERAstar FS plate reader and analysed using MARS Data analysis software (BMG Labtech).

Human T cell activation assays T cells were isolated and activated as above and the respective TCRs were delivered by lentiviral transduction. After 48 h TCR surface presence was evaluated by flow cytometric analysis of the expression of the mouse TCRbeta constant region. After confirmation of TCR surface expression T cells were used for in vitro T cell activation and cytotoxicity assays using NLGN4X peptide loaded U87 glioma cells and NLGN4X overexpressing U87 glioma cells as target cells and incubated overnight. For assays using PB1 glioma cells the latter were irradiated at Subsequently, cytotoxicity was measured using a CytoTox 96® Non-Radioactive Cytotoxicity Assay (Promega) and T cells were stained extra- and intracellularly for flow cytometric analysis of Perforin, TNF-alpha, IFN-y and Granzyme B expression. For PB-1 glioma cells, cells were resuspended at a concentration of 1 x 10^6 cells/ml, irradiated at 5 Gy and stimulated with human Interferon-γ (Peprotech) at a concentration of 300 IU/ml.

3.4.15 Murine cytotoxicity assays

T cells were cocultured with target cells expressing their corresponding epitope or peptide loaded antigen presenting cells and with unmodified target cell lines as a control at serial dilutions of the effector cells or at equal numbers of 2 x 104 cells per well in a 96 well plate if not stated differently

3.4.16 LDH release assay

After 12-36 h of co-culture a LDH maximum release control of target cells was generated by incubation with 10 X Lysis solution (Promega) according to manufacture's instructions. After centrifugation 50 μl of the supernatant were used and incubated with CytoTox 96 Reagent (Promega) for 30 minutes in the dark at room temperature. Absorbance at 490 nm was recorded. Minimum LDH release of T cells and Target cells and media background signal were measured for subsequent analysis. For TCR transgenic T cells GFP-IRES-GFP transduced T cells were used to control for unspecific TCR stimulation. All values were corrected for cell culture medium background and cytotoxicity was calculated as follows if not stated differently:

$$\%\text{cytotoxcitiy} = \frac{\text{Experimental} - \text{effector spontaneous} - \text{target spontaneous}}{\text{target maximum} - \text{target spontaneous}} \quad (1)$$

3.4.17 Vital-FR cytotoxicity assay and FACS-based cytotoxicity assays

T cell receptor transduced human T cells were used on day 4 after transduction and co-cultured overnight at different effector to target cell ratios with different target cell lines previously labeled with CellTrace reagents according to manufacturer's instructions at a dilution of 1:5,000. If peptide loaded target cells were used antigen presenting cells were peptide pulsed at indicated peptide dilution for 1 hour at 37°C, 5 % CO_2 prior to the assay. After overnight coculture plates were centrifuged and resuspended in PBS. T cells were discarded and 30 μl Trypsin per well was added and after 10 min tumor cells were resuspended and subjected to extracellular FACS staining using eFluor780 conjugated fixable viability dye (1:1000 eBioscience) and PE-conjugated anti-human CD3 (1:100, BioLegend) for negative selection of tumor cells. 123 Counting beads were added in 50μl at a 1:5 dilution.
Cytotoxicity was calculated using normalized count of tumor cells. % cyotoxicity was calculated as the quotient of live tumor cells after T cell co-culture to either a tumor cell only or unloaded tumor cell control.

3.5 Statistical analysis

All results were analyzed with Prism version 9.4.0. Used statistical tests are indicated in the respective figure legends. Results were considered as siginificant if the p value was below 0.05.

4 Results

4.1 Development of an adoptive transfer with NLGN4X reactive TCR engineered T cells

The first part of this thesis aims at developing a preclinical model using an adoptive transfer of T cell receptor engineered T cells targeting the NLGN4X antigen that was found to be overexpressed in human glioblastomas and potent to induce a response of peripheral lymphocytes in a small cohort of patients. [Hilf et al., 2019]
Based on these results a reactive T cell receptor was identified and assessed for its *in vitro* reactivity and therapeutic potential in an immunodeficient mouse model.

4.1.1 NFAT reporter assay enables sensitive detection of transgene T-cell-receptor restricted activation

First, I developed an assay to specifically detect recognition of the target protein by the transgene TCR. Therefore, two different assays using either flow cytometry or a Luciferase-based approach were tested. The melanoma antigen recognized by T cells 1 (MART1) specific T cell receptor was utilized as a positive control and peptide specific activation of TCR expressing Jurkat cells was assessed wa assessed. The NanoGlo Luciferase Assay is based on the co-transfection of Jurkat cells with an NFAT reporter consisting of a luciferase under the control of a promoter responsive to the transcription factor Nuclear factor of activated T cells (NFAT). During the TCR-related activation with upregulation of NFAT, the luciferase gene is transcribed and enables detection of activation. Analysis methods were compared for sensitivity and specificity to detect peptide specific activation of TCR transfected Jurkat cells.
Assessment of T cell receptor functionality by flow cytometric analysis of TCR expressing Jurkat cells was hampered by low levels of IFN-γ and TNF-α production in Jurkat cells. Maximum stimulation using para-Methoxyamphetamine (PMA) and Ionomycin resulted in 11,5 % IFN-γ and 3,33 % TNF-α positive Jurkat cells and no reaction to CD3 and CD28 based TCR stimulation was observed. Only limited antigen specific reactions were detected in response to MART 1 peptide in flow cytometric analysis of Jurkat T cells.
Secondly, the NanoGlo Luciferase Assay was assessed for evaluation of TCR-target binding. In order to determine optimal conditions for the testing of the previously described T cell receptors by the means of the NanoGlo Luciferase Assay, I compared different durations of peptide loading of the antigen presenting cells. Furthermore, I evaluated the suitability of a NFAT reporter with and without a Luciferase degradation sequence. I hypothesized that degradation of the Luciferase would decrease the sensitivity to detect a T cell receptor with suboptimal activation but also decrease the background signals which normally occur due to unspecific stimulation.
Jurkat cells transfected with a NFAT Reporter lacking the Luciferase degradation domain (NFATstable) showed log 10 higher RLU (relative luminescence units) signal in response to stimulation of MART 1 TCR by the respective TCRs compared to the NFAT reporter with a Luciferase degradation domain (NFATpest) against peptide loaded HLA-A2 PBMCs (comp. Fig. 6c). However, NFATpest co-transfected MART1 TCR positive Jurkats showed

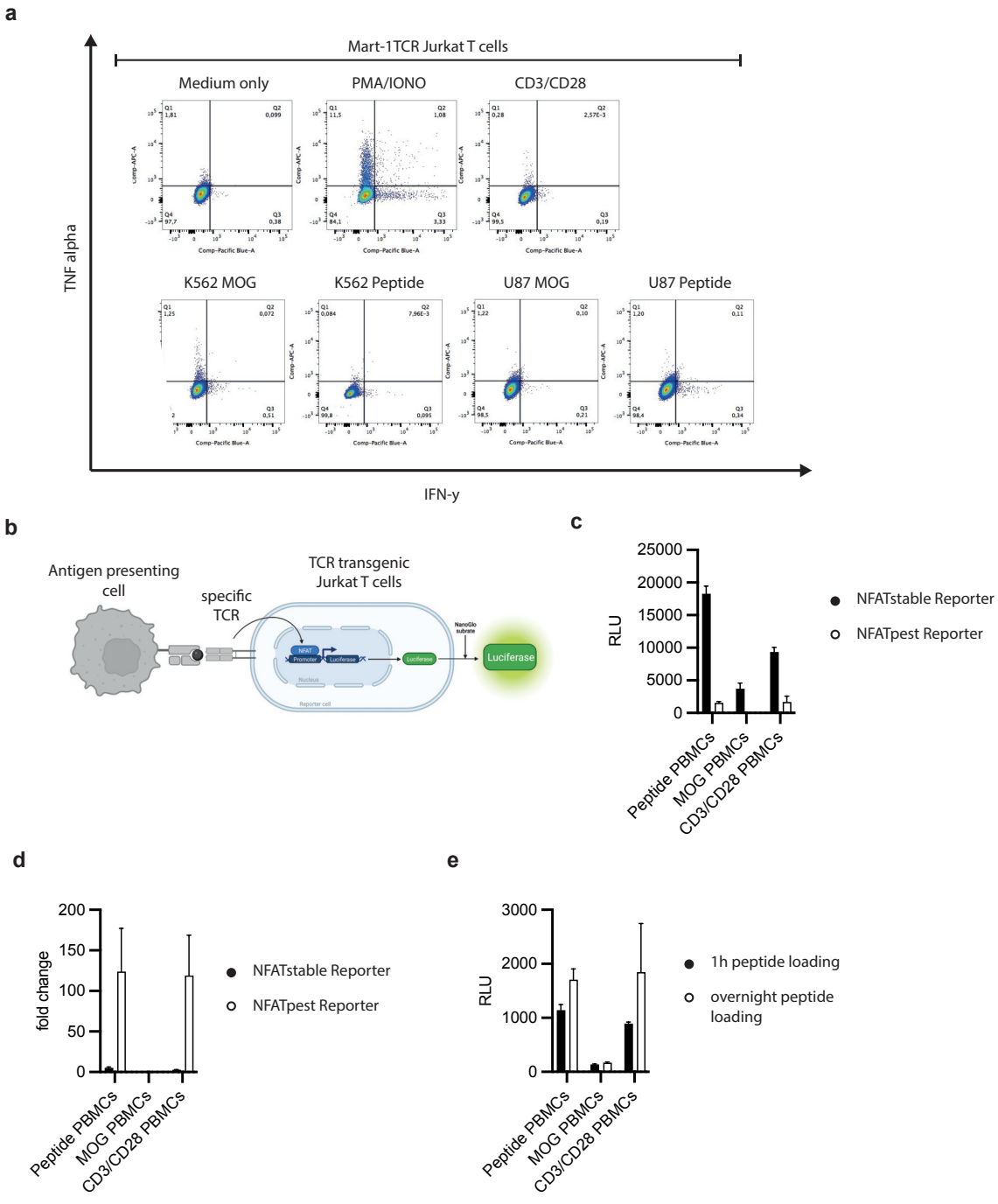

Figure 6: *Continued on next page.*

Figure 6: **The NFAT reporter assay enables detection of transgene TCR restricted activation of Jurkat T cells *in vitro***
a Flow cytometric analysis of an overnight co-culture of peptide loaded antigen presenting cells (K562 HLA-A2+ cells and U87 glioma cells) and MART1 transfected Jurkats. PMA/IONO and CD3/CD28 served as positive controls, medium only as a negative control. APCs were either loaded with irrelevant MOG Peptide or a MART-1 peptide. **b** Schematic overview of Nano-Glo Luciferase based Jurkat T cell assays. **c** NFAT Nano-Glo Luciferase assay of MART1 TCR and either NFAT with (NFATpest) or without (NFATstable) Luciferase degradation domain (PEST domain) co-transfected into TCR deficient Jurkat cells. Absolute RLU and **d** Fold change against HLA-A2+ human PBMCs **e** Comparison of overnight loading of PBMCs vs. 1 h of peptide loading for MART1 transfected CD8 positive Jurkats. *For all samples: n=3 technical replicates, Mean with SEM*

a log2 higher fold change of peptide driven signal compared to unspecific stimulation by an irrelevant MOG peptide (comp. Fig. 6d). For subsequent validation of the NLGN4X TCR the NFATpest reporter was used. There was no difference if cells were pulsed with the respective peptides overnight in contrast to only one hour of peptide stimulation (comp. Fig. 6e).

4.1.2 A monoclonal TCR directed against the NLGN4X epitope is specifically reactive against its target epitope

As previously described [Hilf et al., 2019] patient individual vaccines directed against overexpressed tumor antigens with a high likelihood for binding to the patient's HLA immunopeptidomes resulted in vaccine driven expansion of antigen-specific CD8 T cell responses. NLGN4X transfected healthy donor PBMCs have been shown to be reactive against a target antigen expressing tumor cell line, but further characterization regarding specific activation and cytotoxicity *in vitro* is required. Additionally, there is yet no evidence regarding in vivo reactivity of NLGN4X directed T cells.
Briefly, TCR sequences identified in patients after personalized vaccination with patient individual tumor antigens [Hilf et al., 2019] were used to construct TCR transgenic T cells for subsequent *in vitro* testing of tumor antigen specific activation and lysis of target cells. Finally, the potential of NLGN4X TCR engineered T cells to hamper tumor growth of an antigen overexpressing human glioma cell line in an immunodeficient mouse model with an additional knock-out in murine MHC molecules was evaluated.
First TCGA analysis of the Neuroligin 4, X-linked expression in human healthy brain and Glioblastoma multiforme was performed confirming that NLGN4X is overexpressed in this human brain malignancy. (comp. Fig. 7 a) TCR CDR3 sequences obtained from single cell TCR sequencing of multimer sorted T cells after vaccination in the context of the GAPVAC study ([Hilf et al., 2019]) showed a monoclonal T cell population (comp. Fig. 7 b), as the top clone made up more then 90 % of all sequencend barcodes. TCR sequences of the top 4 clones were then cloned into a pSMARter S/MAR vector (scaffold matrix attachment region) with the advantage of lower immunogenicity compared to viral vectors. First, TCR containing plasmids were used for transfection of TCR deficient CD8a and CD8b positive Jurkat cells to verify recognition of the target peptide sequence by the T cell

receptor. The S/MAR vector encoding for the T cell receptor comprises a murine sequence allowing the detection of transfected T cell receptors by a specific antibody directed against the murine TCR beta constant chain. Transfection efficiency of the T cell receptor was evaluated prior to co-culture by flow cytometric analysis. NLGN4X reactive TCRs depicted stable expression of approximately 35 % and thus showed a similar transfection efficiency as the MART 1 TCR as a positive control. Mock transfected Jurkats were used a negative control for efficiency assessment (comp. Fig. 7 h)
Four TCR sequences were identified from TCR sequencing results after GAPVAC vaccination. In order to assess the functional TCR binding of the top 4 clones NLGN4X frequent types (ft) 1-4 TCR transfected Jurkats were cocultured with BOLETH presenter cells and CD69 expression was assesed by flow cytometry revealing no reacitivity of ft 2-4 but showing highly specific reactivity against the NLGN4X epitope by the NLGN4X ft1 TCR (comp. Fig. 7 c, *Assay performed by Tamara Borschert, DKFZ Department of Neuroimmunology*).
The NLGN4X ft1 TCR was subsequently tested against different presenter cell lines. NLGN4X TCR transgenic Jurkats showed specific activation in an NFAT-NanoGlo Luciferase Assay in response to the relevant peptide presented on HLA-A2 matched PBMCs as well as on U87 glioma cells (comp. Fig. 7 d,e). Thus, the NLGN4X ft1 TCR proved to specifically recognize the NLGN4X epitope presented on different cell lines in two different Jurkat based activation assays. Therefore this TCR was used for further testing of reactivity and therapeutic potential.

4.1.3 Development of efficient gene delivery of the NLGN4X TCR to human T cells

For downstream application of the NLGN4X TCR different vector systems were evaluated for their efficiency to deliver the T cell receptor to primary human T cells. Therefore different GFP expresssing lentiviral vectors using different promotors and two retroviral vectors were used for transduction of human T cells and GFP expression was assessed by flow cytometry. Transduction with either the retroviral *SFG-IRES-GFP* vector or the lentiviral *pLEX307* vector under the EF-1 alpha promoter resulted in the highest median fluorescence intensity of GFP (comp. Fig. 8 a-d). Consequently, the *pLEX307 EF1-alpha* vector and the *SFG-IRES-GFP* vector were used for further evaluation of the expression of the transgene TCR. For first *in vitro* and *in vivo* application the *pLEX307 EF1-alpha* vector was applied. The *SFG-IRES-GFP* vector is currently in use in a clinical trial for manufacturing of CD19-CAR T cells [Schmitt, 2018]. Transduction of human T cells with both TCR constructs encoding the NLGN4X TCR resulted in robustly detecable TCR surface expression as illustrated by flow cytometric detection of the murine TCRbeta constant chain (comp. Fig. 8 e). However, only transduction with the *NLGN4X-SFG-IRES-GFP* vector resulted in highly efficient gene delivery with up to 90 % TCRbeta positive T cells.
For TCR transduction a T cell product containing both CD4 and CD8 T cells was used. TCR transduced T cells were then subjected to repetitive FACS multicolour assessment of typical phenotypic T cell markers over time during *in vitro* expansion (comp. Fig. 8 f). Up to three different donors with two different TCRs (NLGN4X and Mart-1) were assessed on

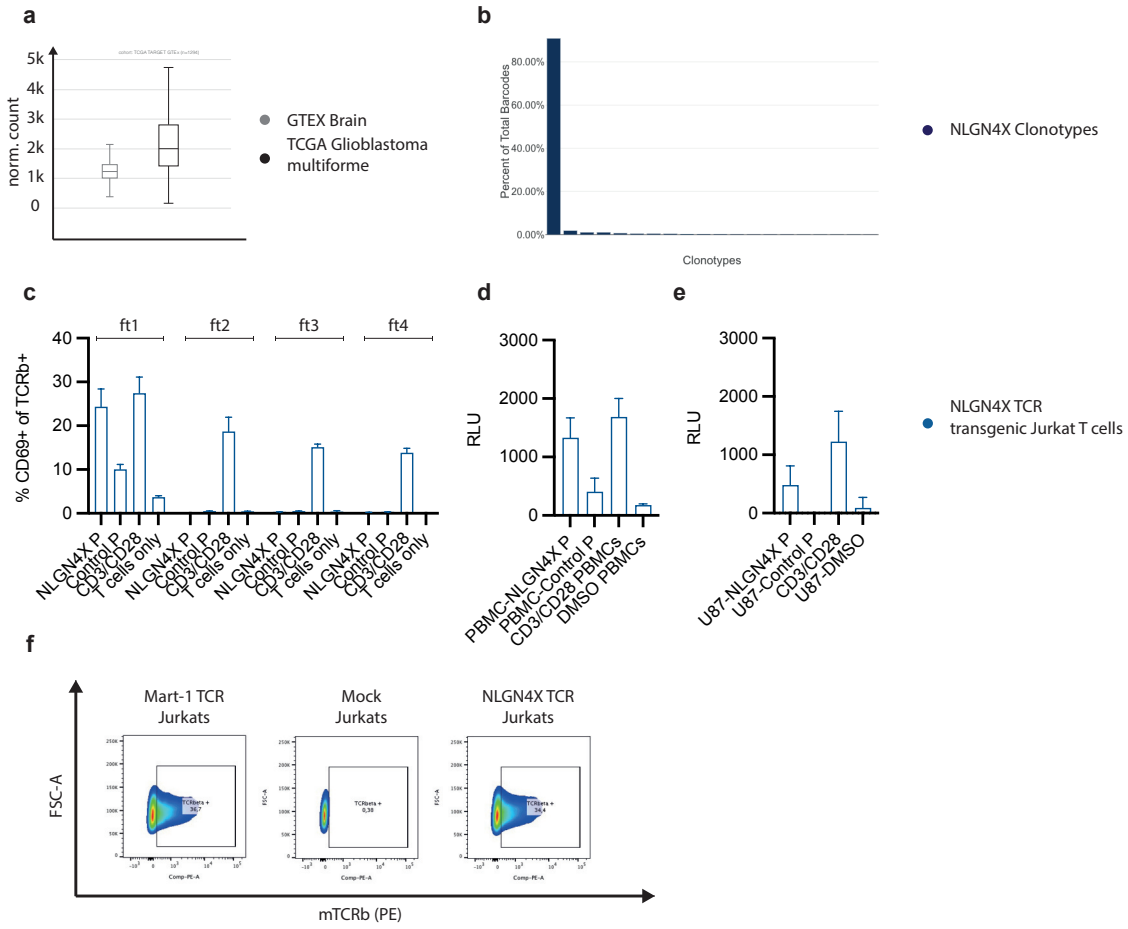

Figure 7: *Continued on next page.*

Figure 7: **NLGN4X ft1 TCR shows specific and consistent activation patterns against different peptide loaded presenter cells**

a TCGA analysis of NLGN4X expression in TCGA datasets of human glioblastoma multiforme samples compared to healthy brain. *Normalized counts shown* **b** Frequencies of CDR3 sequences of different clonotypes obtained by TCR single cell sequencing (*data from GAPVAC consortium, [Hilf et al., 2019]*) **c** Flow cytometric analysis of CD69 expression of Jurkats transfected with the frequent types 1-4 (ft1-4) of the NLGN4X TCR and cocultured with BOLETH antigen presenting cells loaded with either the NLGN4X peptide or a control peptide (*n=3 technical replicates, Mean with SEM, experiment performed by Tamara Borschert.* **d** and **e** NFAT assay of NLGN4X ft1 TCR transgenic Jurkats against HLA-A2 matched PBMCs (**d**) and U87 glioma cells (**e**) *n=3 technical replicates, Mean with SEM, RLU = Relative luminescence units* **f** Exemplary FACS plots of TCRbeta expression on transfected Jurkats cells.

day 0, 4, 11, 17 and 24 of culture. T cells showed stable and high expression of CD45RA and CCR7 confirming a central memory like phenotype. In line with this expression of CD45RO and of the exhaustion markers Lag-3, Tim-3 and PD-1 was low. CX3CR1 a marker for CD8 effector cells increased over time. Thus, gene delivery with a retroviral SFG vector resulted in highly efficient gene transfer and the manufacturing and expansion process resulted in a T cell product that matches the previously described favourable central memory like phenotype. [Vitanza et al., 2021].

4.1.4 NLGN4X-TCR-T show reactivity against different glioma cell lines in vitro

I then aimed to assess functionality of $NLGN4X_{131\text{-}139}$-specific TCR-expressing primary human T cells in vitro using flow cytometric profiling following co-culture with exogenously peptide-loaded non-adherent HLA-A*02^+ K562 leukemia cells. As most relevant effector proteins, Granzyme-B (GrzB), interferon-γ (IFN-γ), and tumor necrosis factor-α (TNF-α) production was assessed. Independent of healthy T cell donors, I found robust expression of the highly cytotoxic cytokines TNF-α and GrzB by $NLGN4X_{131\text{-}139}$-specific TCR-expressing T cells (comp. Fig. 9 a). Strikingly, when benchmarking $NLGN4X_{131\text{-}139}$-specific TCR-expressing primary human T cells with the well-established high-affinity melanoma antigen recognized by T cells 1 (MART-1)-specific TCR that has been used for phase I and II clinical trials [Morgan et al., 2006] I observed similar expression levels of GrzB, IFN-γ, and TNF-α in the used co-culture systems (comp. Fig. 9 b-d). In order to confirm that the robust expression of cytotoxic proteins by $NLGN4X_{131\text{-}139}$-specific TCR-expressing primary human T cells leads to target cell killing, I utilized a modified version of the Vital-FR assay to detect specific lysis of peptide-loaded K562 target cells (comp. Fig. 9 e)[Stanke et al., 2010]. Importantly, $NLGN4X_{131\text{-}139}$-specific and MART1-specific T cells (MART-1-TCR-T) showed comparable cytotoxic activity against peptide-loaded K562 target cells (comp. Fig. 9 f).
Next, I aimed to evaluate the cytotoxic capacity of NLGN4X-TCR-T against the HLA-A*02^+ adherent glioma cell line U87. U87 wildtype cells loaded with the $NLGN4X_{131\text{-}139}$ peptide induced specific upregulation of GrzB, CD69, and 4-1BB (CD137) in NLGN4X-TCR-T (comp. Fig. 12a and Fig. 10a-c). In line with these findings, $NLGN4X_{131\text{-}139}$-specific T cells were able to specifically lyse U87 cells loaded with the target peptide in lactate dehydrogenase (LDH)-based and flow cytometry-based killing assays (comp. Fig. 12 b,c). In co-culture assays applying synthetic MHC class I-restricted peptides for reactivity testing, MHC molecules are usually saturated and external MHC loading might occur. Although the $NLGN4X_{131\text{-}139}$ was previously identified by HLA-ligandome analysis in some glioblastoma patients[Hilf et al., 2019] I aimed at demonstrating endogenous presentation of $NLGN4X_{131\text{-}139}$ in the used tumor model system. Thus, I expressed the $NLGN4X_{131\text{-}139}$ antigen by using either a tandem-minigene (TMG) with different MHC class I epitopes including NLGN4X (U87 TMG) or a retroviral vector containing full-length NLGN4X (U87 NLGN4X). Overexpression of the NLGN4X antigen was confirmed by qPCR and Western blot (comp. Fig. 11 a-c) Similar to the findings with K562 cells as target cells, I found specific upregulation of GrzB, CD69, and 4-1BB when I co-cultured NLGN4X-TCR-T with U87 NLGN4X or U87 TMG target cells (comp. Fig. 12

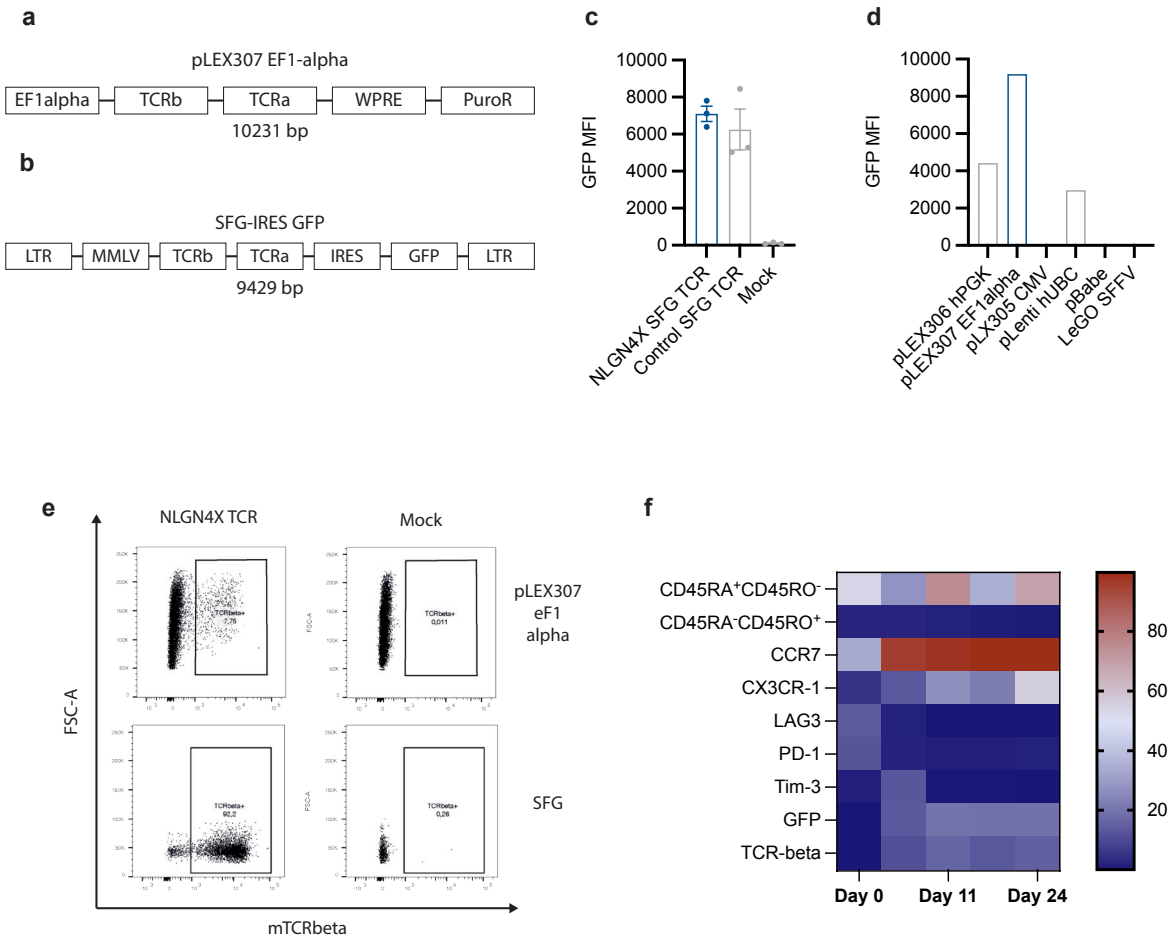

Figure 8: **Development of efficient TCR delivery to human T cells**
a and **b** Schematic structure of **a** *pLEX307 EF-1 alpha* lentiviral construct and **b** *SFG-IRES-GFP* retroviral construct: *TCRa/b = T cell receptor alpha / beta chain, WPRE = Woodchuck-Hepatitis-Virus Posttranscriptional regulatory element, PuroR = Puromycin resistance, LTR = long terminal repeat, IRES =Internal ribosomal entry site* **c** GFP median fluorescence intensity of NLGN4X-TCR-SFG and Flu-TCR-SFG transduced human T cells compared to Mock transduced T cells. *n=3 biological replicates, Mean with SEM* **d** GFP median fluorescence intensity after transduction of human T cells with five different lentiviral constructs using the hPGK (Phosphoglycerate Kinase), EF1-alpha, CMV (cytomegaly virus), hUBC (Polyubiquitin C) and SFFV (spleen focus forming virus) promoter and the pBabe retroviral construct. (*GFP expressing constructs were provided and transduction of human T cells was performed by Rainer Will, German Cancer Research Center***e** Exemplary FACS analysis of murine TCR beta constant region expression in human transduced T cells **f** Heatmap of extracellular flow cytometric expression of different phenotypic markers *n= 3 biological replicates for day 0 and 4 n=2 for day 11-24, Mean depicted*

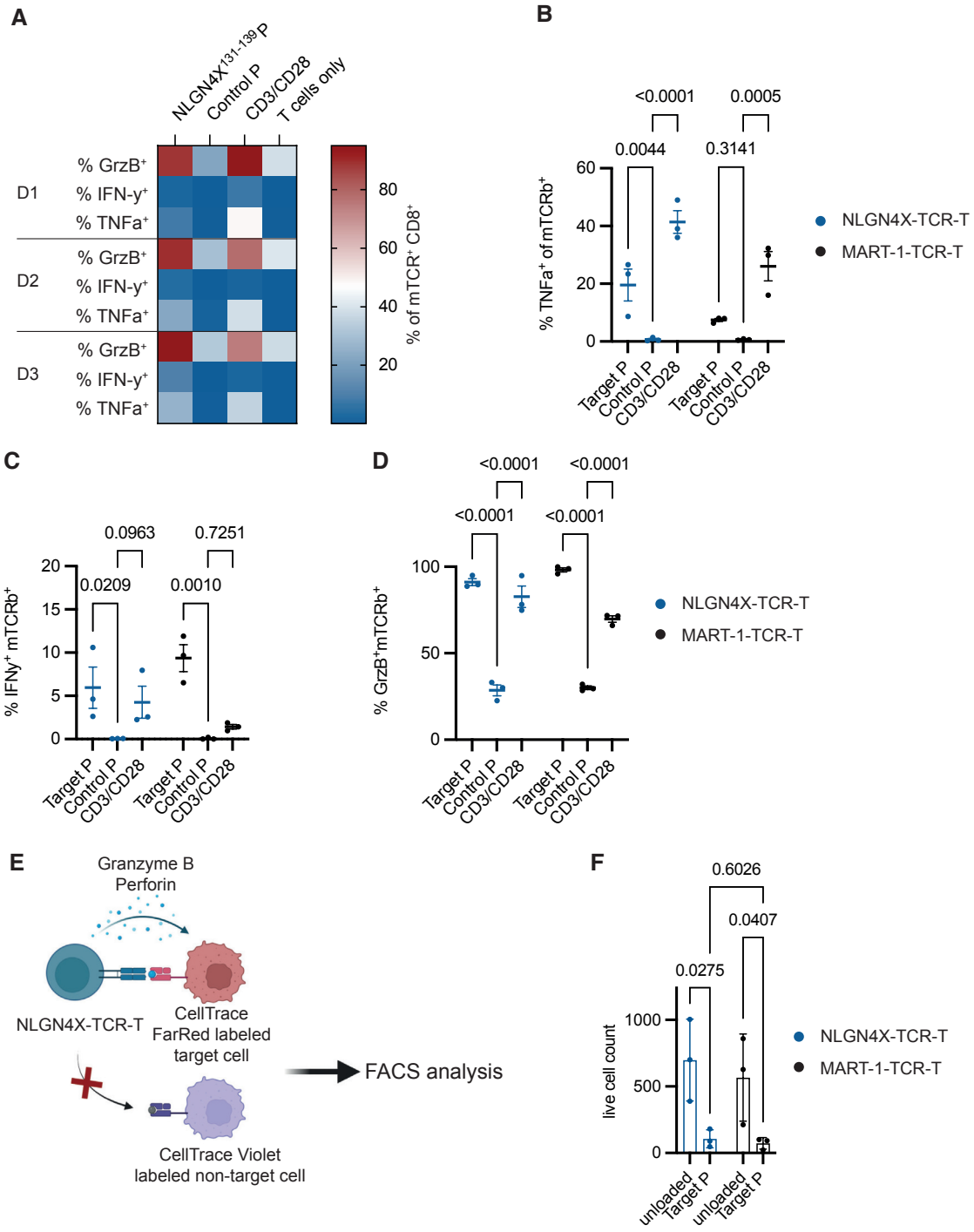

Figure 9: *Continued on next page.*

Figure 9: **NLGN4X-TCR-T showed comparable effective in vitro recognition and lysis of target cells as a clinically used control TCR a**Heatmap of the functional response (IFN-γ, TNF-α, GrzB) of three different donors transduced with a $NLGN4X_{131\text{-}139}$ TCR and cocultured with peptide loaded HLA-A*02^+ K562 leukemia cells. For statistical analysis compare Fig. 9 b-d. n=3 biological replicates. **b**TNF-α production of NLGN4X-TCR-T and Mart-1-TCR-T cultured with peptide loaded HLA-A*02^+ K562 leukemia cells. Target peptide: NLGN4X-TCR-T vs. MART-1 TCR T cells p = 0.0863. Mean with SEM of n=3 biological replicates. Twoway-ANOVA. **c** IFN-γ production of NLGN4X-TCR-T and MART-1-TCR-T cultured with peptide loaded HLA-A*02^+ K562 leukemia cells. Target peptide: NLGN4X-TCR-T vs. MART-1-TCR-T p = 0.2926. Mean with SEM of n=3 biological replicates. Twoway-ANOVA. **d** Granzyme B expression of NLGN4X-TCR-T vs. MART-1-TCR-T cultured with peptide loaded HLA-A*02^+ K562 leukemia cells. Target peptide: NLGN4X-TCR-T vs. MART-1-TCR-T p = 0.3461.Mean with SEM of n=3 biological replicates. Twoway-ANOVA. **e** Exemplary overview of the modified Vital-FR assay28 used in this study: target cells that either endogenously expressed the target epitope or were exogenously loaded with the respective peptide were labeled with CellTraceTM FarRed and non-target cells (irrelevant peptide or no target expression) were labeled with CellTraceTM Violet and cultured with target-specific TCR transduced T cells in the same well. Created with Biorender.com. **f** Live cells of either target peptide loaded or unloaded K562 cells after overnight co-culture with NLGN4X-TCR-T or MART-1-TCR-T at an effector - target (E:T) cell ratio of 10:1 assessed by flow cytometric analysis. Mean with SEM of n=3 biological replicates. Twoway-ANOVA.

d and Fig. 10 d-f). Moreover, U87 TMG and U87 NLGN4X were specifically lysed by NLGN4X-TCR-T (comp. Fig. 12 e). Next, the reactivity of NLGN4X-TCR-T against a patient-derived glioblastoma cell line that endogenously expresses NLGN4X was assessed (comp. Fig. 12 f). When co-culturing PB-1 cells with NLGN4X-TCR-T, I observed specific upregulation of the activation marker 4-1BB and the effector protein perforin (comp. Fig. 12g and Fig. 10 g) and ratio-dependent killing of the target cell line (comp. Fig. 12 h). In summary, I could demonstrate that TCRft1-SFG-IRES-GFP-expressing primary human T cells specifically recognize and lyse tumor cells expressing the $NLGN4X_{131\text{-}139}$ epitope including a patient-derived glioblastoma cell line with natural processing of NLGN4X protein in vitro.

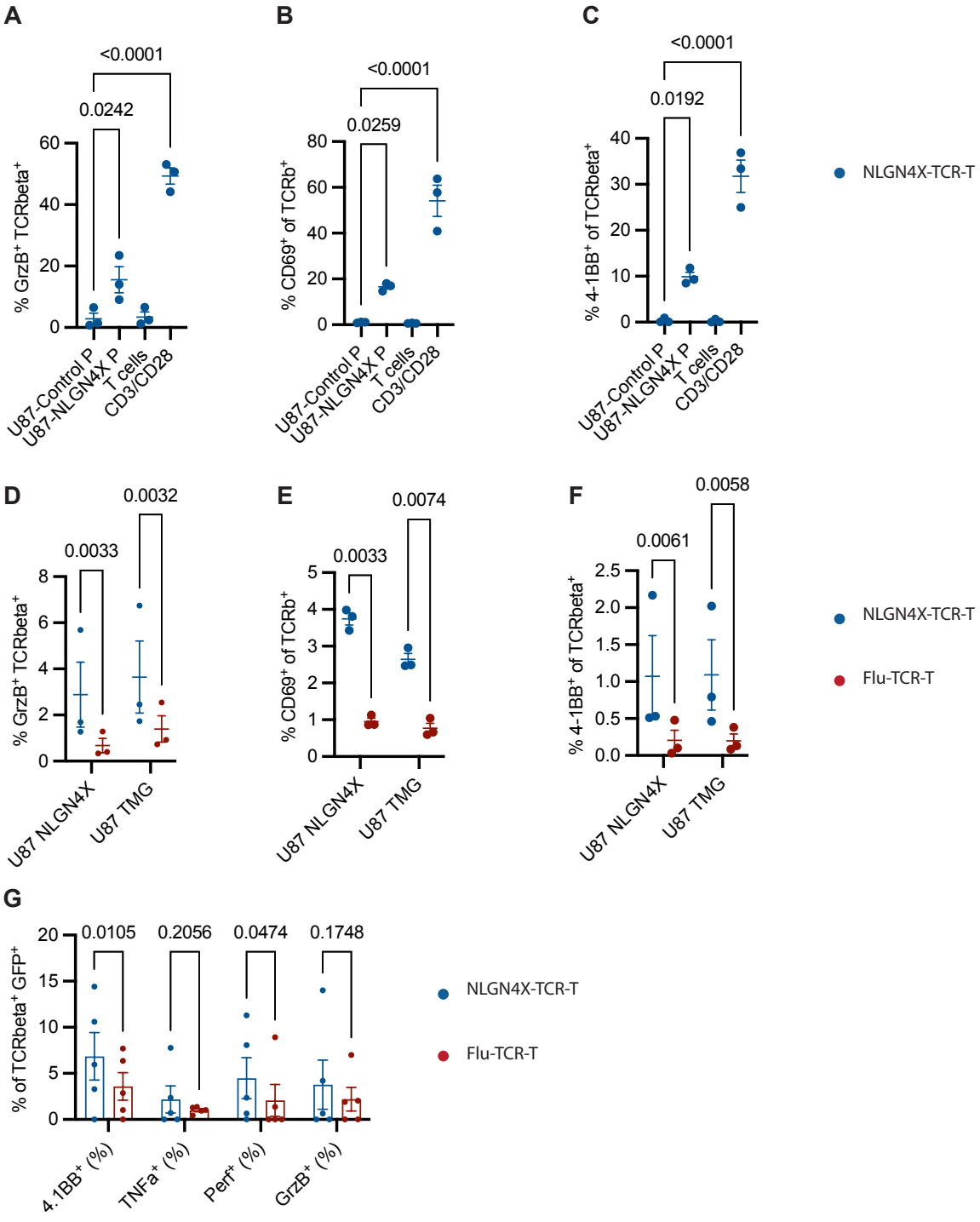

Figure 10: *Continued on next page.*

Figure 10: **Additional Figure: NLGN4X-TCR-T recognizes and lyse U87 glioma cells and are specifically activated by an NLGN4X expressing patient-derived glioblastoma cell line in vitro a** Flow cytometric assessment of an overnight co-culture of NLGN4X-TCR-T from three different donors with U87 glioma cells loaded with either a control or target peptide: percentage of GrzB+ of TCRft1-expressing T cells. Mean with SEM of n=3 biological replicates. Oneway-ANOVA. **b** Percentage of CD69+ cells of TCRft1-expressing T cells. Mean with SEM of n=3 biological replicates. Oneway-ANOVA. **c** Percentage of 4-1BB+ cells of TCRft1-expressing T cells. Mean with SEM of n=3 biological replicates. Oneway-ANOVA. **d** Flow cytometric assessment of an overnight co-culture of NLGN4X-TCR-T from three different donors with U87 NLGN4X or U87 TMG glioma cells, Flu-TCR-T were used as negative control T cells: percentage of GrzB+ of TCRft1-expressing T cells. Mean with SEM of n=3 biological replicates. Twoway-RM-ANOVA. **e** Percentage of CD69+ cells of TCRft1-expressing T cells. Mean with SEM of n=3 biological replicates. Twoway-RM-ANOVA. **f** Percentage of 4-1BB+ cells of TCRft1-expressing T cells. Mean with SEM of n=3 biological replicates. Twoway-RM-ANOVA. **g** Flow cytometric assessment after an overnight co-culture of NLGN4X-TCR-T (n=5) with NLGN4X expressing patient-derived glioblastoma cell line (PB-1), Flu-TCR-T were used as negative control T cells. Percentages of 4-1BB+, TNF-α+, Perf+ and GrzB+ cells of TCRft1-expressing T cells. Mean with SEM of n=5 biological replicates. Twoway-RM-ANOVA.

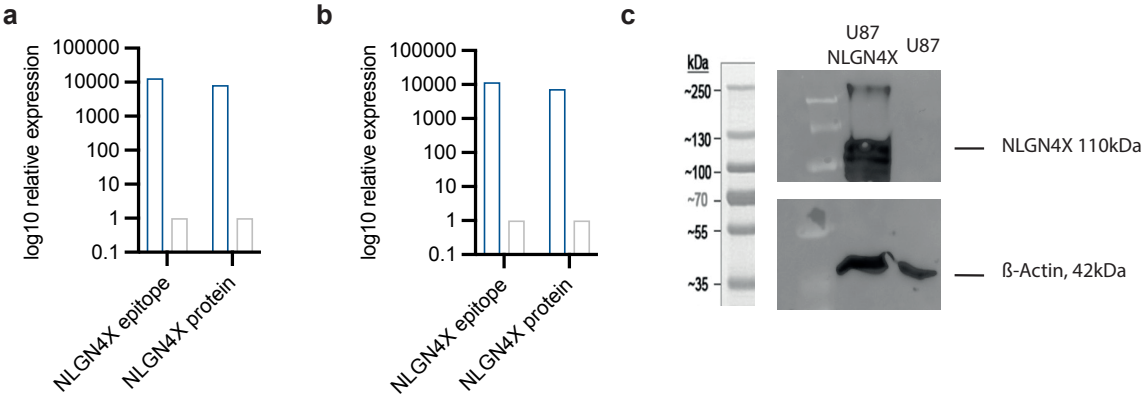

Figure 11: **Generation of U87 glioma cell line with overexpression of the NLGN4X protein a** and **b** Quantitative PCR based assessment of the expression of the NLGN4X RNA in U87 NLGN4X and untransfected U87 glioma cells: normalized to **a** GAPDH and **b** ß-Actin. **c** Western Blot of the expression of the NLGN4X protein in U87 NLGN4X and U87 glioma cells.

Secondly, a tandem-minigene containing different HLA-A2 restricted epitopes was constructed (Design and cloning was performed by Ed Green, Department of Neuro-Immunology, German Cancer Research Center) and transfected into U87 glioma cells resulting in the U87 TMG cell line (performed by Yu-Chan Chih, Department of Neuro-Immunology, German Cancer Research Center).
Both newly generated cell lines were then assessed for functional *in vitro* characterisation of NLGN4X TCR transgenic T cells. Overnight co-culture with the respective target cell lines and a U87 control cell line resulted in specific activation of NLGN4X TCR transduced T cells: TNF-α and the extracellular activation markers CD69 and 41.BB showed increased expression after coculture with NLGN4X TCR in contrast to Flu TCR transgenic T cells (comp. Fig. 12 a-c). Importantly, Granzyme B expression was also increased in NLGN4X-TCR-T compared to Flu TCR control T cells (comp. Fig. 12 d) resulting in effcient lysis of both U87 NLGN4X and U87 TMG target cells in an LDH release assay (comp. Fig. 12 e). Lysis of U87 TMG target cells was also assessed by flow cytometric analysis of a Vital-FR based assay (exemplary FACS gating comp. Fig. 12 f) and specific cytotoxicity was about 50 % of U87 TMG target cells(comp. Fig. 12 g). Killing of U87 glioma cells in this context is most-likely due to trans-killing of non-target cells in proximity to target cells, as target and non-target cells were cultured in a single well.

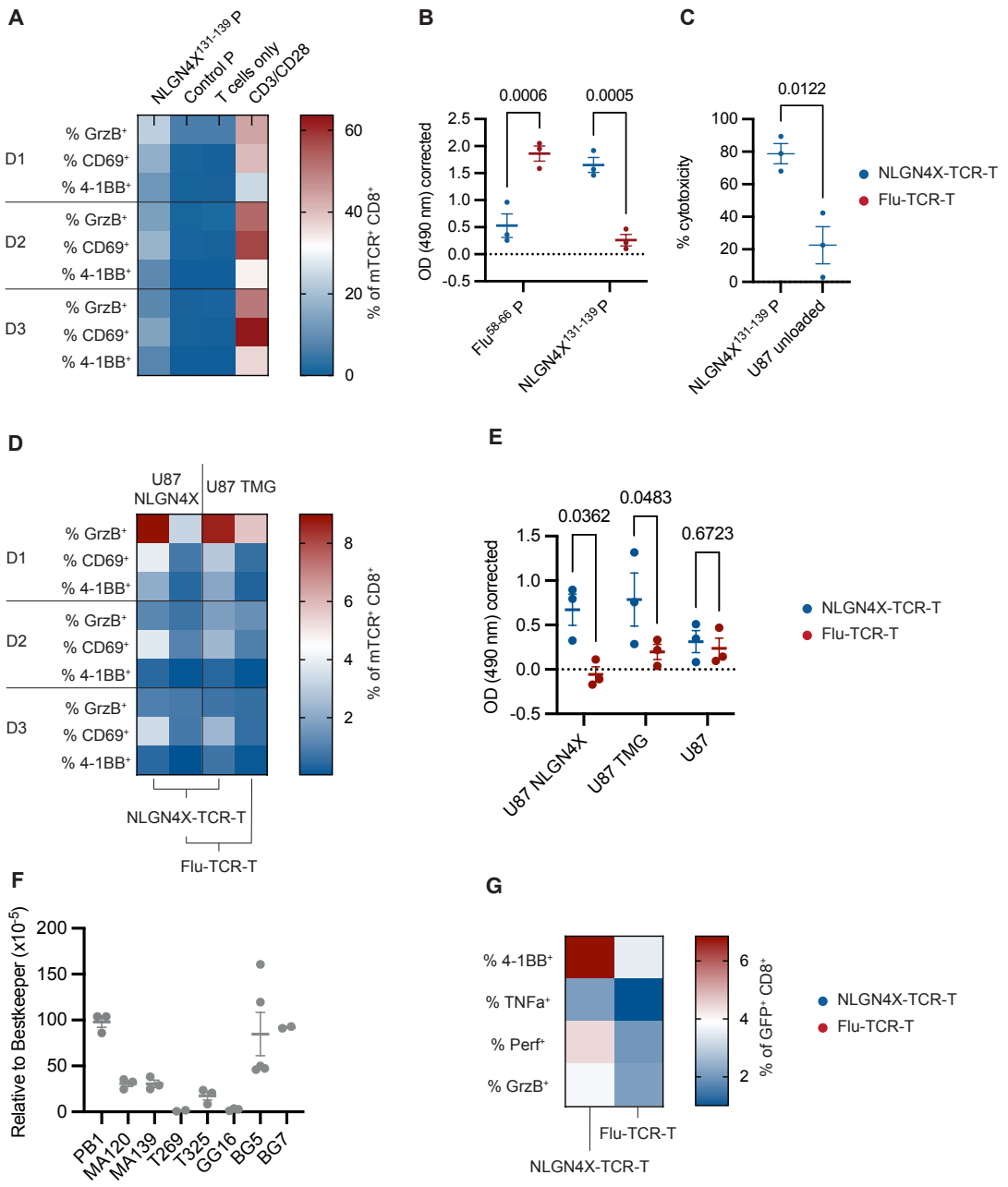

Figure 12: *Continued on next page.*

Figure 12: **The NLGN4X TCR specifically recognizes and lyses glioma cells expressing the NLGN4X target epitope**
a Heatmap of the functional response (CD69, 4.1BB, GrzB) of three different donors transduced with a NLGN4X TCR and cocultured with peptide-loaded HLA-A*02$^+$ U87 glioma cells. For statistical analysis compare Fig. 10 a-c **b** Optical density (OD) measured detecting LDH release after overnight coculture of NLGN4X-TCR-T and Flu (MHCI epitope) TCR transgenic T cells (Flu-TCR-T) with NLGN4X or Flu peptide loaded U87 glioma cells. The E:T ratio was 2:1. Mean with SEM of n=3 biological replicates. Twoway-ANOVA. **c** NLGN4X-TCR-T were cocultured with either peptide loaded U87 glioma cells or unloaded cells and specific cytotoxicity was calculated using FACS based counting of tumor cells. The E:T ratio was 2:1. Mean with SEM of n=3 biological replicates. Unpaired t-Test. **d** Heatmap of the functional response (CD69, 4-1BB, GrzB) of three different donors transduced with a NLGN4X TCR or Flu TCR (here: negative control TCR) and cocultured with U87 glioma endogenously expressing the NLGN4X protein sequence including the relevant epitope (U87 NLGN4X) or a tandem-minigene (U87 TMG) containing the antigenic sequence of NLGN4X. For statistical analysis compare Fig. 10 d-f **d**LDH release assay of NLGN4X-TCR-T vs. Flu-TCR-T (TCR negative control) targeting either U87 NLGN4X, U87 TMG or U87 (target negative control) glioma cells. The E:T ratio was 2:1. Mean with SEM of n=3 biological replicates. Twoway-RM-ANOVA. **f** Different patient-derived glioblastoma cell lines were evaluated for NLGN4X expression by Taqman quantitative PCR. PB1 was used for further in vitro testing. Normalized to Bestkeeper. Mean with SEM. *Cell line provided and experiment performed by D.Hoffmann, German Cancer research centre* **g** Heatmap of the functional response (4-1BB, TNF-α, Perf, GrzB) of five different donors expressing either the NLGN4X TCR or Flu TCR and cocultured with PB-1 patient-derived glioblastoma cells naturally expressing the $NLGN4X_{131\text{-}139}$ epitope. For statistical analysis see Fig. 10 g **h** Optical density (OD) measured detecting LDH release of an overnight coculture NLGN4X-TCR-T vs. Flu-TCR-T (TCR negative control) targeting PB-1 glioma cells with endogenous NLGN4X expression. E:T ratio as indicated below. Mean with SEM of n=3 biological replicates. Twoway-RM-ANOVA.

4.1.5 NLGN4X TCR transgenic T cells provide a therapeutic benefit in a subcutaneous model of U87 NLGN4X glioma cells in an immunodeficient environment

Of note for the following *in vivo* experiment the *pLEX307* lentiviral vector was used generating T cell products with lower TCR surface expression.
NSG MHC I/II knockout mice were used for all in vivo studies as these mice don't develop Graft-versus-host disease caused by an mismatch of the human T cell product with MHC molecules. NSG MHC I/II KO mice are completely deprived of endogenous T cells meaning that any T cell detected by anti human-CD3 antibodies in subsequent analysis resulted from adoptive transfer of human T cells.
First, NSG MHC I/II KO mice were challenged with subcutaneous flank tumors of U87 NLGN4X glioma cells. Tumor growth was monitored daily and treatment was iniated after confirmation of tumor growth in all experimental animals on day 11 after tumor cell inoculation. Healthy donor T cells were engineered to express the NLGN4X TCR and expanded *in vitro* prior to infusion as previously established. Animals received two doses of up to 3.5 Mio. NLGN4X TCR transgenic T cells or Mock control T cells intravenously or were left untreated. Treatment with NLGN4X-TCR-T but not Mock T cells resulted in a significant survival benefit both compared to the Mock T cells and tumor only group (comp. Fig. 13 b). This survival benefit was driven by slowed tumor growth rate after the second adoptive transfer on day 18 until day 25 illustrated by a significantly reduced tumor growth rate (comp. Fig. 13 c-g).
Importantly, immunofluorescence of NLGN4X-TCR-T treated mice compared to Mock treated mice showed a tendency showed increased numbers of T cells in representative fields of interest (comp. Fig. 13 h). Interestingly, CD3 positive T cells in NLGN4X TCR treated mice were detecable within the tumor tissue (comp. Fig. 13 i, circled line), while in Mock T cell treated animals T cells were mainly localized at the tumor border (white arrow).
Taken together, NLGN4X-TCR-T were capable of mediating a therapeutic effect in a subcutaenous tumor model resulting in prolonged survival. Importantly, CD3 positive T cells as correlates of the observed effects could be detected in the tumor tissue.

4.1.6 Local delivery of NLGN4X TCR transgenic T cells in an intracranial glioma model shows therapeutic efficacy

As systemic delivery of human NLGN4X TCR transgenic T cells resulted in slowed tumor progression in a flank tumor model the capacities of these cells to hamper intracranial tumor growth was to be investigated. Recently, it has been shown that local delivery of T cells in brain cancer tumor models results in superior tumor control [Theruvath et al., 2020]. Therefore, intraventricular injection of T cells was applied.
Therefore, NOD scid gamma (NSG) MHC class I and MHC class II knockout (NSG MHCI/II KO) mice, that do not develop graft versus host disease after T cell transfer, were challenged with intracranial U87 TMG experimental gliomas. Mice received either $NLGN4X_{131\text{-}139}$-specific TCR- or negative control (influenza (Flu)) TCR-engineered human T cells (Flu-TCR-T) via intracerebroventricular transfer or did not receive any T cell treatment (NTC) = No T cell Control) (comp. Fig. 14 a). Two injections of 5 x 10^6

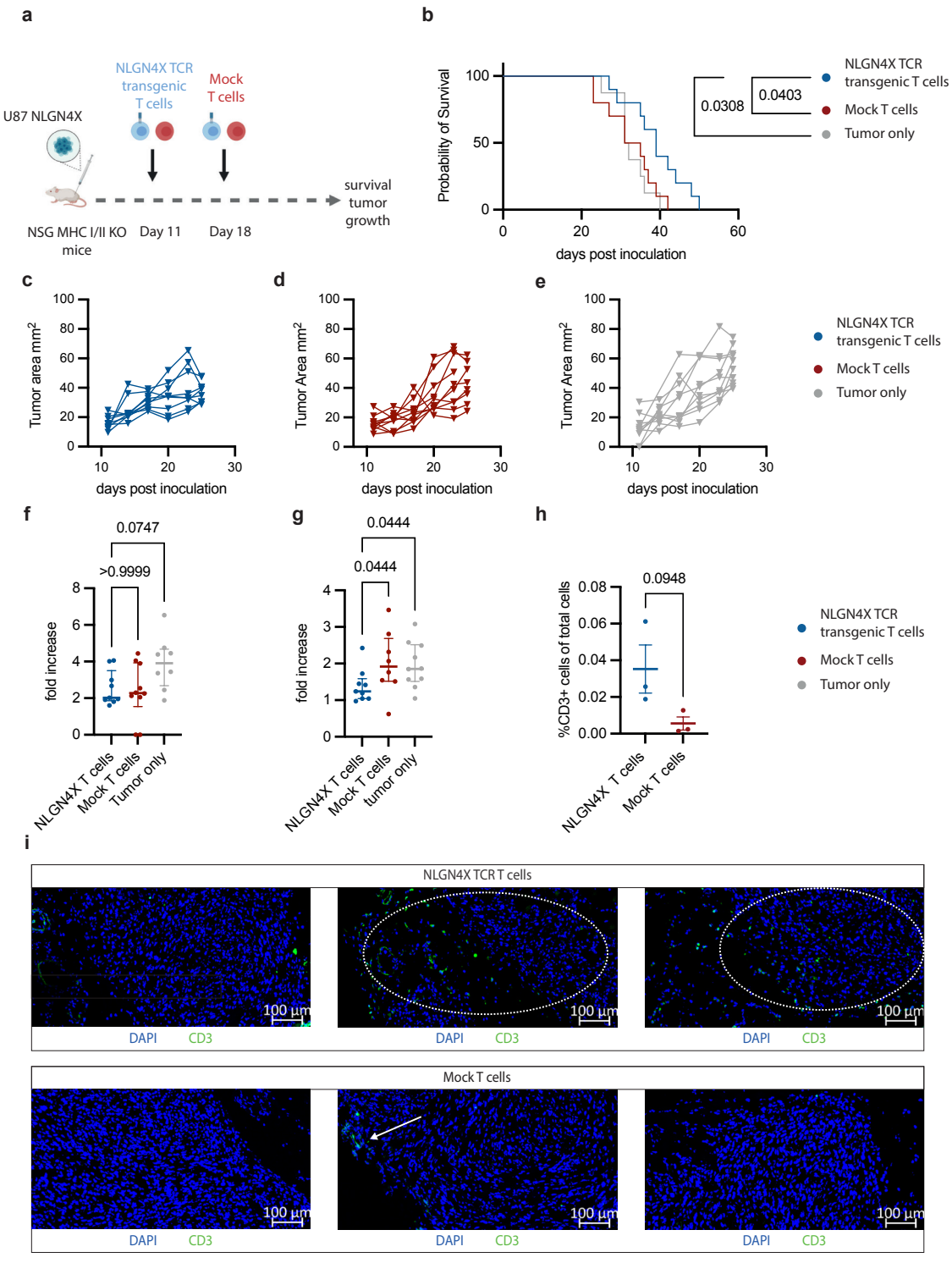

Figure 13: *Continued on next page.*

Figure 13: **NLGN4X TCR transgenic T cells prolong the survival and slow the tumor growth in a subcutaneous model of U87 NLGN4X glioma cells**
a Schematic overview of the experimental workflow: NSG MHCI/II KO mice were challenged with 1 Mio. U87 NLGN4X glioma cells and treated intravenously with two doses of either NLGN4X TCR transgenic T cells or Mock control T cells or were left untreated. **b** survival curves of n= 10 animals per group for NLGN4X and Mock T cells and n=8 animals in the tumor only group, *Log-Rank-test* **c**-**e** individual tumor growth curves of **c** NLGN4X transgenic T cells **d** Mock T cells-treated or **e** untreated mice. **f** and **g** fold increase between day 11 and 25 (**f**) and day 18 and 25 (**g**) *Median with 95% CI, Kruskal-Wallis-Test* **h** Quantification of CD3 positive cell in immunofluorescence images of n=3 animals per group *n=3 biological replicates, Mean with SEM, Unpaired t-Test* **i** Representative immunofluorescence images of n=3 mice per group showing intratumoral CD3 positive cells only in NLGN4X-TCR-T-treated mice

TCR-engineered primary human HLA-A*02$^+$ T cells with 86.6 to 87.4 % mTCRb surface expression after transduction were performed at day 15 and 22 (comp. Fig. 14 a) into the lateral ventricle of the non-tumor-bearing hemisphere. Treatment with NLGN4X-TCR-T resulted in prolonged survival of glioma-bearing animals compared to Flu-TCR-T or NTC mice (comp. Fig. 14 b). By using longitudinal MRI, I aimed to investigate if treatment with NLGN4X-TCR-T leads to objective radiographic responses, therefore tumor volumes were assessed between day 11 and day 67 according to the modified RANO criteria. [Ellingson et al., 2017] At day 67 as the timepoint of best response, I observed stable disease in 11.1 %, partial responses (PR) in 22.2 % and complete response (CR) in 22.2 % of NLGN4X-TCR-T treated mice resulting in an objective response rate (ORR: CR + PR) of 44.4 % in comparison to 0.0 % in both Flu-TCR-T and NTC mice (comp. Fig. 14 c, Fig. 15 a,c). In addition to the assessment of radiographic responses upon $NLGN4X_{131\text{-}139}$-specific TCR-engineered T cell therapy, longitudinal MRI enabled the local assessment of tumor growth (comp. Fig. 14 d,e). Interestingly, two mice with late recurrence of U87 TMG tumors (comp. Fig. 14 e, Fig. 15 b) had shown radiographic responses (one PR, one CR) in previous MRI (comp. Fig. 14 e). Thus, flow cytometric analysis of tumor-infiltrating leukocytes was performed from recurrent late-stage tumors (comp. Fig. 14 f). In these tumors, 78 days after the second administration of NLGN4X-TCR-T, I found predominantly CD4+ T cells with low GFP expression within the experimental tumors. These CD4+ T cells were CD45RA- CCR7- and had low expression of the proliferation marker Ki67 and high PD-1 expression (comp. Fig. 14 f). Notably, recurrent U87 TMG tumors maintained expression of the $NLGN4X_{131\text{-}139}$ antigen as demonstrated by qPCR and in addition, MHC class I expression was still detectable by immunofluorescent staining (comp. Fig. 14 g,h, Fig. 16 a-c). Overall, the findings suggest that late recurrence results from the absence of intratumoral cytotoxic $NLGN4X_{131\text{-}139}$-specific CD8+ T cells (comp. Fig. 14 f-h, Fig. 16 a-c).

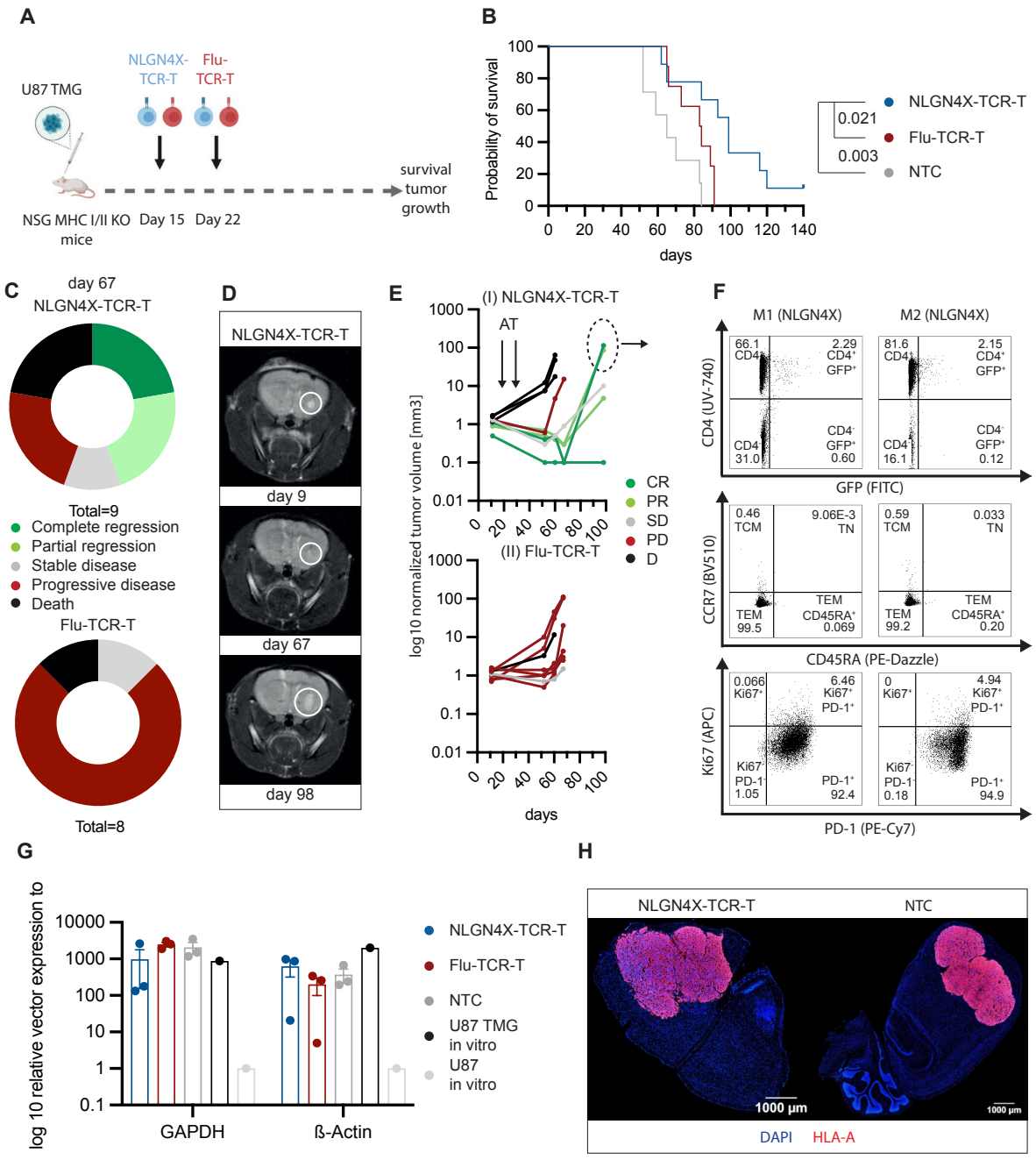

Figure 14: *Continued on next page.*

Figure 14: **NLGN4X TCR transgenic T cells show therapeutic efficacy in intracranial glioma model**
a Schematic experimental overview: NSG MHC I/II KO mice were challenged with intracranial U87 NLGN4X antigen overexpressing gliomas and after confirmation of tumor growth NLGN4X-TCR-T or Flu-TCR-T were injected at day 15 and 22 after tumor inoculation. Created with Biorender.com. **b** Preclinical survival of mice treated either with NLGN4X-TCR-T or Flu-TCR-T targeting intracranial NLGN4X antigen overexpressing U87 cells. NTC = No T cell Control. n=9 mice for NLGN4X-TCR-T, n=8 mice for Flu-TCR-T, n=7 for NTC. Log-Rank-Test. **c** Radiographic response assessment according to the mRANO criteria [Ellingson et al., 2017] between day 11 and 67 complete response (CR) was defined as a change in tumor volume of -100 %, partial response (PR) as $<$ -65 %, stable disease (SD) between $>$ -65 % and +40 % and progressive disease (PD) as $>$ +40 %. **d** MRI image of one long-term surviving NLGN4X-TCR-T treated animal showing tumor regression at the initial tumor site until day 67 and tumor progression at day 98. **e** Individual growth curves of U87 NLGN4X antigen expressing glioma cells of NLGN4X-TCR-T (I) and Flu-TCR-T (II) treated animals. Circled mice were analyzed by FACS as shown in (comp. Fig. 14 f). Log10-scaled growth. Thus, tumor volumes with V = 0 μl are not displayed in the graph. CR = complete response, PR = partial response, SD = stable disease, PD = progressive disease, D = death. For visualization of the tumor growth the detection limit for tumor volumes was set to 0.1 μl. **f** Representative flow cytometric analysis from two animals (M1 = mouse 1, M2 = mouse 2) with late-stage recurrence of the tumor showing persistence of primarily CD4+ T cells at the tumor site with a predominantly CCR7-CD45RA- effector memory phenotype and impaired proliferation with high PD-1 expression. Gated on live hCD3+ T cells. **g** Realtime quantitative PCR of the U87 TMG plasmid sequence in tumors of NLGN4X-TCR-T, Flu-TCR-T treated or NTC animals at late-stage time point compared to in vitro cultured U87 TMG and U87 cells. Relative expression to hGAPDH or hß-Actin. Log10-scaled. n=3 biological replicates. **h** Exemplary immunofluorescence staining of HLA-A expression: One NLGN4X-TCR-T treated animal and one untreated animal at late stage timepoint shown. Immunofluorescence images of additional animals are shown in (comp. Fig. 16 c).

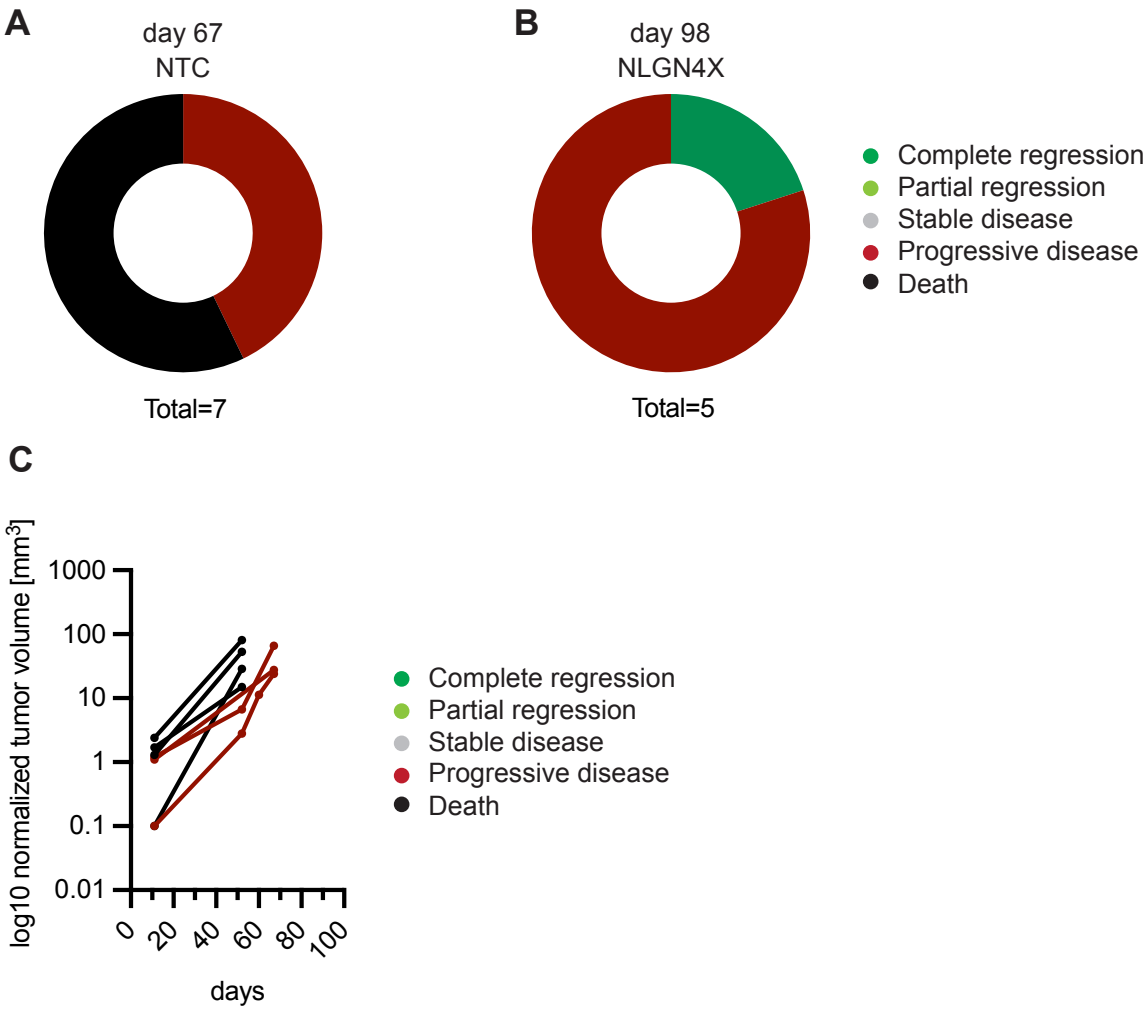

Figure 15: **NMRI-based radiographic response assessment and individual preclinical tumor growth**
a Response assessment in NTC (No T cell Control) on day 67. **b** Response assessment in NLGN4X-TCR-T treated mice on day 98 after all animals in the Flu-TCR-T treated group and in the NTC group had died. **c** Individual growth curves of U87 NLGN4X antigen expressing glioma cells of NTC animals. For visualization of the tumor growth the detection limit for tumor volumes was set to 0.1 μl.

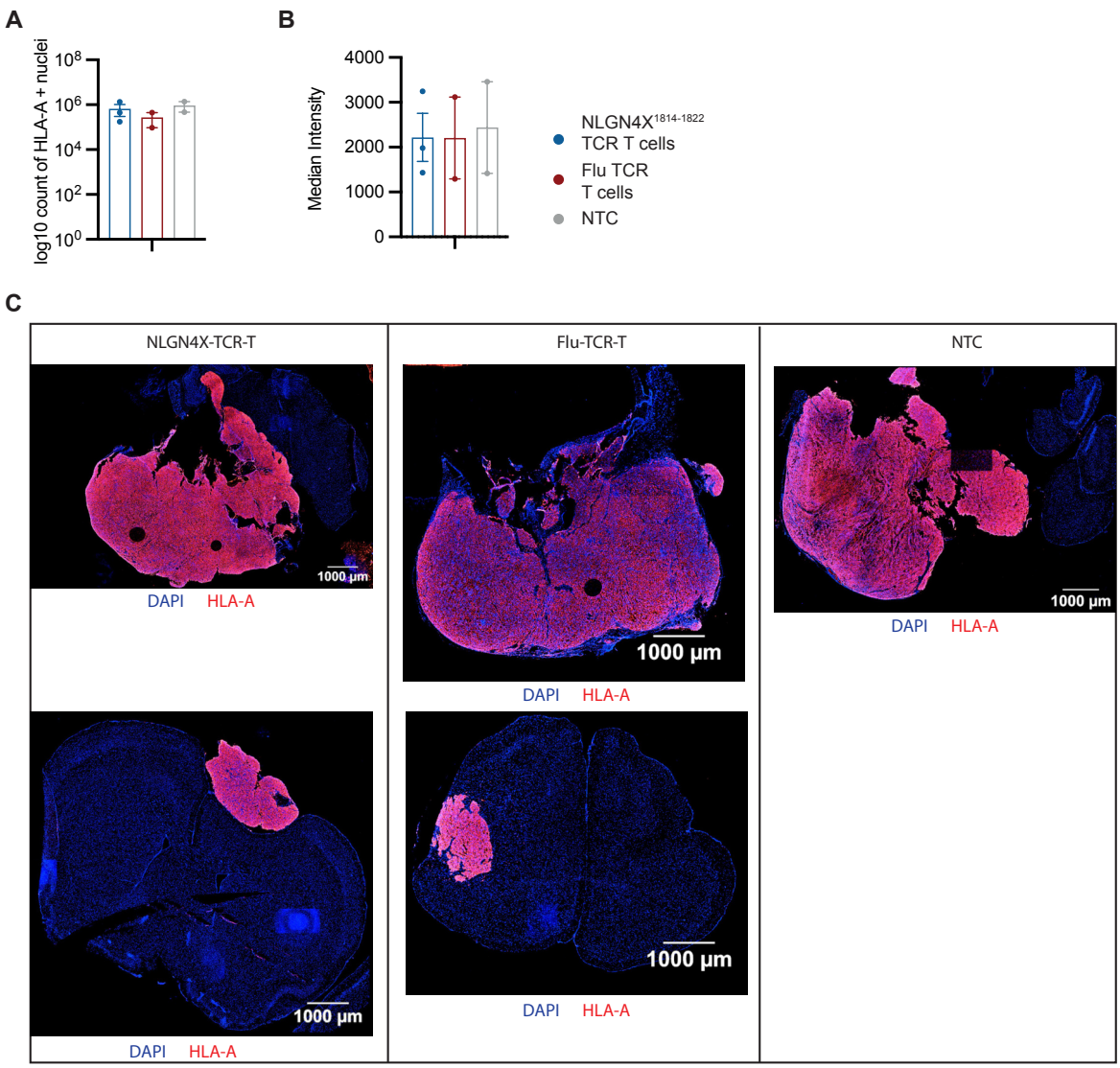

Figure 16: **MRI-based radiographic response assessment and individual preclinical tumor growth**
a Count of HLA-A positive cells (HLA-A positive area colocalized to DAPI positive nuclei) normalized to the percentage of the HLA-A positive area of the total area. Mean with SEM of n=3 (NLGN4X-TCR-T) – 2 (Flu-TCR-T, NTC) biological replicates. Log10-scaled. **b** Median intensity analysis of HLA-A immunofluorescence signal. Mean with SEM of n=3 (NLGN4X) – 2 (Flu and NTC, respectively) biological replicates. **c** Additional images of immunofluorescence stainings of experimental brain tumor slices at the experimental endpoint using an HLA-A-specific antibody and DAPI.

4.1.7 NLGN4X-TCR-T phenotypically adapt within the tumor microenvironment

At late recurrence, I found exhausted CD4+ T cells with low TCR transgene expression. Hence, this observation prompted me to assess the intratumoral phenotype of NLGN4X-TCR-T at an early timepoint after intracerebroventricular delivery in U87 TMG glioma-bearing animals (comp. Fig. 17 a). 6 days after intracerebroventricular transfer, T cells were present in the contralateral experimental glioma and $NLGN4X_{131\text{-}139}$-specific TCR positivity was confirmed on the CD8+ T cell subset (comp. Fig. 17 b). Quantitatively, U87 TMG gliomas treated with NLGN4X-TCR-T and Flu-TCR-T were not differentially infiltrated by CD3+ T cells in immunocompromised mice (comp. Fig. 17 c). CD8+ T cells mainly showed a T effector memory (TEM) phenotype with expression of CD45RA and high expression of Ki67 compared to low expression of the exhaustion markers PD-1 and TIM-3 (comp. Fig. 17 d,e). Specific upregulation of various activation and effector cell markers in NLGN4X-TCR-T compared to Flu-TCR-T (comp. Fig. 17 f), suggests antigen recognition and specific intratumoral T cell activation. However, the fundamental difference between the early phenotypes of intratumoral NLGN4X-TCR-T (comp. Fig. 17 d) and those found at late recurrence (comp. Fig. 14 e) support the hypothesis that loss of cytotoxic CD8+ NLGN4X-TCR-T results in late tumor recurrence.
Of note for the following in vivo experiment the pLEX307 lentiviral vector was used generating T cell products with lower TCR surface expression.
Next, I investigated if NLGN4X-TCR- T were able to recognize endogenously processed NLGN4X in vivo. Thus, NSG MHC class I/II KO mice were challenged with intracranial U87 NLGN4X expressing gliomas and treatment with adoptive transfer was initiated after confirmation of tumor growth using MRI. After manufacturing of the T cell product tumor bearing mice were treated with two doses of intraventricularly delivered T cells expressing either the NLGN4X TCR or with control T cells with no modification of gene expression on day 15 and 22 or were left untreated. (comp. Fig. 18 a)
Tumor growth was then monitored with weekly MRI measurements. Of note 81 % of NLGN4X T cells treated animals had tumor volumes under 50yl on day 49, while only 54 % in the Mock T cells treated group had tumor volumes below the same threshold. (comp. Fig. 18 c,d) Treatment with NLGN4X TCR transgenic T cells resulted in a significant survival benefit compared to both the Mock T cells group and the tumor only group. (comp. Fig. 18 b) MRI magnet resonance imaging of tumor challenged mice on day 42 showed animals with slowed tumor progression in the NLGN4X TCR treated group (exemplary images comp. Fig. 18 e).
Altogether, I could demonstrate that human T cells engineered with a patient-retrieved off-the-shelf TCR targeting the $NLGN4X_{131\text{-}139}$ antigen are capable of lysing tumor cells in vitro and mediating temporary tumor control in experimental gliomas.

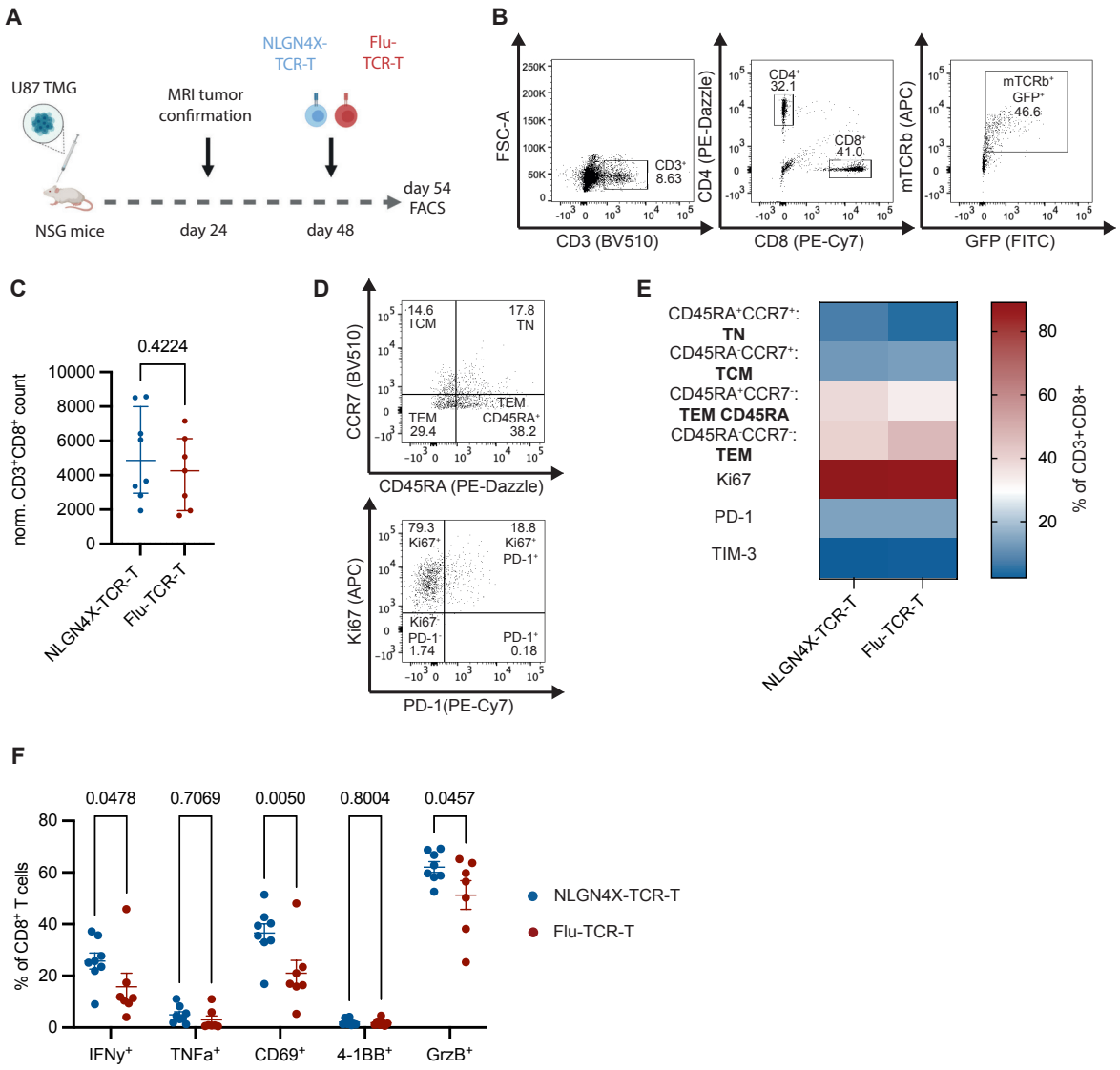

Figure 17: **Local delivery of NLGN4X TCR transgenic T cells prolongs the survival in an intracranial model of U87 NLGN4X gliomas**

a Experimental overview: U87 NLGN4X antigen overexpressing gliomas were injected intracranially and NLGN4X-TCR-T or Flu-TCR-T were injected into the contralateral ventricle. After 6 days T cells were analyzed by flow cytometry and ex vivo activation was assessed. Created with Biorender.com **b** s(B) Exemplary flow cytometry plots showing intratumoral CD3+ T cells, CD4-CD8 distribution and mTCRb and GFP expression **c** (C) Normalized (to tumor volume) count of CD3+CD8+ T cells in the TME. n=8 (NLGN4X-TCR-T), n=7 (Flu-TCR-T). Unpaired t-Test. **d** Exemplary FACS plots showing the CD45RA and CCR7 as well as Ki67 and PD-1 expression on intratumoral CD3+CD8+ T cells (TCM = T central memory cells, TN = naïve T cells, TEM = T effector memory cells, TEM-CD45RA+ = TEM re-expressing CD45RA). **e** Heatmap of phenotypic markers of intratumoral CD3+CD8+ T cells. n=8 (NLGN4X-TCR-T), n=7 (Flu-TCR-T). **f** Assessment of activation and effector cells markers of intratumoral CD8+ T cells. n=8 (NLGN4X-TCR-T), n=7 (Flu-TCR-T). Twoway-ANOVA.

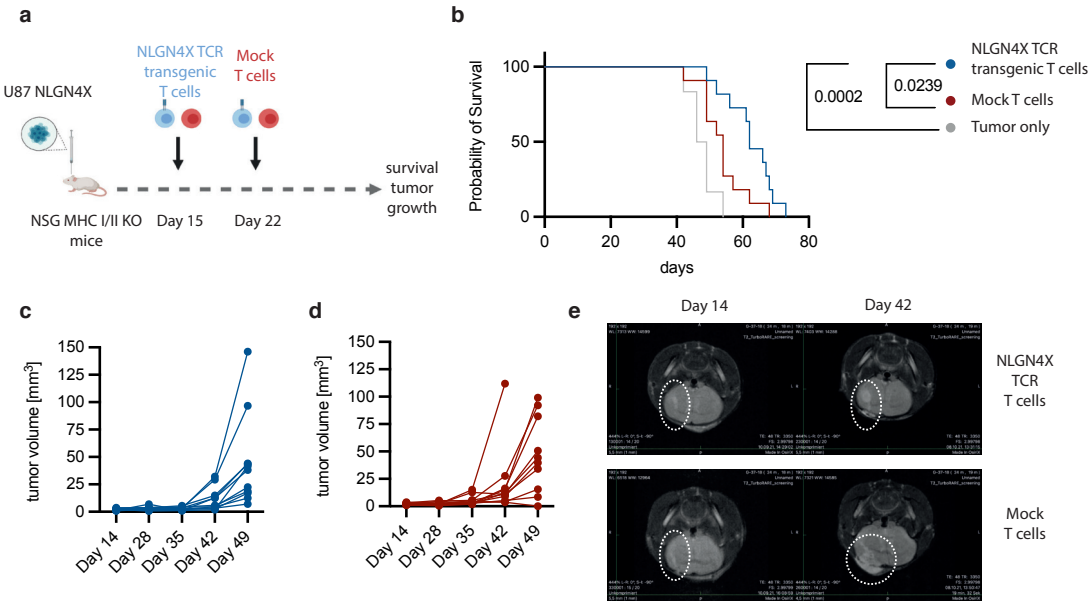

Figure 18: **Local delivery of NLGN4X TCR transgenic T cells prolongs the survival in an intracranial model of U87 NLGN4X gliomas**
a Schematic overview of the experimental workflow: NSG MHCI/II KO mice were challenged with 0.1 Mio. U87 NLGN4X glioma cells and treated with injection into the contralateral ventricle with two doses of either NLGN4X TCR transgenic T cells or Mock control T cells or were left untreated. **b** survival curves of n=11 animals per group for NLGN4X and Mock T cells and n=6 animals in the tumor only group, *Log-Rank-test* **c** and **d** individual tumor growth curves of **c** NLGN4X-TCR-T, **d** Mock T cells-treated animals. **e** exemplary magnet resonance tomography images on day 14 and 42 after tumor cell inoculation for a NLGN4X-TCR-T treated mouse compared to a matched animal of the Mock T cell group (white circles indicate the area of tumor growth: hyperdense tumors visible)

4.2 Part-2 Characterisation of the mechanisms of antigen presentation in the local tumor microenvironment and its implications for CD8 T cell driven immune responses

This part of the thesis was conducted in cooperation with Micheal Kilian. If not stated differently presented results or analysis were obtained by myself. Michael Kilian established and validated the Cx3cr1^{CreERT2}-MHCII^{flox} mouse model and provided evidence of an impaired survival and response to immune checkpoint blockade in case of MHC class II deletion. I validated the genetic knock-out of MHC class II by immunofluorescence and investigated the immune cell compartments by the means of immunofluorescence. I then used the GL261 Full OVA tumor model to assess the impact of the genetic MHC class II depletion in the context of a tumor model with a defined antigen. Using single cell sequencing and in vitro co-culture experiments Michael Kilian, Chin Leng Tan (both Department of Neuroimmunology, German Cancer Research Center) and Ron Sheinin (Systems Immunology, Madi Lab, University of Tel Aviv) deciphered the molecular mechanism that Osteopontin on Macrophages drives TOX-mediated T cell exhaustion through NFAT signalling. Using these results I investigated a second single cell data set of MHC class II depleted and MHC II proficient GL261 tumor bearing mice to validate these findings and added the CCL3/4-CCR5 interaction to that dataset.

4.2.1 Validation of Cx3cr1$^{\mathbf{CreERT2}}$-MHCII$^{\mathbf{flox}}$ mouse model in the context of EAE and GL261 brain tumors – development of immunofluorescence staining of MHC II expression

A Cx3cr1$^{\mathrm{CreERT2}}$-MHCII$^{\mathrm{flox}}$ mouse model (similiar to [Wolf et al., 2018]) was utilized to study the impact of a genetic deletion of MHC class II on tumor growth. The model had previously been verified in the setting of experimental autoimmune encephalomyelitis by Michael Kilian.
Following these results I aimed to validate the genetic deletion of MHC class II in Cx3cr1$^{\mathrm{CreERT2}}$-MHCII$^{\mathrm{flox}}$ mice in the setting of brain tumors by immunofluorescence (IF) staining. Therefore cryofixed sections of GL261 MOKO gliomas from cre^{+} vs. cre^{-} mice treated with immune checkpoint blockade were obtained from Micheal Kilian. To specifically detect MHC class II in murine brain tumors I established an immunofluorescence staining of MHC class II on myeloid cells and tumor cells. Cryosections of brain tumors of PBS perfused mice were stained with a MHC class II targeting antibody. Widefield microscopy revealed specific binding of a MHC II specific antibody. MHC II KO animals showed a clear reduction of MHCII compared to MHC II WT animals. Confocal microscopy confirmed specific colocalization of the MHC class II staining and corresponding nuclei. (comp. Fig. 19 a)

4.2.2 MHC class II deletion on myeloid cells drives reduced T cell infiltration in gliomas

As illustrated previoulsy MHC class II driven antigen presentation has a decisive impact on the progression of tumors and thus the efficiency of immunotherapeutic approaches might

a

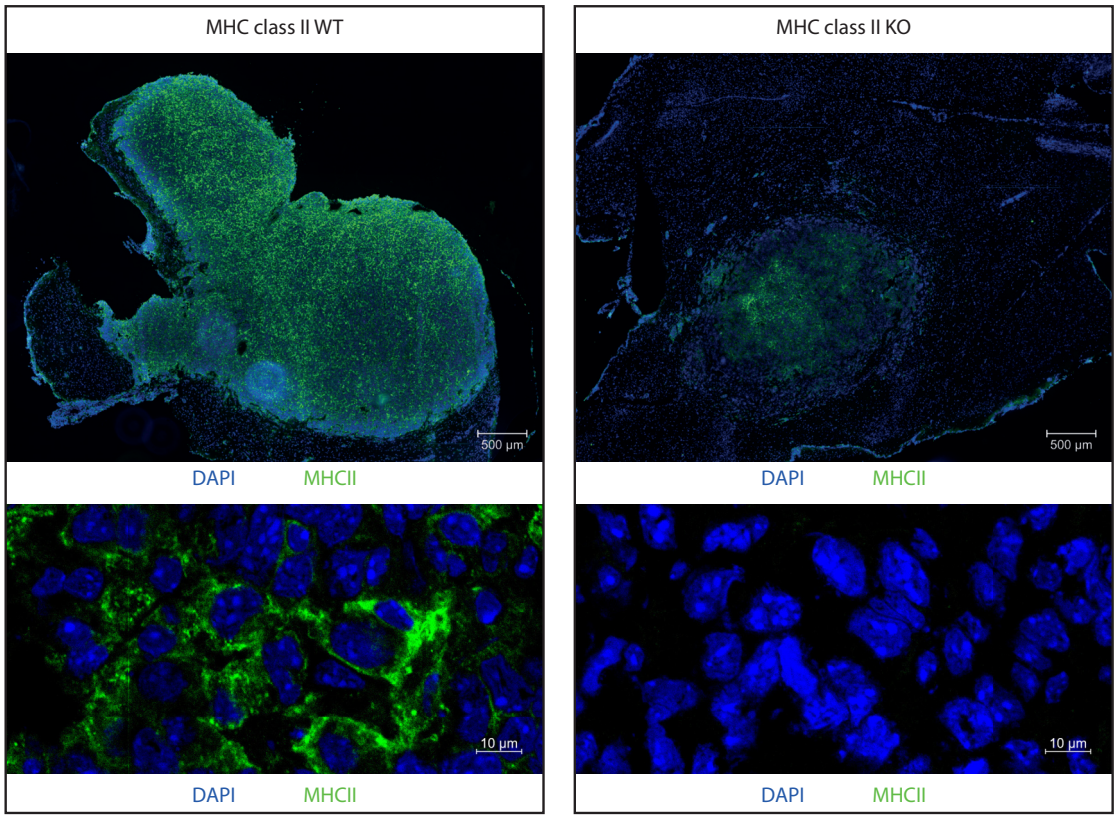

Figure 19: **MHC II expression of GL261 tumor bearing TAM-treated Cx3cr1$^{\mathbf{CreERT2}}$-MHCII$^{\mathbf{flox}}$ mice**
a Immunofluorescence images of GL261 tumors: Representative pictures of one MHC class II KO and one MHC class II WT mice: Widefield microscopy overview showing specific staining of MHC class II within the tumor region and maximal magnification shows specific labeling of cells.

be impacted by the level of MHC class II expression on immune cells in the tumor microenvironment as well.
Michael Kilian assessed the effect of reduced MHC II expression on myeloid cells on the treatment success of immune checkpoint blockade by challenging Cx3cr1^{CreERT2}-MHCII^{flox} mice with intracranial GL261 tumors in the context of combined checkpoint therapy. A treatment effect of the Immune checkpoint blockade was diminshed in MHC II KO mice resulting increased tumor volumes and impaired survival. This effect was not detecable if only microglia cells were deprived of MHC II expression. (*Kilian et al. , Manusscript submitted*)
To investigate the cause of the reduced survival of MHC II deleted mice I hypothesized that reduced immune infiltration alters the tumor microenvironment to be less immunogenic. Therefore, I developed immunofluorescence imaging of the different immune cell compartments in the context of MHC class II deletion in order to evaluate the effects on the tumor microenvironment. Additionally, flow cytometric analysis was performed by Michael Kilian and me to evaluate possible findings of immunofluorescence microscopy.

Development of MHC class II and myeloid cell marker co-staining In order to specifically detect expression of MHC class II on tumor associated antigen-presenting cells by the use of immunofluorescence microscopy three different myeloid cell markers were tested. Ionized calcium-binding adapter molecule 1 (Iba-1) also known as allograft inflammatory factor 1 is commonly considered to be expressed on microglia and macrophages and is up-regulated during activation [Watano et al., 2001]. CD11b and F4/80 are commonly used for myeloid cell differentiation in flow cytometric analysis with F4/80 as a characterizing marker for macrophages.
Different concentrations of all three markers were evaluated for binding specificity. Usage of Iba-1 could not specifically label myeloid cells (comp. Fig. 20 a), but F4/80 specifically stained cells of myeloid compartment and was correctly colocalized with MHC II+ cells in MHC II WT mice (comp. Fig. 20 b) and not in MHC II KO mice (white asterisks, comp. Fig. 20 b).

Validation of reduced MHC class II expression on myeloid cells in the tumor microenviroment Using immunofluorescence miscroscopy the hypothesis if genetic depletion of MHC class II results in reduced infiltration or local proliferation of myeloid cells in the tumor microenvironment was analyzed. To further validate this hypothesis MHC II+ cells and F4/80+ as well as double+ cells were quantified by the means of immunofluorescence in four ICB treated MHC II KO and MHC II WT mice respectively. Confocal microscopy of the tumor border of GL261 gliomas showed clearly reduced amount of MHCII+ cells. Subsequent quantitative analysis of representative images from three different animals per group revealed significantly decreased expression of MHC II on both F4/80- and F4/80+ cells in MHC II KO animals (comp. Fig. 21 c), thereby confirming the efficiency of the genetic Knock-out. The percentage of F4/80 and MHC II double+ cells was significantly reduced resulting in decreased numbers of antigen presenting cells via MHC class II (comp. Fig. 21 b). Cell counts for F4/80+ cells as well as the normalized ratio of F4/80+ myeloid cells of all counted cells did not differ compared to MHC II

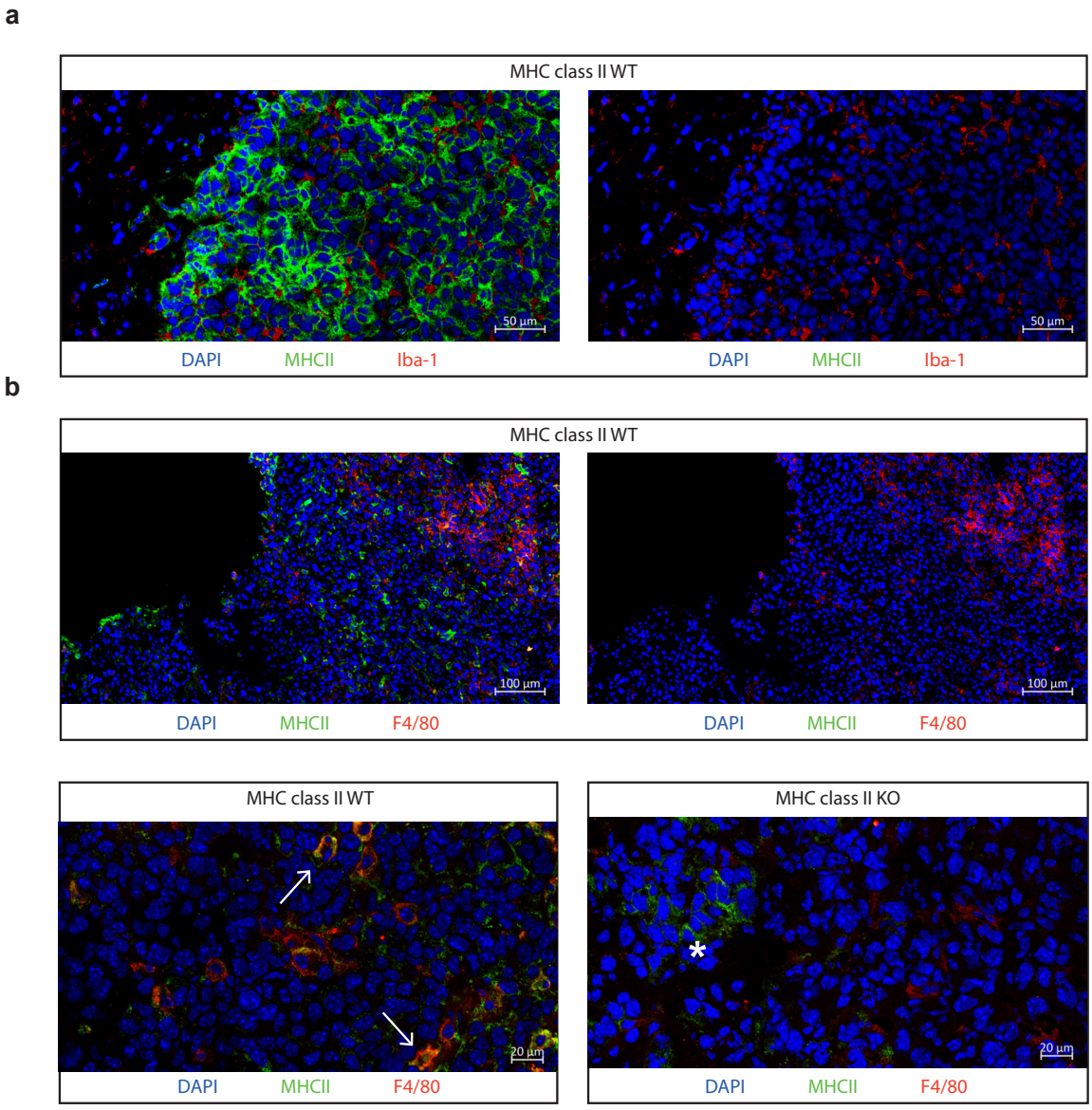

Figure 20: **Detection of MHC II expression on myeloid cells by immunofluorescence**
Confocal microscopy of GL261 gliomas of ICB treated Cx3cr1$^{\mathrm{CreERT2}}$-MHCII$^{\mathrm{flox}}$ mice **a** Iba-1 – MHC II costaining with no detectable Iba-1 and MHC II double positive cells *left overlay, right Iba-1 only* **b** F4/80 – MHC II costaining showing F4/80+-MHC II+ cells which were only present in MHC II wildtype mice (arrows) but not in MHC II knockout mice (asterisks) at maximal magnification *Exemplary immunofluorescence images of the same MHC class II WT mouse and one matched MHC class II KO mouse*

wildtype mice (comp. Fig. 21 a and b). Interestingly, the percentage of MHC class II+ cells of F4/80+ cells was also reduced suggesting a decrease of MHC class II expression on tumor cells as well. To summarize, genetic deletion of MHC class II on myeloid cells did not lead to a reduced number of myeloid cells in the tumor micromilieu.

MHC class II KO reduces the cell numbers of tumor infiltrating T cells Next, other immune cell compartments were analyzed using immunofluorescence imaging of the different T cell subsets in MHC II deleted mice. Histological analysis showed a reduction of CD3+ T cells (comp Fig. 22 a). In order to further differentiate the T cells I tested for expression of CD4 and CD8a. CD4+CD3+ cells could not be detected within tumors of MHC II KO mice (comp. Fig. 22 a). Surprisingly, the amount of CD8a+ T cells was also dramatically decreased in MHC II KO mice (comp. Fig. 22 a). Further analysis of these results by the means of flow cytometry was required in order to validate these results. Nevertheless, the present immunofluorescence images provided interesting starting points for investigations of the involved mechanisms.

Tumoral MHC class II expression in single animals is affected by genetic MHC II deletion on myeloid cells As the previous immunofluorescence data suggests that genetic deletion of MHC class II on myeloid cells influences the infiltration of the T cells, I hypothesized that tumor cells might be subject to changes induced by a MHC class II KO as well.
In order to validate this hypothesis, I aimed to specifically detect MHC II on tumor cells. Since gliomas initially derive from mutations in astrocytes, they still express markers that are typically associated with astrocytes. Glial fibrillary acidic protein (GFAP) is commonly used in the histological diagnosis of gliomas. [van Bodegraven et al., 2019] I developed an immunofluorescence-based assessment of MHC class II expression on GFAP expressing cells and therefore evaluated the impact on genetic deletion of MHC II on myeloid cells for MHC class II expression on non-myeloid cells in the tumor microenvironment. Confocal microscopy revealed that GFAP was highly expressed on cells of the tumor microenvironment (comp. Fig. 23).
The number of GFAP and MHC II doubled+ cells was reduced in both immune checkpoint blockade and isotype control treated (comp. Fig. 23 a) MHC II KO mice suggesting a diminished upregulation of tumoral MHC II expression in the absence of MHC II on myeloid cells. However, as GFAP is not exclusively expressed on tumor cells these findings have to be further validated by a different method.
Thus, I analyzed flow cytometric data of Cx3cr1$^{\mathrm{CreERT2}}$-MHCII$^{\mathrm{flox}}$ mice challenged with intracranial GFP labeled GL261 gliomas (comp. Fig. 23 b). For further analysis of the distinct myeloid subsets I further differentiated them by the use of common markers. Monocytes were classified as either Ly6C$_{\mathrm{low}}$ or Ly6C$_{\mathrm{high}}$ CD45+ CD11b+ cells, while antigen-presenting cells were defined by the dendritic cell marker CD11c. Microglia were defined as CD45$_{\mathrm{intermediate}}$ and CD11b+ cells. As expected, dendritic cells showed the highest amount of myeloid MHC class II surface proteins. According to previously acquired results the amount of MHC II on monocyte derived cells and microglia was significantly reduced in MHC II KO mice (comp. Fig. 23 b).

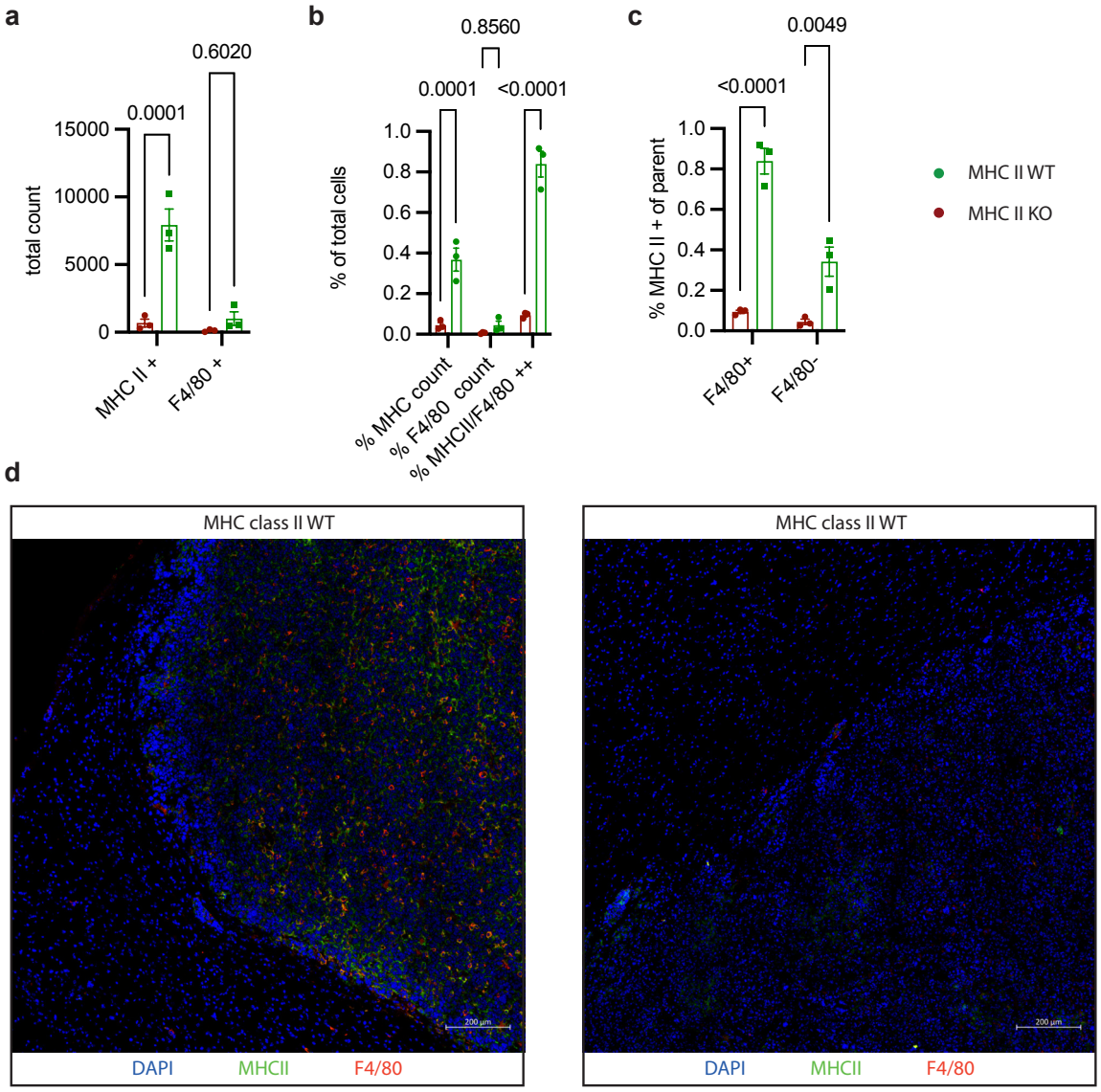

Figure 21: **Immunofluorescence microscopy shows no changes in abundance of myeloid cells in MHC class II KO animals**
Confocal microscopy of GL261 gliomas of ICB treated Cx3cr1^{CreERT2}-MHCII^{flox} mice **a-c** Quantitative analysis in ImageJ of representative confocal images of 3 ICB-treated MHC II KO and MHC II WT mice respectively, counting+ cells and double+ cell **a** Total cell number **b** Percentage of F4/80+, MHC class II+ cells and double positive cells of all counted cells **c** Percentage of MHC class on F4/80+ and F4/80 - cells *n=3, Mean with SEM. Two way ANOVA test.* **d** Confocal microscopy of F4/80+ myeloid cells (representative images of 4 mice per group)

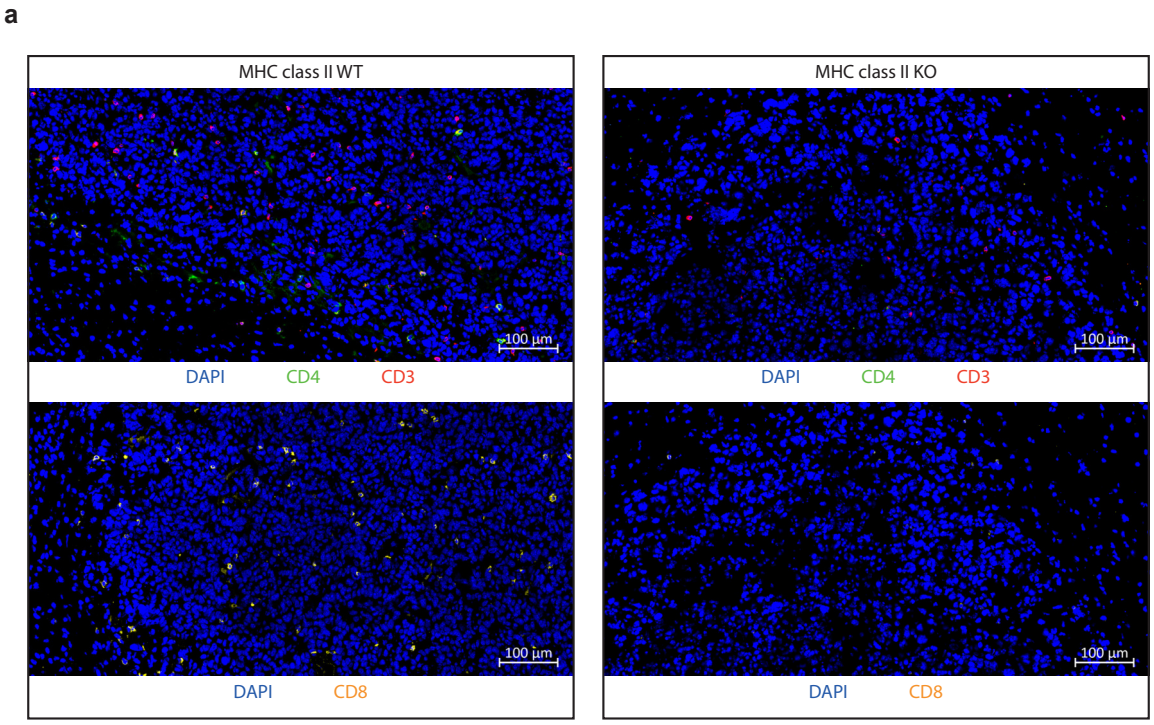

Figure 22: **Immunofluorescence microscopy points to reduced numbers of both the CD8 and CD4 T cell compartment**
Confocal microscopy of GL261 gliomas of ICB treated Cx3cr1$^{\text{CreERT2}}$-MHCII$^{\text{flox}}$ mice **a** CD3+ CD4+ T cells (upper row) and CD8+ T cells (lower row) (representative images of 3 mice per group)

Tumor cells were selected as CD45- and GFP+ cells. Tumor cells in MHC class II KO mice depicted heterogenous expression of MHC class II with a tendency towards decrease expression values compared to MHC class II wildtype animals (comp. Fig. 23 b). Summarizing the results of the flow cytometric and immunofluorescence analysis there are hints that genetic deletion of MHC class II in myeloid cells also affects the tumoral MHC class II expression. However, a clear reduction of MHC II surface expression could only be detected in half the animals that were analyzed. Therefore, further mechanisms seem to be involved in the regulation of tumoral MHC II expression.

MHC II deletion does not affect the morphological properties of tumoral vessel
Due to the reduced amounts of cells of both the myeloid and the T cell compartment I hypothesized that MHC II deletion either affects the infiltration of immune cells or their local proliferation or possibly both.
As CD4+ T cells depict reduced activation in the absence of MHC class two (comp. Fig. 26d), the levels of inflammatory cytokines such as IFN-γ might be reduced in the tumor microenvironment of MHC II knockout mice. IFN-γ is known to be involved in the regulation of cellular adhesion molecules like intercellular adhesion molecule 1 (ICAM-1) on astrocytes [Shrikant et al., 1994] and endothelial cells [Bittner et al., 2013]. IFN-γ blocks the inhibition of ICAM-1 expression by the TWIK-related potassium channel-1 (TREK1) and thus increases leucocyte migration. [Bittner et al., 2013] Consequently, I hypothesized that MHC class II deleted mice exhibit a downregulation of ICAM-1 on endothelial cells due to reduced signaling via IFN-γ and thereby are characterized by limited transendothelial immune cell migration.
To assess the expression of ICAM-1 on endothelial cells I developed an immunofluorescence staining of ICAM-1 and CD31 in GL261 glioma bearing Cx3cr1$^{\mathrm{CreERT2}}$-MHCII$^{\mathrm{flox}}$ mice. Confocal imaging of MHC class II knock-out and wildtype mice revealed specific labeling of CD31+ brain endothelial cells. ICAM-1 was detectable on both non-endothelial (CD31 negative) and endothelial CD31+ cells (comp. Fig. 24 a and b). Double+ cells were considered as endothelial cells expressing ICAM-1 for leucocyte transmigration. However, there were no obvious differences in absolute expression levels of ICAM-1 on either endothelial or non-endothelial cells (comp. Fig. 24 a and b) between MHC II KO and MHC II WT animals. Genetic deletion did not result in diverse vascularization patterns and did not affect the presence of CD31 and ICAM-1 double+ cells. Consequently, the absence of MHC class II rather impacts the local proliferation and functional state of infiltrating and brain resident immune cells than the migration from the blood stream into the tumor site.

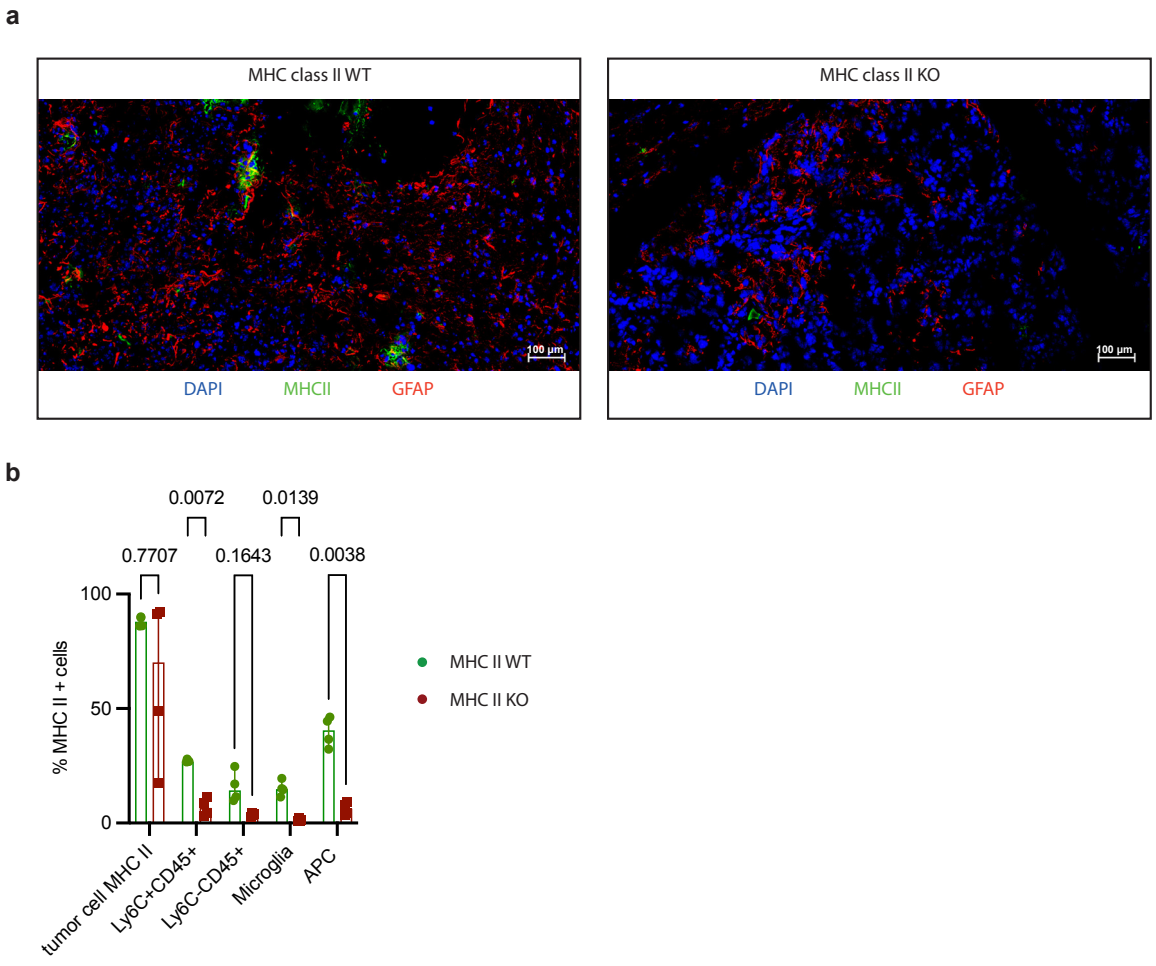

Figure 23: **MHC class II KO results in differences in tumoral MHC class II expression**
Confocal microscopy of GL261 gliomas of isotype control treated Cx3cr1$^{\text{CreERT2}}$-MHCII$^{\text{flox}}$ mice **a** GFAP and MHC class II co-Staining **b** Flow cytometric analysis of MHC class II WT and KO animals that were challenged with GFP+ GL261 tumors. After termination tumors were subjected to FACS analysis: % of MHC II+ cells per cell type *n=4 per group, Twoway-ANOVA, Mean with SEM*

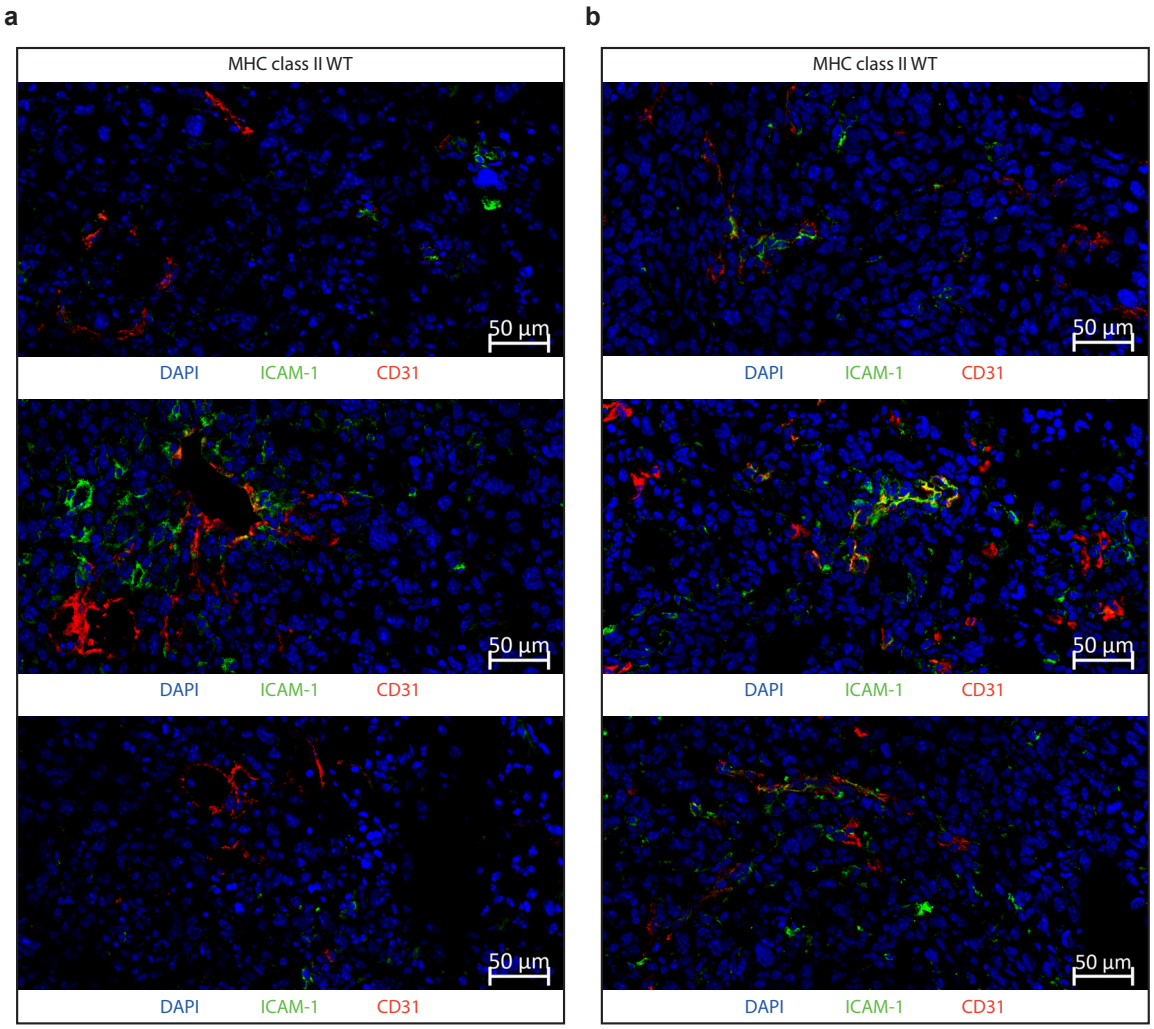

Figure 24: **MHC class II depletion does not alter the morphology of the tumoral vessels**
Confocal microscopy of GL261 gliomas of isotype control treated Cx3cr1$^{\text{CreERT2}}$-MHCII$^{\text{flox}}$ mice **a** and **b** Representative images of ICAM-1 and CD31 Co-Staining *n=3*

4.2.3 Generation of GL261-OVA cell lines and subsequent *in vitro* validation

After transfection GL261 cell lines were tested against T cells isolated from OT-I T cell receptor transgenic C57Bl/6J mice by the means of a T cell activation assay and an LDH release cytotoxicity assay. Subsequent flow cytometric analysis revealed increased proportions of IFN-γ positive CD8 T cells when cocultured with OVA – MHC I epitope expressing GL261 cell lines (comp. Fig. 25a). Evaluation of the cytotoxicity against epitope expressing target cells showed effective killing of OVA MHC I epitope and OVA minigene expressing cell lines (comp. Fig. 25b). OVA full length glioma cells were specifically lysed; however, the efficiency was slightly reduced. (comp. Fig. 25b).
OVA MHC class II epitope expressing and untransfected GL261 cell lines did not activate OT-I T cells and were not specifically lysed in the cytotoxicity assay (comp. Fig. 25b). Consequently, Gl261 OVA cell lines showed sufficient surface expression of the MHC class I epitope. OT-I TCR transgenic were able to specifically recognize and kill the related the target cells.

4.2.4 Antigen presentation via MHC class II affects the functionality of both the CD4 and CD8 T cell compartment

The following experiment was conducted in cooperation with Michael Kilian.
The previous data provide starting points for an analysis of the functional impact of MHC class II on T cell infiltration as well as activation and functionality. The ovalbumin (OVA) protein comprises a well defined MHC class I restricted epitope and an MHC class II epitope with high immunogenicity respectively. Therefore, the OVA antigen model allows the assessment of differences in anti-tumor immunity in relation to either the MHC class I or MHC class II epitope.
Consequently, the initially generated GL261-OVA Full epitope glioma cell line was used and Cx3cr1$^{\mathrm{CreERT2}}$-MHCII$^{\mathrm{flox}}$ mice were challenged with the established cell line for further examination of differentially regulated T cell responses.
Tumor growth was monitored by MRI. MHC II knockout mice showed increased tumor growth between the second and third MRI on days 18 and 25 after the initial tumor cell implantation. The tumor volumes between MHC class II KO and WT mice differed significantly on day 25 after tumor cell inoculation. (comp. Fig. 26 a)
Tumor bearing animals were perfused on day 26 and isolation of tumor infiltrating lymphocytes was performed. Tumor infiltrating lymphocytes were re-stimulated with the respective MHC class I and MHC class II restricted peptide of the OVA protein.
In accordance to the findings of the immunofluorescence staining of ICB treated GL261 gliomas the absolute number of CD4 T cells was strongly impaired in MHC II deleted mice (comp. Fig. 26 b). The count of CD8 T cells normalized to the tumor volume was not significantly decreased (comp. Fig. 26 c) suggesting a preserved infiltration or proliferation of CD8 T cells even in the absence of MHC class II. There was a significant difference in the Median Fluorescence Intensity (MFI) of IFN-γ of CD4 T cells in response to the OVA II peptide between MHC class KO and WT mice indicating reduced funcitionality of the CD4 T cell compartment (comp. Fig. 26 d). In line with these findings the amount of IFN-γ+ CD4 T cells was reduced in MHC II KO mice (comp. Fig. 26 f). For CD8 T cells

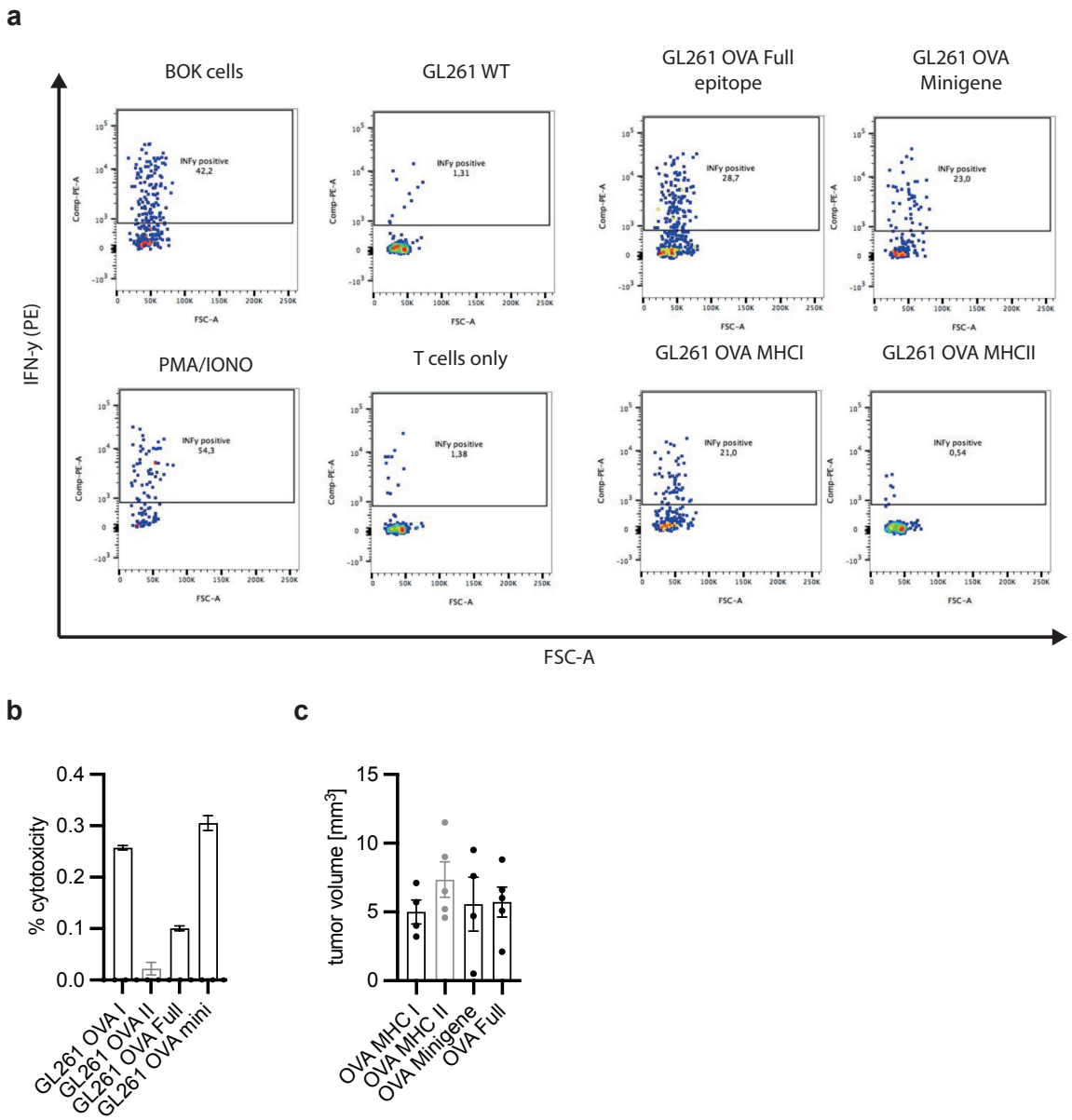

Figure 25: **Validation of OVA expressing GL261 tumor cell lines**
a. Flow cytometric analysis of 48 h cocultures of OVA GL261 cell lines with OT-I TCR transgenic T cells: differential amounts of IFN-γ (IFN-γ) positive CD8 T cells (gating according to FMOs) in the MHC I epitope expressing cell lines compared to negative control GL261 naiv (untransfected) cells. 6 h of PMA/IONO stimulation served as a positive control for maximum IFN-γ release. **b** LDH release cytotoxicity assay. Percentage of maxmium LDH release from target cells normalized to cell culture medium background and spontanous LDH release of cultured cells. *n=3 technical replicates* **c.** Tumor volumes of GL261 OVA glioma cell lines at day 12 after cranial tumor injection into Bl/6J mice. *GL261 OVA MHC I, GL261 OVA Minigene: n=4, GL261 OVA MHC I and II, GL261 OVA MHC II: n=5, Mean with SEM*

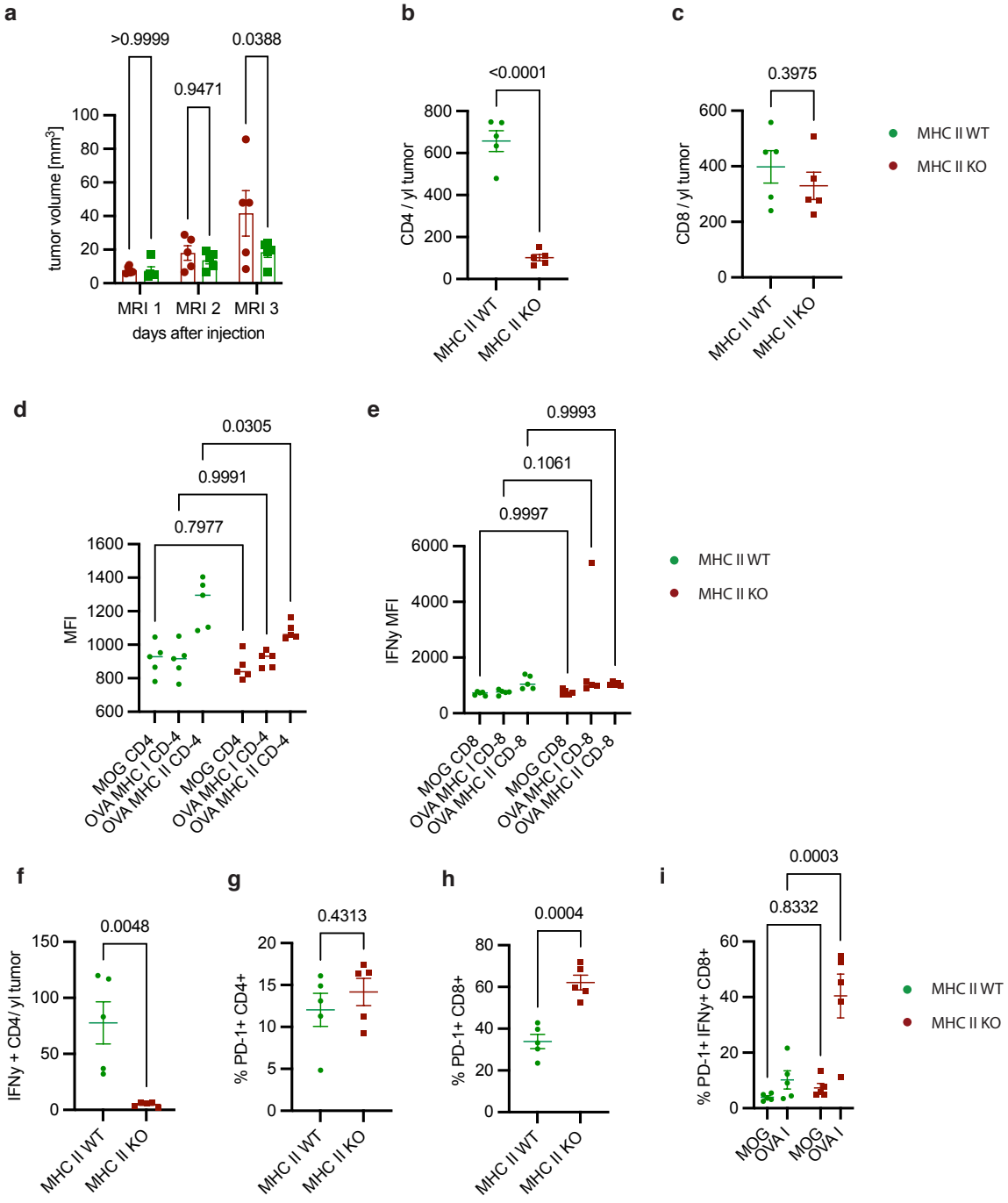

Figure 26: *Continued on next page.*

Figure 26: **MHC class II KO results in reduced functionality of the CD4 T cell compartment and drives exhaustion of antigen-specific CD8 T cells**
a Tumor volumes of MHC II KO and MHC II WT animals on MRI days 11, 18 and 25. *n= 5, Mean with SEM, Twoway-ANOVA* **b** and **c** number of CD4 (b) and CD8 (c) T cell normalized to the tumor volume. *n=5, Mean with SEM, Unpaired t-test* **d** IFN-γ Median Fluorescence intensity (MFI) of CD4 T cells under different restimulation conditions (OVA I = MHC class I OVA peptide, OVA II = MHC class II OVA peptide) *n=5, Mean with SEM, Twoway-ANOVA* **e** IFN-γ MFI of CD8 T cells under different restimulation conditions *n=5, Median with Range, Twoway-ANOVA* **f** Count of CD4 IFN-γ+ cells normalized to the tumor volume. *n=5, Mean with SEM, Unpaired t-Test* **g** and **h** Percentage of PD-1+ CD4 (g) and CD8 (h) T cells *n=5, Mean with SEM, Unpaired t-test* **i** Percentage of IFN-γ+ PD-1+ CD8 T cells *n=5, Mean with SEM, Twoway-ANOVA*

there was no significant difference in the IFN-γ MFI after stimulation with the OVA I peptide. (comp. Fig. 26 e) Further analysis of the different T cell compartment showed a clear increase of the percentage of PD-1+ CD 8 T cells in MHC II KO mice compared to MHC II WT mice demonstrating increased exhaustion of CD8 T cells. (comp. Fig. 26 h) Interestingly, this effect was not visible for CD4 T cells (comp. Fig. 26 g). Analysis of PD-1+ CD8 T cells showed a significant MHC II dependent increase of antigen specific (IFN-γ positive T cells in response to OVA restimulation) PD-1+ CD8 T cells in MHC II KO mice, which suggests exhaustion of antigen-reactive T cells in the abscence of MHC class II (comp. Fig. 26 i).
Together these results highlight two findings concerning the T cell compartment in the abscence of MHC class II: First there is a reduced amount of both antigen-specific and unspecific CD4 T cells and second an increased exhaustion of CD8 T cells in general and of antigen-reactive CD8 T cells in particular. Therefore, the absence of antigen presentation via MHC class II on myeloid cells resulted in an exhausted phenotype of antigen-specific T cells and diminished their capability to efficiently mediate tumor control.
Consequently, these results highlight that MHC class II is essential for the stemness of antigen-specific CD8 T cells, as MHC class II loss drives exhaustion and reduced functionality of these cells. For further analysis of the functional state of CD8 T cells in dependence of an MHC class II proficient immune compartment single cell sequencing was applied to discover possible mechanisms.

4.2.5 Increased Osteopontin expression on M2-like Macrophages and decreased CCL-3/CCL4-CCR5 signaling in the abscence of MHC class II drives dysfunctional CD8 T cell states

Mutual planning and data acquisition with M. Kilian. Development and validation of the Osteopontin-CD29-NFATc1 axis by M.Kilian and Ron Sheinin (Systems Immunology, Madi Lab, University of Tel Aviv). Based on the findings of Kilian et al. I investigated a second single cell data set from murine MHC class II depleted and MHC class II proficient mice bearing intracranial GL261 tumors and validated the previously observed mechanisms in this data set.

Following the previous findings single cell sequencing was applied in order to analyze the mechanisms that drive MHC II dependent T cell exhaustion.

Cx3cr1$^{\text{CreERT2}}$-MHCII$^{\text{flox}}$ mice were challenged with intracranial GL261 wildtype tumors and tumor growth was confirmed on day 17 after tumor cell inoculation with MRI. On day 21 GL261 gliomas were isolated and subjected to FACS sorting for CD45+ CD11b+ myeloid cells and CD45+CD3+ T cells of 6 mice per group. Hashing anitbodies were used in order to combine different animals in one sequencing runs. After sequencing and pre-processing (*performed by Chin Leng Tan* and following standard quality check 1011 T cells and 2433 myeloid cells in total were obtained. MHC class KO cells were represented at lower numbers compared to MHC class WT cells with 1052 and 2392 total cell counts respectively. Integrated analysis and t-SNE (t-Distributed Stochastic Neighbor Embedding) based representation of the dataset resulted in 13 different clusters.

The myeloid cells clustered into three different macrophage clusters (M1-Ma, M2-Ma, Ccr7-Ma), two microglia clusters (hMg, daMg), three different dendrtic cell clusters (CD209a DC, pDC, cDC2) and one cluster of NK cells, neutrophils and mast cells respectively. (comp. Fig. 27 b) T cells in the integrated analysis were seperated into one cluster of CD3+ T cells and one cluster of proliferating CD8a T cells (mKi67 eCD8). (comp. Fig. 27 b).

The myeloid clusters were defined according to common markers to disintinguish myeloid cell types. M1-like macrophages were identified by the M1 marker *Nos2*, high expression of MHC class II molecules like *H2-Ab1* and the co-stimulatory receptor *CD86* (comp. Fig. 27 d) [Orecchioni et al., 2019] M2-like macrophages were defined by the expression of *Tgfb1* and *Arg1*. [Zhang et al., 2016], [DeNardo and Ruffell, 2019] Ccr7 Macrophages expressed the marker *Ccr7* and pro-inflammatory markers like *CD80*, *Il1b* and the chemokine Ccl22 that is also known as Macrophage-derived chemokine (comp. Fig. 27 d). [Orecchioni et al., 2019] The microglial clusters expressed the common microglial markers *HexB*, *Sparc* and *P2ry12*. (comp. Fig. 27 d) While one clusters was defined as homoestatic microglia and one clusters as disease associated microglia with high expression of *Cd68* and *ApoE* (comp. Fig. 27 d) in accordance to Jordao et al. [Jordao et al., 2019] and downregulated expression of *Tmem119* and *P2ry12* [Jordao et al., 2019]. CD209a dendritic cells were identified by their expression of *CD209a*, MHC class II (*H2-Ab1*) and Cxcl10 [Hirako et al., 2016] (comp. Fig. 27 d) . Other subtypes of dendritic cells (*Ptprc*$^{\text{high}}$ and *Itgax*+) that were identified in the dataset included plasmocytoid dendritic cells (pDC) classified by high expression of *Irf8* and *Zeb2* and cDC2 dendritic cells with high levels of *Irf4* and *Id2* (comp. Fig. 27 d). [Collin and Bigley, 2018]

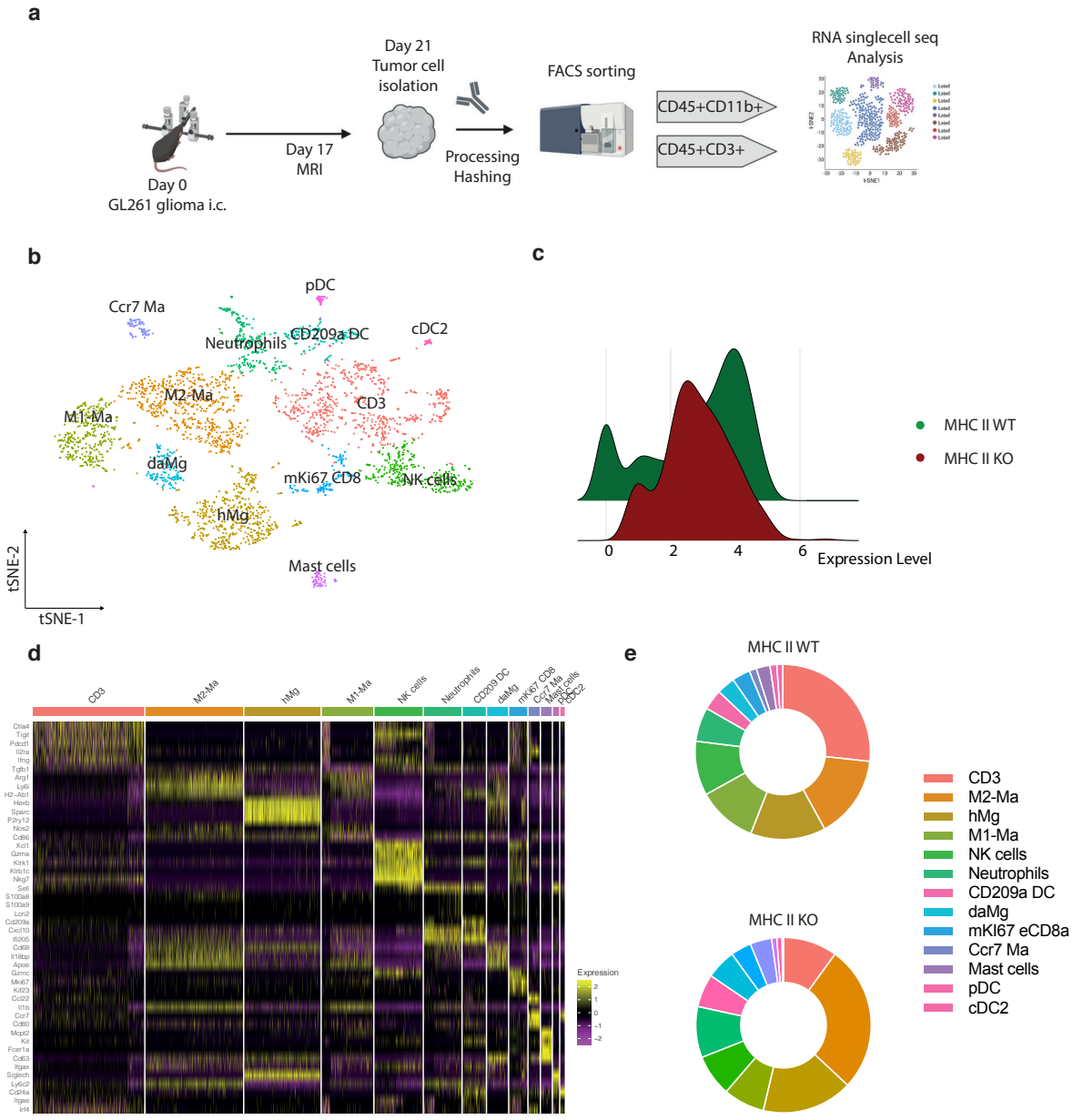

Figure 27: *Continued on next page.*

Figure 27: **Single cell sequencing of GL261 gliomas in Cx3cr1^{CreERT2}-MHCII^{flox} mice reveals differential enrichment of myeloid cell clusters between MHC class II wildtype and knock-out mice**
a Experimental overview: Intracranial GL261 were isolated on day 21 and subjected to RNA single cell sequencing after FACS sorting for T cells (CD45+CD3+) and myeloid cells (CD45+CD11b+). **b** t-SNE (t-Distributed Stochastic Neighbor Embedding) based representation of n=3444 single cells into 13 clusters. **c** Global MHC class II expression of all myeloid cell subsets confirming MHC class II KO. **d** Heatmap of cluster defining markers. **e** Cell numbers per cluster as relative percentage of all cells of all MHC II WT single cells (CD3 = 26.71% - M2-Ma = 15.34 % - hMg = 13.87 % - M1-Ma= 10.99 % - NK cells = 10.03 - Neutrophils = 6.31 % - CD209a DC = 3.76 % - daMg = 3.38 % - miK67 eCD8a = 3.34 % - Ccr7 Ma = 1.34 % - Mast cells = 2.55 % - pDC = 1.25% - cDC = 1.08 %, n=2392 cells) and MHC II KO single cells (CD3 = 9.98% - M2-Ma = 26.99 % - hMg = 16.73 % - M1-Ma= 7.60 % - NK cells = 7.7 % - Neutrophils = 9.41 % - CD209a DC = 6.08 % - daMg = 5.51 % - miK67 eCD8a = 3.80 % - Ccr7 Ma = 3.99 % - Mast cells = 0.95 % - pDC = 0.95 % - cDC = 0.28 % n=1052 cells).

NK cells showed high abundance of the common markers *Nkg7, Klrb1c, Klrk1, Xcl1* and *GzmA*. [Bottcher et al., 2018][Ng et al., 2020] Neutrophils had upregulated gene expression of *Lcn2* [Schroll et al., 2012] and *S100A8* and *S100A9* [Ryckman et al., 2003]. Mast cells were defined by *Mcpt2* and *Mcpt4* (comp. Fig. 27 d). [Dwyer et al., 2016]
The MHC class II deletion resulted in different relative proportions of cell clusters in MHC II KO vs. WT tumors. In the myeloid cell compartment an increase in the relative percentage of M2 like macrophages in MHC class II deleted animals was observable, while inflammatory M1-like macrophages were reduced in MHC II KO mice and Ccr7 macrophages were only present in the MHC class II KO animals suggesting a strong effect of the genetic knock-out on the local tumor microenvironment. (comp. Fig. 27 e)
T cells were identified by typical T cell markers *Cd3e*, *Ifng*, *Pdcd1*, *Ctla-4* and were seperated into two seperate cluster with expression of *GrzC* and *mKi67* in the mKi67 CD8a cluster (comp. Fig. 27 d). T cells were then seperately analysed resulting in 8 clusters with 3 Cd8a+ clusters, two CD4 clusters, two Treg clusters and one cluster of gamma-delta T cells. (comp. Fig. 28 a). The CD4 T cells clustered in one cluster with the naive T cells marker *Il7r* and reduced expression of *Ifng*, while the activated CD4 T cells showed high expression of *Ifng* and *Ctla-4*. The three CD8a T cell clusters differed in their expression of activation markers, while the naive T cells had high abundance of the stemness markers *Tcf7* [Siddiqui et al., 2019] and *Sell* [Szabo et al., 2019], there also two clusteres showing an activated and proliferating genotype with high levels of *GzmA* and *mKi67* (Ki-67). The Tregs were classified by high expression of *Icos* for one cluster and *Ctla-4* and *Foxp3* for the other Treg cluster. [Guo et al., 2018]
The MHC class II KO also resulted in a clear reduction in the abdunance of T cells in MHC II KO animals.
As antigen specific CD8 T cells showed an exhausted phenotype in the abscence of MHC class II in previous experiments, CD8a T cells were checked for the expression of different exhaustion markers. GzmA CD8a T cells showed significantly increased expression of Tim3

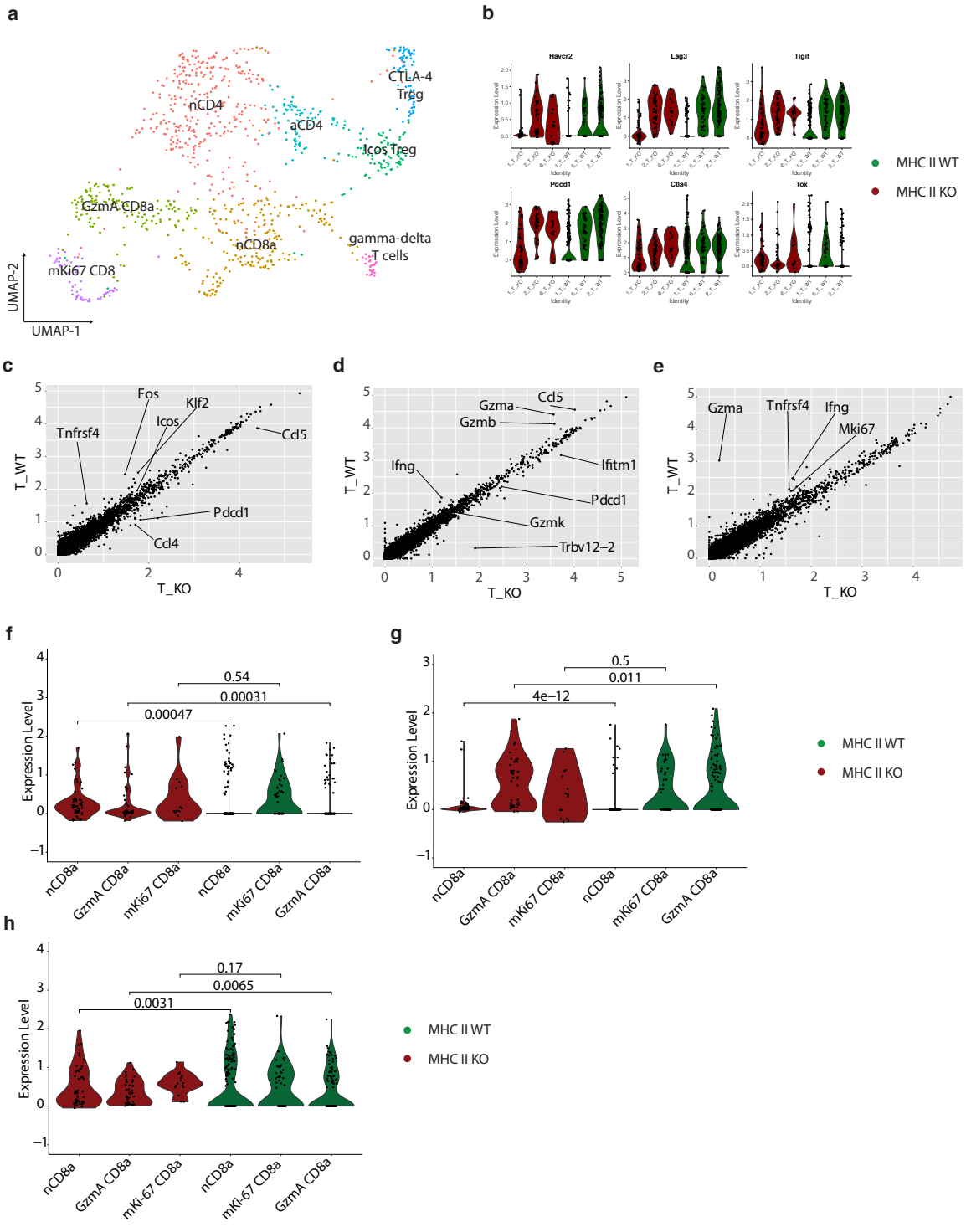

Figure 28: *Continued on next page.*

Figure 28: **CD8a T cells show upregulated expression of exhaustion markers in the abscence of MHC class II and downregulation of effector molecules**
a UMAP-based representation of CD3+ sorted T cells in 8 disintinct clusters. **b** Exhaustion markers for CD8a+ T cell clusters: Tim3 (*Havcr2*), Lag3, Tigit, PD-1 (*Pdcd1*), Ctla4 and Tox **c-e** Differential expression plots of **c** naive CD8a T cells, **d** GzmA Cd8a T cells and **e** mKi67 CD8a T cells. **f-h** Expression plots of the three Cd8a T cell clusters for **f** Tox, **g** Tim3 and **h** NFATC1 *Wilcoxon Test for statistical significance*

(*Havcr2*) and *Tox* (comp. Fig. 28f and g) and therefore matching the exhausted phenotype of T cells that occur at the late stage of murine GL261 gliomas (comp. Fig. **??**), suggesting that the abscence of MHC class II drives T cells into early exhaustion.
Other common exhaustion markers (*Lag3, Pdcd1, Ctla4 and Tigit*) only showed slight changes between MHC class II WT and KO animals (comp. Fig. 28 b). Subsequently, differentially expressed genes were investigated between different MHC class II WT and KO mice in the three different Cd8a T cell clusters. Naive CD8a T cells showed upregulation of the naive marker *Klf2* [Sebzda et al., 2008] and increased expression of *Tnfrsf4* (OX40L) that is known to be expressed on activated T cells [Ware, 2011]. *Fos* as part of the NFATc1 complex [Jain et al., 1992] was also upregulated in MHC class II WT naive T cells. In contrast Pdcd1 was enriched in MHC class II KO T cells, suggesting a rather exhausted state of naive CD8a T cells in MHC II KO mice, while activation markers were enriched in MHC II WT CD8a T cells. (comp. Fig. 28 c) Due to its high expression of Tox and Tim3, the GzmA CD8a T cell cluster was further investigated. The activation marker *Ifng* and the transcripts for the effector molecules Granzyme A and B were enriched in this cluster in the prescence of MHC class II. Interestingly Ccl5 was highly expressed in MHC class II WT driving homing of effector T cells in response to binding to Ccr5 [Seo et al., 2020]. (comp. Fig. 28 d) Similarly, mKi67 Cd8a T cells showed enrichment of the activation markers *Tnfrsf4*, *Gzma*, *Ifng* and *Mki67* (Ki-67) (comp. Fig. 28 e) highlighting the importance of MHC class II to maintain the activation response of the CD8 T cell compartment. Tox has been shown to be a critical regulator of T cell exhaustion [Khan et al., 2019][Scott et al., 2019] and is induced upon chronic NFAT signalling [Scott et al., 2019]. Therefore, CD8a T cell clusters were tested for NFATc1 expression and indeed GzmA CD8a T cells showed signifcantly elevated expression of NFATc1 (comp. Fig. 28 h). Naive CD8a T cells that also had elevated expression of the exhaustion marker PD-1 in differential gene expression analysis showed increased NFATc1 expression (comp. Fig. 28 c,h). Thus, effector CD8a T cells progress into NFATc1 driven *Tox* exhaustion in the abscence of MHC class II signalling.
Next, the mechanisms by which MHC class II abscence results in chronic NFATc1 signalling leading to *Tox* upregulation was investigated in this single cell data set. Therefore, myeloid cell clusters and CD4 T cells as immediate targets of a genetic deletion of MHC class II were analyzed. Differential expression analysis of M2-like makrophages showed upregulation of *Arg1*, *Nos2* and *Cd274* as well as *Ccl5* in MHC class II wildtype mice. *Arg1* and *Cd274* (PD-L1) are generally associated with a rather immunosuppressive phenotype, while Nos2 is a typical pro-inflammatory M1-like marker (comp. Fig. 29 a). MHC class II KO mice showed an enrichment of *Rps28* (Ribosomal protein S28) and

Rps29 (Ribosomal protein S29) as well as increased expression of the mitochondrial ATPase 8 (*mt-ATP8*) suggesting increased protein synthesis and cellular metabolism that could be indicative of increased proliferation of this cluster in case of an MHC class II KO. Interestingly, this cluster exhibited also an upregulation of osteopontin (*Spp1*) in MHC class deleted animals (comp. Fig. 29f). Receptor-ligand analysis (*performed by R.Sheinin, Systems Immunology, Madi Lab, University of Tel Aviv*) predicted osteopontin to bind to CD29 on CD8 T cells. CD29 has been described as a marker of highly cytotoxic human T cells [Nicolet et al., 2020] and has been shown to increase Akt signalling in hepatocellular carcinomas [Jiang et al., 2015]. Akt-signalling results in regulation of the GSK3β NFATc1 cascade that is known to induce increased NFATc1 expression in the context of osteoclast differentiation. [Moon et al., 2012] Therefore, *M.Kilian et al.* (*manuscript submitted*) described the following mechanism: Osteopontin on M2-like macrophages binds to CD29 on CD8a T cells inducing Akt-GSK3 signalling which results in NFAT transcription and TOX upregulation and finally T cell exhaustion.
To analyse why osteopontin is upregulated on M2-like macrophages in the context of MHC class II deficiency CD4 T cells in this data set were assessed for differential marker expression (comp. Fig. 29 c and d). Naive CD4 T cells showed upregulation of the activation markers *Ifng*, *CD40L* and *Lag3* in MHC II WT mice (comp. Fig. 29 c). In line with these findings activated CD4 T cells also exhibited strong upregulation of *Ifng*, the cytotoxic marker *Nkg7* [Szabo et al., 2019] and the chemokines *Ccl3* and *Ccl4*. (comp. Fig. 29 d) Therefore, MHC class II signalling shifted the CD4 compartment towards T cell activation with increased production of IFN-γ. To further validate this finding I performed Geneset enrichment analysis showing that cytokine production ranked among the top differentially regulated gene sets between MHC class II proficient and deficient animals in CD4 T cells (comp. Fig. 29 e). These findings support the hypothesis of *Kilian et al.* that in dependence of MHC class II signalling intratumorally released IFN-γ suppressess osteopontin expression in macrophages and therefore is essential to hamper chronic CD8a T cell activation and subsequent exhaustion. This was validated *in vitro* by M. Kilian and supported by detailed single cell analysis by Ron Sheinin (Systems Immunology, Madi Lab, University of Tel Aviv).
Interestingly, Ccl3 and Ccl4 were strongly upregulated in CD4 T cells from MHC class II proficient mice. Ccl3 and Ccl4 on activated CD4 T cells are known to guide Ccr5 expressing naive Cd8a T cells towards the tumor site [Castellino et al., 2006].Ccl4 expression differed significantly between activated T cells of MHC class II and WT animals. I then assessed the differential Ccr5 expression between the MHC class WT and KO mice, only proliferating CD8a T cells (comp. Fig. 29 i) in MHC class II WT mice had a expression level of Ccr5 of above 1 suggesting that this signalling pathway might be impaired in the absence of MHC class II as well which would be in line with immunofluorescence microscopy of murine GL261 gliomas with reduced numbers of CD8 T cells.

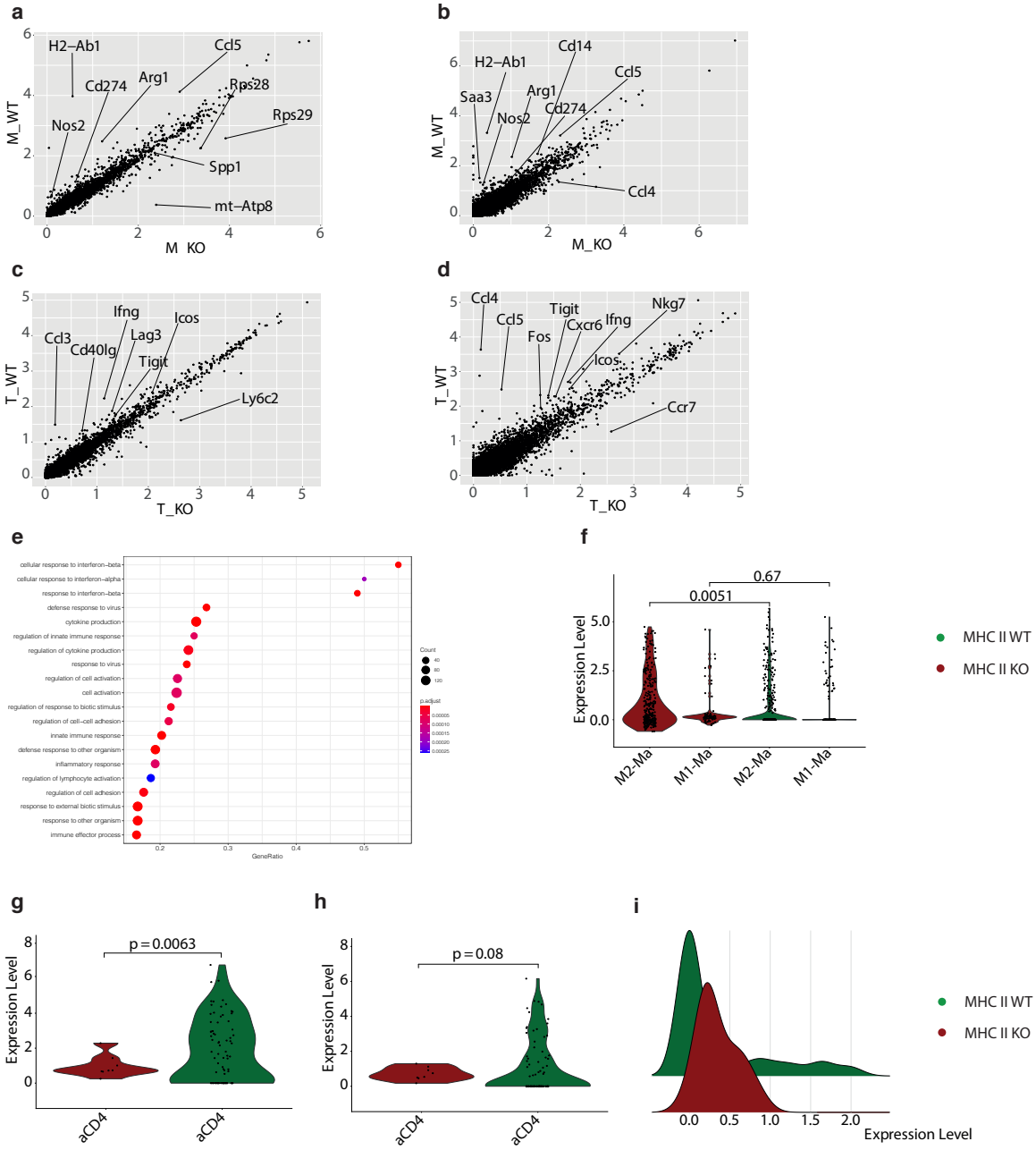

Figure 29: *Continued on next page.*

Figure 29: **Increased osteopontin expression on M2-like macrophages and decreased expression of the Ccl3/4-Ccr5 pathway in activated CD4 T cells could be drivers of T cell exhaustion in the abscence of MHC class II signalling**
a-d Differential expression plots of **a** M2-like macrophages, **b** M1-like macrophages, **c** naive CD4 T cells and **d** activated T cells. **e** GenSet-Enrichment analysis of CD4 T cells. **f** Expression of Spp1 (Osteopontin) on M2-like and M1-like macrophages between MHC class II KO and Wildtype animals *Wilcoxon Test for statistical significance* **g** and **h** expression of Ccl4 (**g**) and Ccl3 (**h**) in activated CD4 T cells *T-Test for statiscal significance* **i** Expression of Ccr5 between MHC class II KO and WT animals

Therefore the suggested final mechanism can be illustrated as following (comp. Fig. 30): Antigen-specific binding of CD4 T cells to MHC class II results in activation and IFN-γ release of activated CD4 T cells. IFN-γ leads to reduced expression of Osteopontin on macrophages. In the abscence of IFN-γ osteopontin binds to CD29 on antigen-specific CD8a T cells resulting in downstream Akt-NFATc1 signalling. Chronic NFATc1 signalling results in TOX expression and T cell exhaustion. Secondly, upon MHC class II dependent activation CD4 T cells express Ccl3 and Ccl4 that guides Ccr5 expressing CD8 T cells towards the tumor microenvironment. In summary, MHC class II is essential for the recruiment and functional fitness of antigen specific CD8a T cells in glioblastomas.

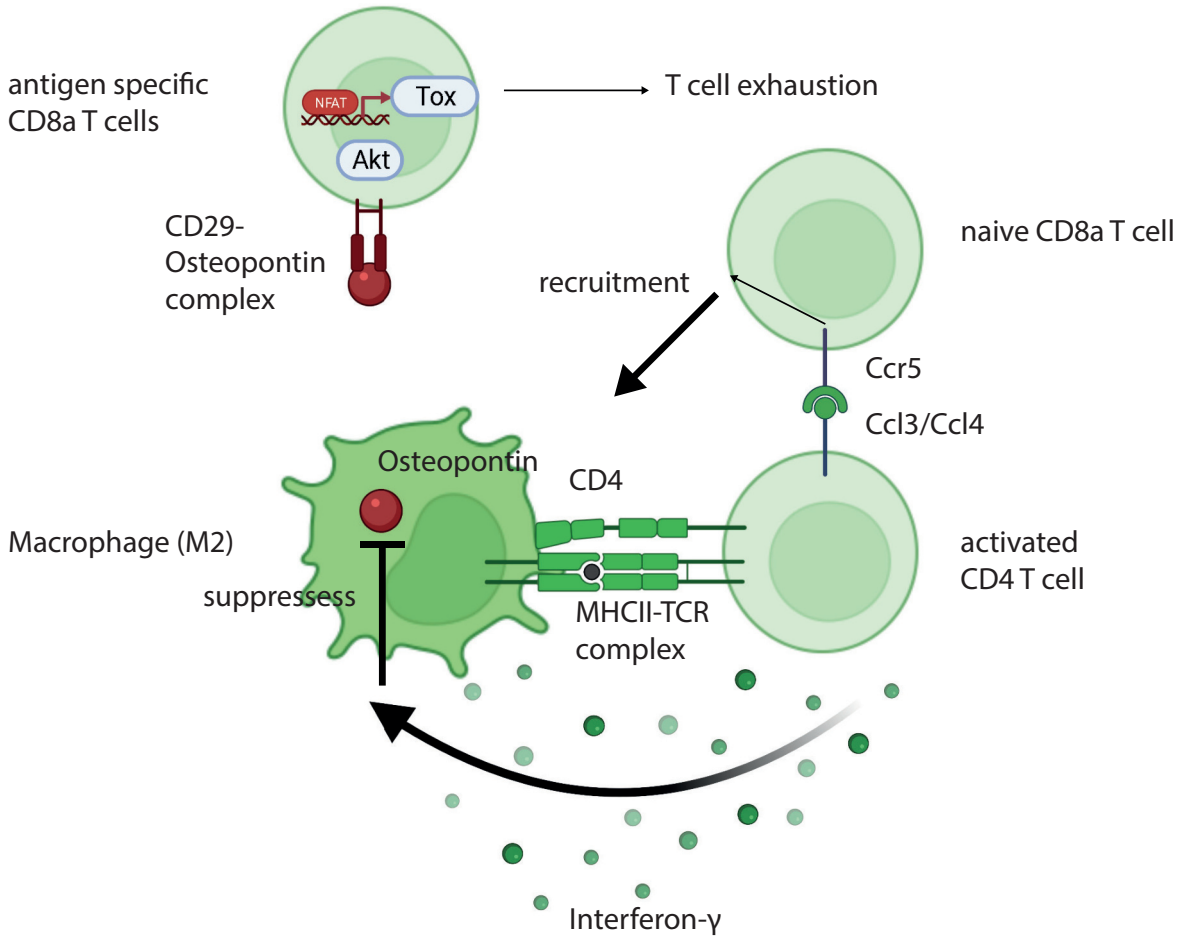

Figure 30: **MHC class II dependent CD8a T cell recruitment and fitness** Scheme of the interaction deciphered using the MHC class II KO mouse model.

5 Discussion

5.1 Adoptive T cell transfer as a treatment for brain cancer

The survival in newly-diagnosed patients with glioblastoma multiforme is still limited to a median overall survival between 29 months [Hilf et al., 2019] and 33 month [Lim et al., 2022] under maximal therapeutic concepts underlining the urgent need for efficient therapies. Adoptive cell therapy has proven to be an efficient therapeutic concept in different cancer entities like multiple myeloma, lymphoma and metastatic melanoma. [Dudley et al., 2002],[Morgan et al., 2006],[Munshi et al., 2021],[Frigault et al., 2022] Therapeutic approaches using adoptively transferred T cells engineered to recognize different surface antigens in brain cancer are yet limited to early clinical studies. [Majzner et al., 2022], [Vitanza et al., 2021], [Brown et al., 2015], [O'Rourke et al., 2017] However, these studies demonstrate promising starting points for further research using genetically engineered T cells for therapy of brain tumors. Recently published trials exclusively report the application of Chimeric-antigen-receptor (CAR) transgenic T cells. However, CAR T cells have two major limitations, as they are only able to target surface antigens that are often not completely tumor-specific and secondly are characterised by the potential severe off-target cytotoxicity like neurotoxcity [Morgan et al., 2013] [Morgan et al., 2010]. Recent approaches are aiming at overcoming these challenges using tumor or location site-specific induction of CAR T cells [Choe et al., 2021]. However, due to the low mutational load in glioblastomas [Hodges et al., 2017] the selection of target antigens remains challenging. Here, T cell receptor engineered T cells as used in this thesis feature a main advantage, as they enable the selection of intracellular target antigens that are bound on HLA-molecules for immunotherapeutic strategies. The GAPVAC-101 study has demonstrated a new and safe mechanism to select new targets for immunotherapy by vaccination of patients with an individualized peptide cocktail resulting in the expansion of tumor-reactive T cells. In this context Neuroligin 4, X-linked emerged as a potential new target for immunotherapy. Developing TCR transgenic T cells against NLGN4X expressing brain tumors thus enables targeting of an epitope that is not only presented on the cell surface but on HLA-A2 molecules and promises to be safe due to its origin as a target derived from an endogenous immune response. In contrast to preclinical and clinical studies employing CAR T cells, there is only rare evidence for the application of T cell receptor engineered T cells in brain cancer. A single preclinical study demonstrates the efficiency of a TCR transgenic cell product directed against the H3.3K27M mutation that is present in diffuse midline gliomas [Chheda et al., 2018]. For the treatment of glioblastoma this work provides the first preclinical evidence for the feasibility and efficiency of TCR transgenic T cell products targeting an antigen overexpressed in human glioblastomas and that was identified from patient-derived immune responses.

The presented results highlight the potential of NLGN4X TCR engineered T cells to limit tumor growth and enable prolonged survival and thereby demonstrating the potential for further application in clinical studies. However, a main limitation of this study is the use of an immunodeficient mouse model hampering the assessment of off-target cytotoxicity as some on and off-target epitopes might not be shared between mouse and human. Recently, it has been shown that the usage of an HLA-A2 and HLA-DR1 humanized mouse model

allows the investigations of the effects of cellular therapies in a fully immunocompetent mouse model [Kilian et al., 2022]. The immune response shown in this thesis is purely driven by the adoptively transferred T cells. However, results presented in the second part of this thesis and current studies [Zander et al., 2019] highlight the role other immune cell subsets to maintain CD8 effector T cell functionality. In this context, the application of T cell products containing both CD4 and CD8 T cells has proven to generate optimal tumor responses [Turtle et al., 2016], which was adapted in this study.
NLGN4X TCR transgenic T cells showed a highly specific effector phenotype *in vitro* with robust cytotoxicity and were capable of prolonging survival, but compared to current pre-clinical work under the usage of different CAR constructs NLGN4X TCR transgenic were not able to induce long term complete responses. [Choe et al., 2021] [Vitanza et al., 2021]. *Choe et al.* show complete regression of tumors after injection of *Syn-Notch* CAR T cells and up to 100% long term-survivors and *Vitanza et al.* demonstrate equal efficiency for spacer length-engineered CAR T cells which were translated into clinical application in the *Brain-Child trial*. The limited preclinical efficiency is most probably driven by loss of functional intratumoral TCR positive effector cells highlighting the need for repetitive T cell product infusion in a phase I clinical study.
The study by *Chheda et al.* using TCR engineered T cells in brain cancer targeting the H3.3K27M mutation is the only comparable current study to the *in vitro* and *in vivo* results demonstrated in this thesis. H3.3.K27M TCR transgenic T cells show equal efficient activation and lysis pattern to NLGN4X TCR transgenic T cells with a peptide specific induction of about 30 % CD69 positive T cells in response to the H3.3.K27M peptide [Chheda et al., 2018] compared to 20 % CD69 positive T cells in response to the NLGN4X peptide presented on glioma cells. Both, *Chheda et al.* and this thesis report a cytotoxicity of about 80% against peptide loaded U87 target cells. [Chheda et al., 2018] This thesis additionally provides a deep insight in polyfunctional T cell effector induction in response to different endogenously and exogenously target-epitope-presenting cell lines and an in depth analysis of the therapeutic capacity of these cells in flank and intracranial tumor models and under usage of local intraventricular delivery of T cells.
This thesis utilizes the U87 glioma cell line engineered to overexpress either the target epitope or the target protein to study therapeutic efficiency of T cell receptor transduced T cells. The U87 cell line is a rather artificial cell line with a high mutational load limiting the transferability of this tumor model overexpressing the NLGN4X epitope to primary human gliomas. However, NLGN4X-TCR-T were also capable to recognize and lyse a patient-derived glioma line with endogenous expression of NLGN4X highlighting the clinical relevance of the presented results.

5.2 The efficiency of immune-checkpoint blockade in brain malignancies

The application of immune checkpoint therapy has been extensively investigated in several cancer entities with diverse results. [Topalian et al., 2012] [Diaz et al., 2022] [Luke et al., 2022] In melanoma *Luke et al.* demonstrate efficiency of checkpoint therapy compared to a placebo control. *Diaz et al.* show that treatment with Pembrolizumab demonstrate equal

efficiency in the treatment of colorectal carcinoma compared to chemotherapy. The role of immune checkpoint blockade in the context of glioblastomas has been subjected to extensive discussions. *Bouffet et al.* demonstrated that immune checkpoint therapy is in principle capable of inducing responses in hypermutated glioblastomas. [Bouffet et al., 2016] Additionally, is has been demonstrated that neoadjuvant therapy with Pembrolizumab (PD-1 Inhibitor) was superior compared to adjuvant application after surgical resection only. [Cloughesy et al., 2019] *Cloughesy et al.* additionally support these findings with evidence of clonal T cell expansion in responder patients. However, a phase 3 clinical trial in patients with recurrent glioblastoma failed to demonstrate an improvement in the overall survival of patients treated with nivolumab targeting PD-1 compared to bevacizumab targeting VEGF-C. [Reardon et al., 2020]
Non-responders to immune checkpoint therapy are characterised by expansion of immunosuppressive myeloid cells in the tumor microenvironment. [Aslan et al., 2020] Accordingly, these findings provided the rational to target the PD-L1 immune checkpoint molecule additionally to CTLA-4 and PD-1. Also, single treatment with PD-L1 demonstrated promising results in a phase II clinical trial in metastatic urothelial carcinoma. [Balar et al., 2017] The combination therapy scheme was used to evaluate the responses of immune checkpoint therapy in the context of MHC class II deficiency in this thesis. Treatment with ICB resulted in enhanced survival in MHC class II proficient mice, while this effect was significantly reduced in MHC class II deleted animals. However, in the presented results no complete tumor regression but only partial regression was observable in treated animals. Limited efficiency of immune checkpoint therapy has also been reported in different cancer entities. [Wu et al., 2022] Yet, the application of immune checkpoint blockade remains a controversial therapy regimen in brain cancer.

5.3 MHC class II prevents CD8 T cell exhaustion

Starting with *Kreiter et al.* the role of the MHC class II - CD4 T cell interaction in tumor immunology has gained increasing interest. [Kreiter et al., 2015] The study of *Kreiter et al.* demonstrated that an unexpected amount of cancer mutations is recognized by CD4 T cells via MHC class II restricted presentation. Additionally, successful tumor rejection requires the prescence of CD4+ T cells in the tumor microenvironment even in the absence of MHC class II epitopes on the tumor. [Alspach et al., 2019] *Alspach et al.* highlight that MHC class II restricted T cell activation of CD4 T cells is a crucial factor in anti-tumor immunity. This thesis also provides evidence of the importance of MHC class II in a MHC class I epitope driven tumor model, where the lack of MHC class II-CD4 T cell interaction results in increased exhaustion of antigen specific CD8 T cells in MHC class II deficient mice. Interestingly, T cell exhaustion is has been shown to be restricted to specific regions of the tumor, in which tumor associated macophages triggered exhaustion of CD8 T cells. [Kersten et al., 2021] Importantly, these regions localised within the tumor core were characterised by decreased antigen presentation signatures suggesting that the abscence of signaling cascades induced by antigen presentation resulted in increased exhaustion of CD8 T cells. [Kersten et al., 2021] The data presented in this work highlights that a specific subtype of M2-like macrophages is abdundant in the tumor microenviroment of MHC class II deleted animals. Moreover, deletion of MHC class II resulted in an upregulation of the

exhaustion marker TOX on a subset of tumor reactive T cells. Therefore, this thesis, additionally to the previously described importance of CD4-MHC class II interaction, provides evidence that MHC class II prevents tumor-reactive CD8 T cells from TOX driven exhaustion.
TOX has been previously described as a key driver of T cell exhaustion in dependence of chronic NFAT activation and T cell stimulation [Khan et al., 2019]. Here, it is additionally shown that MHC II signalling hampers chronic NFAT signalling via suppression of osteopontin in a specific subset of macrophages. Osteopontin binding to CD44 on CD8 T cells has been previously shown to suppress T cell responses in colorectal carcinoma. [Klement et al., 2018] According to the presented results, this suppression is driven by Interferon-γ released by CD4 T cells that are activated through binding to MHC II presented epitopes. Osteopontin was also identified as a negative predictor for patient overall survival in different cancer entities [Weber et al., 2010] fitting to the presented survival benefit in MHC class II proficient mice.
These data provide evidence for the complex cross-talk of immune cell subsets in different tumor regions. *Pelka et al.* extensively characterised the spatial relationship of different immune cell subtypes in colorectal cancer demonstrating that a subset of myeloid cells with a transcriptional programme associated with MHC class II antigen presentation co-localized with clusters of activated T cells. [Pelka et al., 2021] Interestingly, tumors that do not form specific MHC class II rich regions are lacking T cell infiltration and result in progressive disease in those patients [Jansen et al., 2019]. These MHC class II rich regions are essential to maintain a rather stem-like phenotype of tumor infiltrating T cells. [Jansen et al., 2019] Coming back to the initially presented evidence for optimization of cellular products in adoptive cell transfer by defining a specific ratio CD4 and CD8 T cells, the data presented in this study underlines the importance of MHC-II CD4 T cell interaction to maintain functional CD8 effector responses.

5.4 Conclusion

The therapy of malignancies of the brain is still lacking curative and truly efficient therapies, however, promising results of preclinical and early clinical trials applying immunotherapeutic concepts encourage further investigations of both new therapeutic options and the underlying mechanisms of resistance.
With the aim to understand the relevance of MHC class II restriced antigen presentation in the tumor microenvironment and to develop a new therapeutic concept with the delivery of NLGN4X T cell receptor engineered T cells this thesis tries to add new evidence to both the mechanisms of anti-tumor immunity and the discovery of new immunotherapeutic regiments.
Neuroligin 4, X-linked as a target for T cell therapy originated from a novel approach to induce specific T cell responses in glioblastoma patients with individualized vaccines. The conept of delivering T cells engineered with a T cell receptor that was identified by this novel approach continues this idea of highly individualized tumor therapy starting with a tumor sample of an individual patient and ending with a therapy of TCR engineered T cells specifically adjusted to the antigen landscape of the tumor. This thesis demonstrates that this approach is in principle feasible and therapeutically efficient in a preclinical model. NLGN4X TCR engineered T cells showed a highly functional effector phenotype *in vitro* and proved to provide a therapeutic benefit in intracranial tumor models. Despite all limitations of the employed model the presented data could provide the starting point for early clinical therapy with NLGN4X TCR engineered T cells.
Secondly, recent research and the results presented in the second part of this thesis highlight that efficient tumor therapy is highly dependent on the prescence of MHC class II restricted antigen presentation in the tumor microenvironment to maintain fitness of CD8 effector cells. This thesis was part of a larger project that discovered a mechanism by which MHC class II suppresses osteopontin induced chronic activation and exhaustion of CD8 T cells. The understanding how anti-tumor immunity depends on the complex interplay of different immune cell subsets, is essential for the development of efficient immunotherapeutic concepts.
In essence, this thesis provides first evidence of the therapeutic potential of a highly individualized T cell receptor engineered T cell product directed against the Neuroligin 4, X-linked antigen and deciphers a mechanism by which MHC class II signalling maintains the fitness of intratumoral effector T cells.

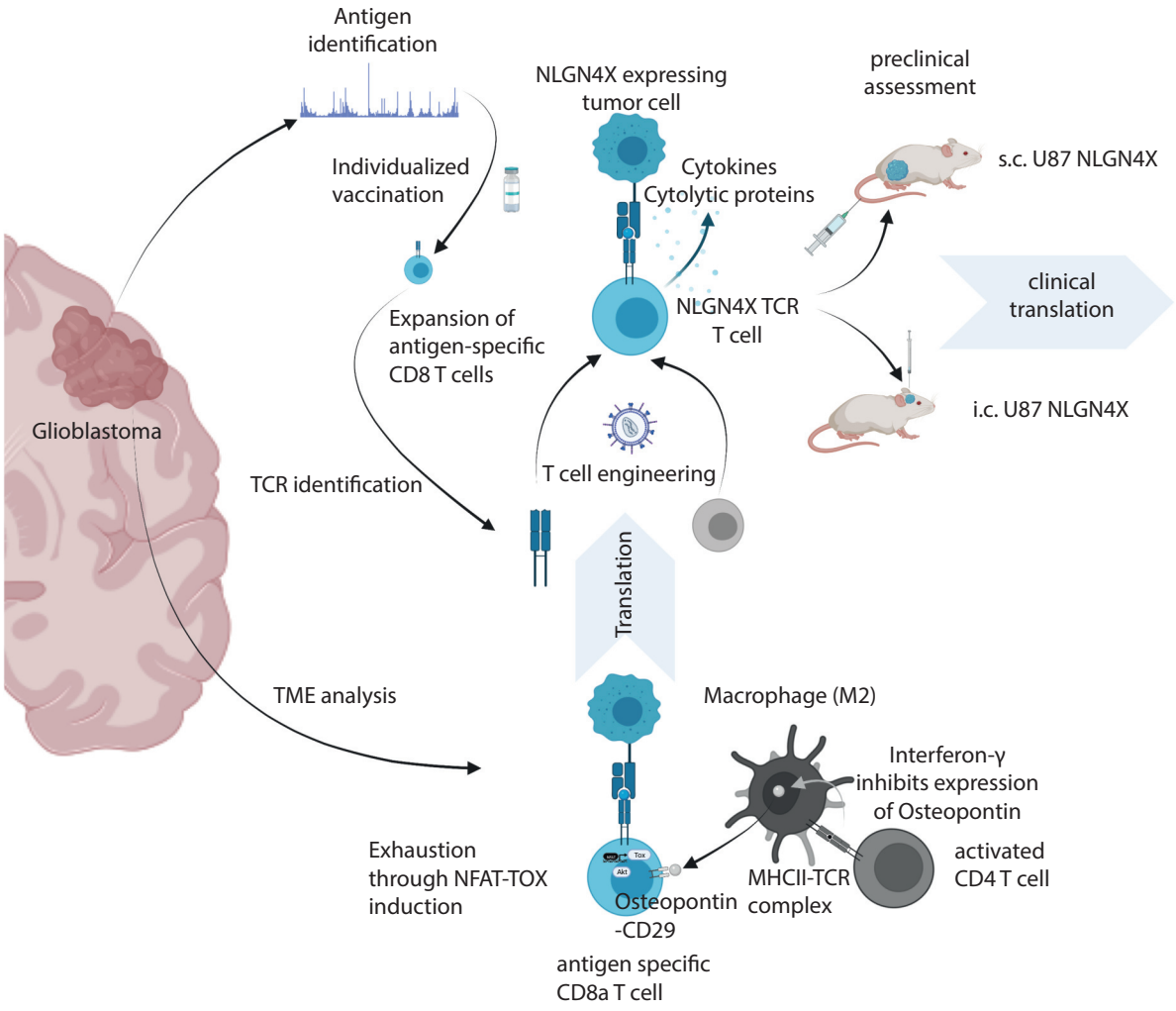

Figure 31: **Graphical abstract**
In brief, the NLGN4X tumor antigen was identified in the context of the GAPVAC study [Hilf et al., 2019] after patient-individualized vaccination. The identified T cell receptor (TCR) was delivered to human T cells and assessed for its reactivity *in vitro* and in preclinical immunodeficient mouse models. Secondly, the interaction of MHC class II and CD4 T cells keeps the functional fitness of CD8 effector cells via decreased signaling of Osteopontin resulting in decreased TOX expression. These findings can be translated to adoptive cellular therapeutic concepts.

6 Summary

Adoptive cell therapy has shown to be an effective treatment for different cancer entities. This thesis investigated the therapeutic potential of T cells engineered with a T cell receptor that targets the Neuroligin 4, X-linked (NLGN4X) antigen which is overexpressed in human glioblastomas.
The specifity of the T cell receptor derived from T cell receptor single cell sequencing was evaluated *in vitro* using an immortalized T cell line. The NLGN4X specific T cell receptor of the most frequent clonotype proved to robustly bind the NLGN4X antigen on different target cells, while exhibiting limited binding to previoulsy predicted off-target peptides. Human T cells equipped with the NLGN4X recognizing T cell receptor were assessed for their functional capacity *in vitro* and demonstrated polyfunctional effector cell activation upon antigen encounter and efficient lysis of different NLGN4X-antigen-presenting target cell lines. NLGN4X TRC transgenic T cells showed therapeutic efficacy in different glioma cell models expressing the NLGN4X target antigen when implanted in an immunodeficient mouse model carrying a knock-out of the murine major histocompatibility complex I and II. A temporary objective response rate (complete or partial response) was observed in 44.4% of the NLGN4X-TCR-T cells treated animals. The therapeutic effects were driven by specific intratumoral activation of NLGN4X-TCR-T cells.
Secondly, the role of major histocompatibility complex (MHC) class II restricted antigen presentation to T helper cells in anti-tumor immunity to glioblastomas was investigated. A mouse model with tamoxifen inducible knockout-out of MHC class II in all myeloid cells or specifically in microglial cells was utilized to evaluate effects of a genetic depletion of MHC II. Mice with a deletion of MHC II had siginificantly reduced survival and response to immune checkpoint blockade. Analysis of the immune cell compartments in the tumor microenvironment showed a decrease in the amount of both T helper and T effector cells. Further analysis of the T cell effector compartment revealed that even in an MHC class I driven tumor model deficiency of MHC class II resulted in exhaustion of antigen-specific CD8+ T effector cells. Single cell sequencing of the tumor infiltrating leukocytes demonstrated the expansion of an immunosuppressive macrophage subset with increased expression of osteopontin. Activated T effector cells were prevented from TOX (thymocyte selection associated high mobility group box) mediated exhaustion in the prescence of MHC class II. Binding of MHC class II on myeloid cells to T helper cells results in increased IFN-γ expression with the effect of a downregulation of Osteopontin on macrophages that resulted in increased fitness of T effector cells.
In conclusion, this thesis provides first preclinical evidence of the therapeutic effectiveness and functional phenotype of an highly individualized T cell therapy targeting a patient specific tumor antigen in human glioblastomas. Furthermore, the fitness of intratumoral T effector cells requires MHC class II dependent signalling between T helper cells and myeloid cells to prevent T effector cells from exhaustion through chronic antigen stimulation.

7 Zusammenfassung

Die Behandlung von Patienten mit unterschiedlichen Tumorentitäten mittels Adoptiven Zelltransfer hat sich als vielversprechende Behandlungsmethode herausgestellt. In dieser Arbeit wurde das therapeutische Potential von T-Zell-Rezeptor transgenen T-Zellen, die die Antigensequenz des in humanen Glioblastomen überexprimierten Neuroligin-4, X-linked (NLGN4X) Proteins erkennen.
Der NLGN4X reaktive T-Zell-Rezeptor wurde in einem Datensatz von T-Zell-Rezeptor Einzelzell-Sequenzierungen identifiziert und anschließend *in vitro* auf seine Spezifität mittels einer immortalisierten T-Zell-Linie getestet. Der T-Zell-Rezeptor des häufigsten T-Zell Klonotyps zeigte eine zuverlässige Bindung an das auf dem Haupthistokompatibilitätskomplex (MHC) Klasse I präsentierten NLGN4X Antigens bei einer geringen Affinität zu anderen Antigensequenz-ähnlichen Peptiden, die nicht Ziel der eigentlichen T-Zell-Therapie sind. Humane T-Zellen mit Expression des transgenen NLGN4X-T-Zell-Rezeptors zeigten einen polyfunktionalen Effektorzelltyp *in vitro* and waren in der Lage verschiedenen Tumorzelllinien mit Expression des Zielepitops, darunter eine von Gliompatienten stammende Linie, spezifisch zu lysieren. U87 Gliomzellen, die das NLGN4X Protein überexprimieren, wurden in eine immundefiziente Mauslinie mit zusätzlicher genetischer Deletion von MHC Klasse I und II implantiert und Adoptiven T-Zelltransfers behandelt. NLGN4X-TZR transgene T-Zellen zeigten eine spezifische intratumorale Aktivierung und eine therapeutische Wirksamkeit mit intermittierender kompletter und partieller Regredienz der Tumore in 44.4% der behandelten Tiere.
Im zweiten Teil der vorliegenden Arbeit wurde die Rolle der Antigenpräsentation über Haupthistokompatibilitätskomplex (MHC) Klasse II zwischen myeloiden Zellen und T-Helfer-Zellen für die Antitumorimmunität untersucht. Hierzu wurde ein Mausmodell genutzt, das einen mittels Tamoxifen induzierbaren genetischen Knock-out von MHC II in entweder allen myeloiden Zellen oder ausschließlich in Mikrogliazellen ermöglicht. Mäuse mit genetischer Deletion des MHC II Gens zeigten ein reduziertes Überleben und Ansprechen auf eine Immuncheckpoint-Blockade in einem intrakraniellen murinen Glioblastommodell. Dieser wurde durch eine veränderte Zusammensetzung der intratumoralen Immunzellkompartimente verursacht, wobei sich eine verringerte Zahl der intratumoralen T-Zellen zeigte. Eine genauere Analyse der T-Effektorzellen zeigte einen dysfunktionalen Phenotyp von Antigen-spezifischen T-Effektorzellen im Falle einer genetischen MHC II Deletion in einem Tumormodell, das vornehmlich ein stark immunogenes MHC I Antigen exprimiert. Einzelzell-Sequenzierung des Transkriptoms von Tumor-infiltrierenden Leukozyten zeigte eine Expansion eines immunosuppressiven Subtyps von Makrophagen mit erhöhter Expression von Osteopontin.Aktive MHC II abhängige Signaltransduktion im Tumormikromilieu verhinderte, dass aktivierte T-Effektorzellen in einen dysfunktionalen Zustand übergingen, der durch Überexpression von TOX (Thymozyten-Selektions-assoziierte HMG-Box) gekennzeichnet waren. Die Bindung von T-Helferzellen an MHC II führte zu einer vermehrten Interferon-γ Expression, was zu einer verminderten Osteopontin Expression auf Makrophagen mit dem Effekt eines funktionalen T-Zell-Effektorkompartiments führte.
Zusammenfassend, zeigt diese Arbeit erste präklinische Resultate zur Effizienz und Funktionalität von individualisierten T-Zell-Rezeptor transgenen T-Zellen, die ein

Patienten-spezifisches Tumorantigen in humanen Glioblastomen erkennen. Des weiteren ist für die Funktionalität von intratumoralen T-Effektorzellen die MHC Klasse II abhängige Aktivierung von T-Helferzellen von entscheidender Bedeutung.

8 List of references

References

Y. Agata, A. Kawasaki, H. Nishimura, Y. Ishida, T. Tsubata, H. Yagita, and T. Honjo. Expression of the pd-1 antigen on the surface of stimulated mouse t and b lymphocytes. *Int Immunol*, 8(5):765–72, 1996. doi: 10.1093/intimm/8.5.765.

E. Alspach, D. M. Lussier, A. P. Miceli, I. Kizhvatov, M. DuPage, A. M. Luoma, W. Meng, C. F. Lichti, E. Esaulova, A. N. Vomund, D. Runci, J. P. Ward, M. M. Gubin, R. F. V. Medrano, C. D. Arthur, J. M. White, K. C. F. Sheehan, A. Chen, K. W. Wucherpfennig, T. Jacks, E. R. Unanue, M. N. Artyomov, and R. D. Schreiber. Mhc-ii neoantigens shape tumour immunity and response to immunotherapy. *Nature*, 574(7780):696–701, 2019. doi: 10.1038/s41586-019-1671-8.

K. Aslan, V. Turco, J. Blobner, J. K. Sonner, A. R. Liuzzi, N. G. Nunez, D. De Feo, P. Kickingereder, M. Fischer, E. Green, A. Sadik, M. Friedrich, K. Sanghvi, M. Kilian, F. Cichon, L. Wolf, K. Jahne, A. von Landenberg, L. Bunse, F. Sahm, D. Schrimpf, J. Meyer, A. Alexander, G. Brugnara, R. Roth, K. Pfleiderer, B. Niesler, A. von Deimling, C. Opitz, M. O. Breckwoldt, S. Heiland, M. Bendszus, W. Wick, B. Becher, and M. Platten. Heterogeneity of response to immune checkpoint blockade in hypermutated experimental gliomas. *Nat Commun*, 11(1):931, 2020. doi: 10.1038/s41467-020-14642-0.

J. I. Ausman, W. R. Shapiro, and D. P. Rall. Studies on the chemotherapy of experimental brain tumors: development of an experimental model. *Cancer Res*, 30(9):2394–400, 1970.

A. V. Balar, M. D. Galsky, J. E. Rosenberg, T. Powles, D. P. Petrylak, J. Bellmunt, Y. Loriot, A. Necchi, J. Hoffman-Censits, J. L. Perez-Gracia, N. A. Dawson, M. S. van der Heijden, R. Dreicer, S. Srinivas, M. M. Retz, R. W. Joseph, A. Drakaki, U. N. Vaishampayan, S. S. Sridhar, D. I. Quinn, I. Duran, D. R. Shaffer, B. J. Eigl, P. D. Grivas, E. Y. Yu, S. Li, 3rd Kadel, E. E., Z. Boyd, R. Bourgon, P. S. Hegde, S. Mariathasan, A. Thastrom, O. O. Abidoye, G. D. Fine, D. F. Bajorin, and I. Mvigor210 Study Group. Atezolizumab as first-line treatment in cisplatin-ineligible patients with locally advanced and metastatic urothelial carcinoma: a single-arm, multicentre, phase 2 trial. *Lancet*, 389(10064):67–76, 2017. doi: 10.1016/S0140-6736(16)32455-2.

S. Bittner, T. Ruck, M. K. Schuhmann, A. M. Herrmann, H. Moha ou Maati, N. Bobak, K. Gobel, F. Langhauser, D. Stegner, P. Ehling, M. Borsotto, H. C. Pape, B. Nieswandt, C. Kleinschnitz, C. Heurteaux, H. J. Galla, T. Budde, H. Wiendl, and S. G. Meuth. Endothelial twik-related potassium channel-1 (trek1) regulates immune-cell trafficking into the cns. *Nat Med*, 19(9):1161–5, 2013. doi: 10.1038/nm.3303.

M. F. Bolliger, J. Pei, S. Maxeiner, A. A. Boucard, N. V. Grishin, and T. C. Sudhof. Unusually rapid evolution of neuroligin-4 in mice. *Proc Natl Acad Sci U S A*, 105(17): 6421–6, 2008. doi: 10.1073/pnas.0801383105.

J. P. Bottcher, E. Bonavita, P. Chakravarty, H. Blees, M. Cabeza-Cabrerizo, S. Sammicheli, N. C. Rogers, E. Sahai, S. Zelenay, and C. Reis e Sousa. Nk cells stimulate recruitment of cdc1 into the tumor microenvironment promoting cancer immune control. *Cell*, 172(5):1022–1037 e14, 2018. doi: 10.1016/j.cell.2018.01.004.

E. Bouffet, V. Larouche, B. B. Campbell, D. Merico, R. de Borja, M. Aronson, C. Durno, J. Krueger, V. Cabric, V. Ramaswamy, N. Zhukova, G. Mason, R. Farah, S. Afzal, M. Yalon, G. Rechavi, V. Magimairajan, M. F. Walsh, S. Constantini, R. Dvir, R. Elhasid, A. Reddy, M. Osborn, M. Sullivan, J. Hansford, A. Dodgshun, N. Klauber-Demore, L. Peterson, S. Patel, S. Lindhorst, J. Atkinson, Z. Cohen, R. Laframboise, P. Dirks, M. Taylor, D. Malkin, S. Albrecht, R. W. Dudley, N. Jabado, C. E. Hawkins, A. Shlien, and U. Tabori. Immune checkpoint inhibition for hypermutant glioblastoma multiforme resulting from germline biallelic mismatch repair deficiency. *J Clin Oncol*, 34(19):2206–11, 2016. doi: 10.1200/JCO.2016.66.6552.

R. L. Bowman, F. Klemm, L. Akkari, S. M. Pyonteck, L. Sevenich, D. F. Quail, S. Dhara, K. Simpson, E. E. Gardner, C. A. Iacobuzio-Donahue, C. W. Brennan, V. Tabar, P. H. Gutin, and J. A. Joyce. Macrophage ontogeny underlies differences in tumor-specific education in brain malignancies. *Cell Rep*, 17(9):2445–2459, 2016. doi: 10.1016/j.celrep.2016.10.052.

S. W. Boyer, A. V. Schroeder, S. Smith-Berdan, and E. C. Forsberg. All hematopoietic cells develop from hematopoietic stem cells through flk2/flt3-positive progenitor cells. *Cell Stem Cell*, 9(1):64–73, 2011. doi: 10.1016/j.stem.2011.04.021.

J. Brahmer, K. L. Reckamp, P. Baas, L. Crino, W. E. Eberhardt, E. Poddubskaya, S. Antonia, A. Pluzanski, E. E. Vokes, E. Holgado, D. Waterhouse, N. Ready, J. Gainor, O. Aren Frontera, L. Havel, M. Steins, M. C. Garassino, J. G. Aerts, M. Domine, L. Paz-Ares, M. Reck, C. Baudelet, C. T. Harbison, B. Lestini, and D. R. Spigel. Nivolumab versus docetaxel in advanced squamous-cell non-small-cell lung cancer. *N Engl J Med*, 373(2):123–35, 2015. doi: 10.1056/NEJMoa1504627.

C. E. Brown, B. Badie, M. E. Barish, L. Weng, J. R. Ostberg, W. C. Chang, A. Naranjo, R. Starr, J. Wagner, C. Wright, Y. Zhai, J. R. Bading, J. A. Ressler, J. Portnow, M. D'Apuzzo, S. J. Forman, and M. C. Jensen. Bioactivity and safety of il13ralpha2-redirected chimeric antigen receptor cd8+ t cells in patients with recurrent glioblastoma. *Clin Cancer Res*, 21(18):4062–72, 2015. doi: 10.1158/1078-0432.CCR-15-0428.

C. E. Brown, D. Alizadeh, R. Starr, L. Weng, J. R. Wagner, A. Naranjo, J. R. Ostberg, M. S. Blanchard, J. Kilpatrick, J. Simpson, A. Kurien, S. J. Priceman, X. Wang, T. L. Harshbarger, M. D'Apuzzo, J. A. Ressler, M. C. Jensen, M. E. Barish, M. Chen, J. Portnow, S. J. Forman, and B. Badie. Regression of glioblastoma after chimeric antigen receptor t-cell therapy. *N Engl J Med*, 375(26):2561–9, 2016. doi: 10.1056/NEJMoa1610497.

L. Bunse, S. Pusch, T. Bunse, F. Sahm, K. Sanghvi, M. Friedrich, D. Alansary, J. K. Sonner, E. Green, K. Deumelandt, M. Kilian, C. Neftel, S. Uhlig, T. Kessler, A. von Landenberg, A. S. Berghoff, K. Marsh, M. Steadman, D. Zhu, B. Nicolay, B. Wiestler, M. O. Breckwoldt, R. Al-Ali, S. Karcher-Bausch, M. Bozza, I. Oezen, M. Kramer, J. Meyer, A. Habel, J. Eisel, G. Poschet, M. Weller, M. Preusser, M. Nadji-Ohl, N. Thon, M. C. Burger, P. N. Harter, M. Ratliff, R. Harbottle, A. Benner, D. Schrimpf, J. Okun, C. Herold-Mende, S. Turcan, S. Kaulfuss, H. Hess-Stumpp, K. Bieback, D. P. Cahill, K. H. Plate, D. Hanggi, M. Dorsch, M. L. Suva, B. A. Niemeyer, A. von Deimling, W. Wick, and M. Platten. Suppression of antitumor t cell immunity by the oncometabolite (r)-2-hydroxyglutarate. *Nat Med*, 24(8):1192–1203, 2018. doi: 10.1038/s41591-018-0095-6.

F. Castellino, A. Y. Huang, G. Altan-Bonnet, S. Stoll, C. Scheinecker, and R. N. Germain. Chemokines enhance immunity by guiding naive cd8+ t cells to sites of cd4+ t cell-dendritic cell interaction. *Nature*, 440(7086):890–5, 2006. doi: 10.1038/nature04651.

Z. S. Chheda, G. Kohanbash, K. Okada, N. Jahan, J. Sidney, M. Pecoraro, X. Yang, D. A. Carrera, K. M. Downey, S. Shrivastav, S. Liu, Y. Lin, C. Lagisetti, P. Chuntova, P. B. Watchmaker, S. Mueller, I. F. Pollack, R. Rajalingam, A. M. Carcaboso, M. Mann, A. Sette, K. C. Garcia, Y. Hou, and H. Okada. Novel and shared neoantigen derived from histone 3 variant h3.3k27m mutation for glioma t cell therapy. *J Exp Med*, 215(1): 141–157, 2018. doi: 10.1084/jem.20171046.

T. Chodon, B. Comin-Anduix, B. Chmielowski, R. C. Koya, Z. Wu, M. Auerbach, C. Ng, E. Avramis, E. Seja, A. Villanueva, T. A. McCannel, A. Ishiyama, J. Czernin, C. G. Radu, X. Wang, D. W. Gjertson, A. J. Cochran, K. Cornetta, D. J. Wong, P. Kaplan-Lefko, O. Hamid, W. Samlowski, P. A. Cohen, G. A. Daniels, B. Mukherji, L. Yang, J. A. Zack, D. B. Kohn, J. R. Heath, J. A. Glaspy, O. N. Witte, D. Baltimore, J. S. Economou, and A. Ribas. Adoptive transfer of mart-1 t-cell receptor transgenic lymphocytes and dendritic cell vaccination in patients with metastatic melanoma. *Clin Cancer Res*, 20(9):2457–65, 2014. doi: 10.1158/1078-0432.CCR-13-3017.

J. H. Choe, P. B. Watchmaker, M. S. Simic, R. D. Gilbert, A. W. Li, N. A. Krasnow, K. M. Downey, W. Yu, D. A. Carrera, A. Celli, J. Cho, J. D. Briones, J. M. Duecker, Y. E. Goretsky, R. Dannenfelser, L. Cardarelli, O. Troyanskaya, S. S. Sidhu, K. T. Roybal, H. Okada, and W. A. Lim. Synnotch-car t cells overcome challenges of specificity, heterogeneity, and persistence in treating glioblastoma. *Sci Transl Med*, 13 (591), 2021. doi: 10.1126/scitranslmed.abe7378.

M. J. Clark, N. Homer, B. D. O'Connor, Z. Chen, A. Eskin, H. Lee, B. Merriman, and S. F. Nelson. U87mg decoded: the genomic sequence of a cytogenetically aberrant human cancer cell line. *PLoS Genet*, 6(1):e1000832, 2010. doi: 10.1371/journal.pgen.1000832.

T. F. Cloughesy, A. Y. Mochizuki, J. R. Orpilla, W. Hugo, A. H. Lee, T. B. Davidson, A. C. Wang, B. M. Ellingson, J. A. Rytlewski, C. M. Sanders, E. S. Kawaguchi, L. Du, G. Li, W. H. Yong, S. C. Gaffey, A. L. Cohen, I. K. Mellinghoff, E. Q. Lee, D. A. Reardon, B. J. O'Brien, N. A. Butowski, P. L. Nghiemphu, J. L. Clarke, I. C.

Arrillaga-Romany, H. Colman, T. J. Kaley, J. F. de Groot, L. M. Liau, P. Y. Wen, and R. M. Prins. Neoadjuvant anti-pd-1 immunotherapy promotes a survival benefit with intratumoral and systemic immune responses in recurrent glioblastoma. *Nat Med*, 25(3): 477–486, 2019. doi: 10.1038/s41591-018-0337-7.

M. Collin and V. Bigley. Human dendritic cell subsets: an update. *Immunology*, 154(1): 3–20, 2018. doi: 10.1111/imm.12888.

D. G. DeNardo and B. Ruffell. Macrophages as regulators of tumour immunity and immunotherapy. *Nat Rev Immunol*, 19(6):369–382, 2019. doi: 10.1038/s41577-019-0127-6.

Jr. Diaz, L. A., K. K. Shiu, T. W. Kim, B. V. Jensen, L. H. Jensen, C. Punt, D. Smith, R. Garcia-Carbonero, M. Benavides, P. Gibbs, C. de la Fourchardiere, F. Rivera, E. Elez, D. T. Le, T. Yoshino, W. Y. Zhong, D. Fogelman, P. Marinello, T. Andre, and Keynote Investigators. Pembrolizumab versus chemotherapy for microsatellite instability-high or mismatch repair-deficient metastatic colorectal cancer (keynote-177): final analysis of a randomised, open-label, phase 3 study. *Lancet Oncol*, 23(5):659–670, 2022. doi: 10.1016/S1470-2045(22)00197-8.

H. Dong, S. E. Strome, D. R. Salomao, H. Tamura, F. Hirano, D. B. Flies, P. C. Roche, J. Lu, G. Zhu, K. Tamada, V. A. Lennon, E. Celis, and L. Chen. Tumor-associated b7-h1 promotes t-cell apoptosis: a potential mechanism of immune evasion. *Nat Med*, 8 (8):793–800, 2002. doi: 10.1038/nm730.

H. Du, K. Hirabayashi, S. Ahn, N. P. Kren, S. A. Montgomery, X. Wang, K. Tiruthani, B. Mirlekar, D. Michaud, K. Greene, S. G. Herrera, Y. Xu, C. Sun, Y. Chen, X. Ma, C. R. Ferrone, Y. Pylayeva-Gupta, J. J. Yeh, R. Liu, B. Savoldo, S. Ferrone, and G. Dotti. Antitumor responses in the absence of toxicity in solid tumors by targeting b7-h3 via chimeric antigen receptor t cells. *Cancer Cell*, 35(2):221–237 e8, 2019. doi: 10.1016/j.ccell.2019.01.002.

M. E. Dudley, J. R. Wunderlich, P. F. Robbins, J. C. Yang, P. Hwu, D. J. Schwartzentruber, S. L. Topalian, R. Sherry, N. P. Restifo, A. M. Hubicki, M. R. Robinson, M. Raffeld, P. Duray, C. A. Seipp, L. Rogers-Freezer, K. E. Morton, S. A. Mavroukakis, D. E. White, and S. A. Rosenberg. Cancer regression and autoimmunity in patients after clonal repopulation with antitumor lymphocytes. *Science*, 298(5594): 850–4, 2002. doi: 10.1126/science.1076514.

D. F. Dwyer, N. A. Barrett, K. F. Austen, and Consortium Immunological Genome Project. Expression profiling of constitutive mast cells reveals a unique identity within the immune system. *Nat Immunol*, 17(7):878–87, 2016. doi: 10.1038/ni.3445.

B. M. Ellingson, P. Y. Wen, and T. F. Cloughesy. Modified criteria for radiographic response assessment in glioblastoma clinical trials. *Neurotherapeutics*, 14(2):307–320, 2017. doi: 10.1007/s13311-016-0507-6.

J. Fogh, J. M. Fogh, and T. Orfeo. One hundred and twenty-seven cultured human tumor cell lines producing tumors in nude mice. *J Natl Cancer Inst*, 59(1):221–6, 1977. doi: 10.1093/jnci/59.1.221.

E. Friebel, K. Kapolou, S. Unger, N. G. Nunez, S. Utz, E. J. Rushing, L. Regli, M. Weller, M. Greter, S. Tugues, M. C. Neidert, and B. Becher. Single-cell mapping of human brain cancer reveals tumor-specific instruction of tissue-invading leukocytes. *Cell*, 181(7): 1626–1642 e20, 2020. doi: 10.1016/j.cell.2020.04.055.

M. Friedrich, R. Sankowski, L. Bunse, M. Kilian, E. Green, C. Ramallo Guevara, S. Pusch, G. Poschet, K. Sanghvi, M. Hahn, T. Bunse, P. Munch, H. M. Gegner, J. K. Sonner, A. von Landenberg, F. Cichon, K. Aslan, T. Trobisch, L. Schirmer, D. Abu-Sammour, T. Kessler, M. Ratliff, D. Schrimpf, F. Sahm, C. Hopf, D. H. Heiland, O. Schnell, J. Beck, C. Bottcher, C. Fernandez-Zapata, J. Priller, S. Heiland, I. Gutcher, F. J. Quintana, A. von Deimling, W. Wick, M. Prinz, and M. Platten. Tryptophan metabolism drives dynamic immunosuppressive myeloid states in idh-mutant gliomas. *Nat Cancer*, 2(7):723–740, 2021. doi: 10.1038/s43018-021-00201-z.

M. J. Frigault, J. Dietrich, K. Gallagher, M. Roschewski, J. T. Jordan, D. Forst, S. R. Plotkin, D. Cook, K. S. Casey, K. A. Lindell, G. D. Depinho, K. Katsis, E. L. Elder, M. B. Leick, B. Choi, N. Horick, F. Preffer, M. Saylor, S. McAfee, P. V. O'Donnell, T. R. Spitzer, B. Dey, Z. DeFilipp, A. El-Jawahri, T. T. Batchelor, M. V. Maus, and Y. B. Chen. Safety and efficacy of tisagenlecleucel in primary cns lymphoma: a phase 1/2 clinical trial. *Blood*, 139(15):2306–2315, 2022. doi: 10.1182/blood.2021014738.

K. Ganesh, Z. K. Stadler, A. Cercek, R. B. Mendelsohn, J. Shia, N. H. Segal, and Jr. Diaz, L. A. Immunotherapy in colorectal cancer: rationale, challenges and potential. *Nat Rev Gastroenterol Hepatol*, 16(6):361–375, 2019. doi: 10.1038/s41575-019-0126-x.

S. B. Goldberg, S. N. Gettinger, A. Mahajan, A. C. Chiang, R. S. Herbst, M. Sznol, A. J. Tsiouris, J. Cohen, A. Vortmeyer, L. Jilaveanu, J. Yu, U. Hegde, S. Speaker, M. Madura, A. Ralabate, A. Rivera, E. Rowen, H. Gerrish, X. Yao, V. Chiang, and H. M. Kluger. Pembrolizumab for patients with melanoma or non-small-cell lung cancer and untreated brain metastases: early analysis of a non-randomised, open-label, phase 2 trial. *Lancet Oncol*, 17(7):976–983, 2016. doi: 10.1016/S1470-2045(16)30053-5.

T. Goldmann, P. Wieghofer, P. F. Muller, Y. Wolf, D. Varol, S. Yona, S. M. Brendecke, K. Kierdorf, O. Staszewski, M. Datta, T. Luedde, M. Heikenwalder, S. Jung, and M. Prinz. A new type of microglia gene targeting shows tak1 to be pivotal in cns autoimmune inflammation. *Nat Neurosci*, 16(11):1618–26, 2013. doi: 10.1038/nn.3531.

X. Guo, Y. Zhang, L. Zheng, C. Zheng, J. Song, Q. Zhang, B. Kang, Z. Liu, L. Jin, R. Xing, R. Gao, L. Zhang, M. Dong, X. Hu, X. Ren, D. Kirchhoff, H. G. Roider, T. Yan, and Z. Zhang. Global characterization of t cells in non-small-cell lung cancer by single-cell sequencing. *Nat Med*, 24(7):978–985, 2018. doi: 10.1038/s41591-018-0045-3.

N. Hilf, S. Kuttruff-Coqui, K. Frenzel, V. Bukur, S. Stevanovic, C. Gouttefangeas, M. Platten, G. Tabatabai, V. Dutoit, S. H. van der Burg, P. Thor Straten,

F. Martinez-Ricarte, B. Ponsati, H. Okada, U. Lassen, A. Admon, C. H. Ottensmeier, A. Ulges, S. Kreiter, A. von Deimling, M. Skardelly, D. Migliorini, J. R. Kroep, M. Idorn, J. Rodon, J. Piro, H. S. Poulsen, B. Shraibman, K. McCann, R. Mendrzyk, M. Lower, M. Stieglbauer, C. M. Britten, D. Capper, M. J. P. Welters, J. Sahuquillo, K. Kiesel, E. Derhovanessian, E. Rusch, L. Bunse, C. Song, S. Heesch, C. Wagner, A. Kemmer-Bruck, J. Ludwig, J. C. Castle, O. Schoor, A. D. Tadmor, E. Green, J. Fritsche, M. Meyer, N. Pawlowski, S. Dorner, F. Hoffgaard, B. Rossler, D. Maurer, T. Weinschenk, C. Reinhardt, C. Huber, H. G. Rammensee, H. Singh-Jasuja, U. Sahin, P. Y. Dietrich, and W. Wick. Actively personalized vaccination trial for newly diagnosed glioblastoma. *Nature*, 565(7738):240–245, 2019. doi: 10.1038/s41586-018-0810-y.

I. C. Hirako, M. A. Ataide, L. Faustino, P. A. Assis, E. W. Sorensen, H. Ueta, N. M. Araujo, G. B. Menezes, A. D. Luster, and R. T. Gazzinelli. Splenic differentiation and emergence of ccr5(+)cxcl9(+)cxcl10(+) monocyte-derived dendritic cells in the brain during cerebral malaria. *Nat Commun*, 7:13277, 2016. doi: 10.1038/ncomms13277.

T. R. Hodges, M. Ott, J. Xiu, Z. Gatalica, J. Swensen, S. Zhou, J. T. Huse, J. de Groot, S. Li, W. W. Overwijk, D. Spetzler, and A. B. Heimberger. Mutational burden, immune checkpoint expression, and mismatch repair in glioma: implications for immune checkpoint immunotherapy. *Neuro Oncol*, 19(8):1047–1057, 2017. doi: 10.1093/neuonc/nox026.

K. Ichtchenko, Y. Hata, T. Nguyen, B. Ullrich, M. Missler, C. Moomaw, and T. C. Sudhof. Neuroligin 1: a splice site-specific ligand for beta-neurexins. *Cell*, 81(3):435–43, 1995. doi: 10.1016/0092-8674(95)90396-8.

J. Jain, P. G. McCaffrey, V. E. Valge-Archer, and A. Rao. Nuclear factor of activated t cells contains fos and jun. *Nature*, 356(6372):801–4, 1992. doi: 10.1038/356801a0.

C. S. Jansen, N. Prokhnevska, V. A. Master, M. G. Sanda, J. W. Carlisle, M. A. Bilen, M. Cardenas, S. Wilkinson, R. Lake, A. G. Sowalsky, R. M. Valanparambil, W. H. Hudson, D. McGuire, K. Melnick, A. I. Khan, K. Kim, Y. M. Chang, A. Kim, C. P. Filson, M. Alemozaffar, A. O. Osunkoya, P. Mullane, C. Ellis, R. Akondy, S. J. Im, A. O. Kamphorst, A. Reyes, Y. Liu, and H. Kissick. An intra-tumoral niche maintains and differentiates stem-like cd8 t cells. *Nature*, 576(7787):465–470, 2019. doi: 10.1038/s41586-019-1836-5.

X. Jiang, J. Wang, K. Zhang, S. Tang, C. Ren, and Y. Chen. The role of cd29-ilk-akt signaling-mediated epithelial-mesenchymal transition of liver epithelial cells and chemoresistance and radioresistance in hepatocellular carcinoma cells. *Med Oncol*, 32(5): 141, 2015. doi: 10.1007/s12032-015-0595-x.

M. J. C. Jordao, R. Sankowski, S. M. Brendecke, Sagar, G. Locatelli, Y. H. Tai, T. L. Tay, E. Schramm, S. Armbruster, N. Hagemeyer, O. Gross, D. Mai, O. Cicek, T. Falk, M. Kerschensteiner, D. Grun, and M. Prinz. Single-cell profiling identifies myeloid cell subsets with distinct fates during neuroinflammation. *Science*, 363(6425), 2019. doi: 10.1126/science.aat7554.

S. Jung, J. Aliberti, P. Graemmel, M. J. Sunshine, G. W. Kreutzberg, A. Sher, and D. R. Littman. Analysis of fractalkine receptor cx(3)cr1 function by targeted deletion and green fluorescent protein reporter gene insertion. *Mol Cell Biol*, 20(11):4106–14, 2000. doi: 10.1128/MCB.20.11.4106-4114.2000.

M. E. Keir, S. C. Liang, I. Guleria, Y. E. Latchman, A. Qipo, L. A. Albacker, M. Koulmanda, G. J. Freeman, M. H. Sayegh, and A. H. Sharpe. Tissue expression of pd-l1 mediates peripheral t cell tolerance. *J Exp Med*, 203(4):883–95, 2006. doi: 10.1084/jem.20051776.

Kelly Kersten, Kenneth H. Hu, Alexis J. Combes, Bushra Samad, Tory Harwin, Arja Ray, Arjun Arkal Rao, En Cai, Kyle Marchuk, Jordan Artichoker, Tristan Courau, Quanming Shi, Julia Belk, Ansuman T. Satpathy, and Matthew F. Krummel. Spatiotemporal co-dependency between macrophages and exhausted cd8¡sup¿+¡/sup¿ t cells in cancer. *bioRxiv*, page 2021.09.27.461866, 2021. doi: 10.1101/2021.09.27.461866.

O. Khan, J. R. Giles, S. McDonald, S. Manne, S. F. Ngiow, K. P. Patel, M. T. Werner, A. C. Huang, K. A. Alexander, J. E. Wu, J. Attanasio, P. Yan, S. M. George, B. Bengsch, R. P. Staupe, G. Donahue, W. Xu, R. K. Amaravadi, X. Xu, G. C. Karakousis, T. C. Mitchell, L. M. Schuchter, J. Kaye, S. L. Berger, and E. J. Wherry. Tox transcriptionally and epigenetically programs cd8(+) t cell exhaustion. *Nature*, 571 (7764):211–218, 2019. doi: 10.1038/s41586-019-1325-x.

K. Kierdorf, D. Erny, T. Goldmann, V. Sander, C. Schulz, E. G. Perdiguero, P. Wieghofer, A. Heinrich, P. Riemke, C. Holscher, D. N. Muller, B. Luckow, T. Brocker, K. Debowski, G. Fritz, G. Opdenakker, A. Diefenbach, K. Biber, M. Heikenwalder, F. Geissmann, F. Rosenbauer, and M. Prinz. Microglia emerge from erythromyeloid precursors via pu.1- and irf8-dependent pathways. *Nat Neurosci*, 16(3):273–80, 2013. doi: 10.1038/nn.3318.

M. Kilian, T. Bunse, W. Wick, M. Platten, and L. Bunse. Genetically modified cellular therapies for malignant gliomas. *Int J Mol Sci*, 22(23), 2021. doi: 10.3390/ijms222312810.

M. Kilian, M. Friedrich, K. Sanghvi, E. Green, S. Pusch, D. Kawauchi, M. Lower, J. K. Sonner, C. Kramer, J. Zaman, S. Jung, M. O. Breckwoldt, G. Willimsky, S. B. Eichmuller, A. von Deimling, W. Wick, F. Sahm, M. Platten, and L. Bunse. T-cell receptor therapy targeting mutant capicua transcriptional repressor in experimental gliomas. *Clin Cancer Res*, 28(2):378–389, 2022. doi: 10.1158/1078-0432.CCR-21-1881.

C. A. Klebanoff, L. Gattinoni, D. C. Palmer, P. Muranski, Y. Ji, C. S. Hinrichs, Z. A. Borman, S. P. Kerkar, C. D. Scott, S. E. Finkelstein, S. A. Rosenberg, and N. P. Restifo. Determinants of successful cd8+ t-cell adoptive immunotherapy for large established tumors in mice. *Clin Cancer Res*, 17(16):5343–52, 2011. doi: 10.1158/1078-0432.CCR-11-0503.

J. D. Klement, A. V. Paschall, P. S. Redd, M. L. Ibrahim, C. Lu, D. Yang, E. Celis, S. I. Abrams, K. Ozato, and K. Liu. An osteopontin/cd44 immune checkpoint controls cd8+

t cell activation and tumor immune evasion. *J Clin Invest*, 128(12):5549–5560, 2018. doi: 10.1172/JCI123360.

F. Klemm, R. R. Maas, R. L. Bowman, M. Kornete, K. Soukup, S. Nassiri, J. P. Brouland, C. A. Iacobuzio-Donahue, C. Brennan, V. Tabar, P. H. Gutin, R. T. Daniel, M. E. Hegi, and J. A. Joyce. Interrogation of the microenvironmental landscape in brain tumors reveals disease-specific alterations of immune cells. *Cell*, 181(7):1643–1660 e17, 2020. doi: 10.1016/j.cell.2020.05.007.

S. Kreiter, M. Vormehr, N. van de Roemer, M. Diken, M. Lower, J. Diekmann, S. Boegel, B. Schrors, F. Vascotto, J. C. Castle, A. D. Tadmor, S. P. Schoenberger, C. Huber, O. Tureci, and U. Sahin. Mutant mhc class ii epitopes drive therapeutic immune responses to cancer. *Nature*, 520(7549):692–6, 2015. doi: 10.1038/nature14426.

D. R. Leach, M. F. Krummel, and J. P. Allison. Enhancement of antitumor immunity by ctla-4 blockade. *Science*, 271(5256):1734–6, 1996. doi: 10.1126/science.271.5256.1734.

M. Lim, M. Weller, A. Idbaih, J. Steinbach, G. Finocchiaro, R. R. Raval, G. Ansstas, J. Baehring, J. W. Taylor, J. Honnorat, K. Petrecca, F. De Vos, A. Wick, A. Sumrall, S. Sahebjam, I. K. Mellinghoff, M. Kinoshita, M. Roberts, R. Slepetis, D. Warad, D. Leung, M. Lee, D. A. Reardon, and A. Omuro. Phase 3 trial of chemoradiotherapy with temozolomide plus nivolumab or placebo for newly diagnosed glioblastoma with methylated mgmt promoter. *Neuro Oncol*, 2022. doi: 10.1093/neuonc/noac116.

Y. Lou, G. Wang, G. Lizee, G. J. Kim, S. E. Finkelstein, C. Feng, N. P. Restifo, and P. Hwu. Dendritic cells strongly boost the antitumor activity of adoptively transferred t cells in vivo. *Cancer Res*, 64(18):6783–90, 2004. doi: 10.1158/0008-5472.CAN-04-1621.

D. N. Louis, A. Perry, P. Wesseling, D. J. Brat, I. A. Cree, D. Figarella-Branger, C. Hawkins, H. K. Ng, S. M. Pfister, G. Reifenberger, R. Soffietti, A. von Deimling, and D. W. Ellison. The 2021 who classification of tumors of the central nervous system: a summary. *Neuro Oncol*, 23(8):1231–1251, 2021. doi: 10.1093/neuonc/noab106.

A. Louveau, J. Herz, M. N. Alme, A. F. Salvador, M. Q. Dong, K. E. Viar, S. G. Herod, J. Knopp, J. C. Setliff, A. L. Lupi, S. Da Mesquita, E. L. Frost, A. Gaultier, T. H. Harris, R. Cao, S. Hu, J. R. Lukens, I. Smirnov, C. C. Overall, G. Oliver, and J. Kipnis. Cns lymphatic drainage and neuroinflammation are regulated by meningeal lymphatic vasculature. *Nat Neurosci*, 21(10):1380–1391, 2018. doi: 10.1038/s41593-018-0227-9.

J. J. Luke, P. Rutkowski, P. Queirolo, M. Del Vecchio, J. Mackiewicz, V. Chiarion-Sileni, L. de la Cruz Merino, M. A. Khattak, D. Schadendorf, G. V. Long, P. A. Ascierto, M. Mandala, F. De Galitiis, A. Haydon, R. Dummer, J. J. Grob, C. Robert, M. S. Carlino, P. Mohr, A. Poklepovic, V. K. Sondak, R. A. Scolyer, J. M. Kirkwood, K. Chen, S. J. Diede, S. Ahsan, N. Ibrahim, A. M. M. Eggermont, and Keynote Investigators. Pembrolizumab versus placebo as adjuvant therapy in completely resected stage iib or iic melanoma (keynote-716): a randomised, double-blind, phase 3 trial. *Lancet*, 399(10336): 1718–1729, 2022. doi: 10.1016/S0140-6736(22)00562-1.

R. G. Majzner, S. Ramakrishna, K. W. Yeom, S. Patel, H. Chinnasamy, L. M. Schultz, R. M. Richards, L. Jiang, V. Barsan, R. Mancusi, A. C. Geraghty, Z. Good, A. Y. Mochizuki, S. M. Gillespie, A. M. S. Toland, J. Mahdi, A. Reschke, E. H. Nie, I. J. Chau, M. C. Rotiroti, C. W. Mount, C. Baggott, S. Mavroukakis, E. Egeler, J. Moon, C. Erickson, S. Green, M. Kunicki, M. Fujimoto, Z. Ehlinger, W. Reynolds, S. Kurra, K. E. Warren, S. Prabhu, H. Vogel, L. Rasmussen, T. T. Cornell, S. Partap, P. G. Fisher, C. J. Campen, M. G. Filbin, G. Grant, B. Sahaf, K. L. Davis, S. A. Feldman, C. L. Mackall, and M. Monje. Gd2-car t cell therapy for h3k27m-mutated diffuse midline gliomas. *Nature*, 603(7903):934–941, 2022. doi: 10.1038/s41586-022-04489-4.

S. G. Marro, S. Chanda, N. Yang, J. A. Janas, G. Valperga, J. Trotter, B. Zhou, S. Merrill, I. Yousif, H. Shelby, H. Vogel, M. Y. S. Kalani, T. C. Sudhof, and M. Wernig. Neuroligin-4 regulates excitatory synaptic transmission in human neurons. *Neuron*, 103 (4):617–626 e6, 2019. doi: 10.1016/j.neuron.2019.05.043.

N. D. Mathewson, O. Ashenberg, I. Tirosh, S. Gritsch, E. M. Perez, S. Marx, L. Jerby-Arnon, R. Chanoch-Myers, T. Hara, A. R. Richman, Y. Ito, J. Pyrdol, M. Friedrich, K. Schumann, M. J. Poitras, P. C. Gokhale, L. N. Gonzalez Castro, M. E. Shore, C. M. Hebert, B. Shaw, H. L. Cahill, M. Drummond, W. Zhang, O. Olawoyin, H. Wakimoto, O. Rozenblatt-Rosen, P. K. Brastianos, X. S. Liu, P. S. Jones, D. P. Cahill, M. P. Frosch, D. N. Louis, G. J. Freeman, K. L. Ligon, A. Marson, E. A. Chiocca, D. A. Reardon, A. Regev, M. L. Suva, and K. W. Wucherpfennig. Inhibitory cd161 receptor identified in glioma-infiltrating t cells by single-cell analysis. *Cell*, 184(5): 1281–1298 e26, 2021. doi: 10.1016/j.cell.2021.01.022.

B. C. Miller, D. R. Sen, R. Al Abosy, K. Bi, Y. V. Virkud, M. W. LaFleur, K. B. Yates, A. Lako, K. Felt, G. S. Naik, M. Manos, E. Gjini, J. R. Kuchroo, J. J. Ishizuka, J. L. Collier, G. K. Griffin, S. Maleri, D. E. Comstock, S. A. Weiss, F. D. Brown, A. Panda, M. D. Zimmer, R. T. Manguso, F. S. Hodi, S. J. Rodig, A. H. Sharpe, and W. N. Haining. Subsets of exhausted cd8(+) t cells differentially mediate tumor control and respond to checkpoint blockade. *Nat Immunol*, 20(3):326–336, 2019. doi: 10.1038/s41590-019-0312-6.

J. B. Moon, J. H. Kim, K. Kim, B. U. Youn, A. Ko, S. Y. Lee, and N. Kim. Akt induces osteoclast differentiation through regulating the gsk3beta/nfatc1 signaling cascade. *J Immunol*, 188(1):163–9, 2012. doi: 10.4049/jimmunol.1101254.

R. A. Morgan, M. E. Dudley, J. R. Wunderlich, M. S. Hughes, J. C. Yang, R. M. Sherry, R. E. Royal, S. L. Topalian, U. S. Kammula, N. P. Restifo, Z. Zheng, A. Nahvi, C. R. de Vries, L. J. Rogers-Freezer, S. A. Mavroukakis, and S. A. Rosenberg. Cancer regression in patients after transfer of genetically engineered lymphocytes. *Science*, 314 (5796):126–9, 2006. doi: 10.1126/science.1129003.

R. A. Morgan, J. C. Yang, M. Kitano, M. E. Dudley, C. M. Laurencot, and S. A. Rosenberg. Case report of a serious adverse event following the administration of t cells transduced with a chimeric antigen receptor recognizing erbb2. *Mol Ther*, 18(4):843–51, 2010. doi: 10.1038/mt.2010.24.

R. A. Morgan, N. Chinnasamy, D. Abate-Daga, A. Gros, P. F. Robbins, Z. Zheng, M. E. Dudley, S. A. Feldman, J. C. Yang, R. M. Sherry, G. Q. Phan, M. S. Hughes, U. S. Kammula, A. D. Miller, C. J. Hessman, A. A. Stewart, N. P. Restifo, M. M. Quezado, M. Alimchandani, A. Z. Rosenberg, A. Nath, T. Wang, B. Bielekova, S. C. Wuest, N. Akula, F. J. McMahon, S. Wilde, B. Mosetter, D. J. Schendel, C. M. Laurencot, and S. A. Rosenberg. Cancer regression and neurological toxicity following anti-mage-a3 tcr gene therapy. *J Immunother*, 36(2):133–51, 2013. doi: 10.1097/CJI.0b013e3182829903.

N. C. Munshi, Jr. Anderson, L. D., N. Shah, D. Madduri, J. Berdeja, S. Lonial, N. Raje, Y. Lin, D. Siegel, A. Oriol, P. Moreau, I. Yakoub-Agha, M. Delforge, M. Cavo, H. Einsele, H. Goldschmidt, K. Weisel, A. Rambaldi, D. Reece, F. Petrocca, M. Massaro, J. N. Connarn, S. Kaiser, P. Patel, L. Huang, T. B. Campbell, K. Hege, and J. San-Miguel. Idecabtagene vicleucel in relapsed and refractory multiple myeloma. *N Engl J Med*, 384(8):705–716, 2021. doi: 10.1056/NEJMoa2024850.

S. S. Ng, F. De Labastida Rivera, J. Yan, D. Corvino, I. Das, P. Zhang, R. Kuns, S. B. Chauhan, J. Hou, X. Y. Li, T. C. M. Frame, B. A. McEnroe, E. Moore, J. Na, J. A. Engel, M. S. F. Soon, B. Singh, A. J. Kueh, M. J. Herold, M. Montes de Oca, S. S. Singh, P. T. Bunn, A. R. Aguilera, M. Casey, M. Braun, N. Ghazanfari, S. Wani, Y. Wang, F. H. Amante, C. L. Edwards, A. Haque, W. C. Dougall, O. P. Singh, A. G. Baxter, M. W. L. Teng, A. Loukas, N. L. Daly, N. Cloonan, M. A. Degli-Esposti, J. Uzonna, W. R. Heath, T. Bald, S. K. Tey, K. Nakamura, G. R. Hill, R. Kumar, S. Sundar, M. J. Smyth, and C. R. Engwerda. The nk cell granule protein nkg7 regulates cytotoxic granule exocytosis and inflammation. *Nat Immunol*, 21(10):1205–1218, 2020. doi: 10.1038/s41590-020-0758-6.

B. P. Nicolet, A. Guislain, F. P. J. van Alphen, R. Gomez-Eerland, T. N. M. Schumacher, M. van den Biggelaar, and M. C. Wolkers. Cd29 identifies ifn-gamma-producing human cd8(+) t cells with an increased cytotoxic potential. *Proc Natl Acad Sci U S A*, 117(12): 6686–6696, 2020. doi: 10.1073/pnas.1913940117.

O. I. Olopade, R. B. Jenkins, D. T. Ransom, K. Malik, H. Pomykala, T. Nobori, J. M. Cowan, J. D. Rowley, and M. O. Diaz. Molecular analysis of deletions of the short arm of chromosome 9 in human gliomas. *Cancer Res*, 52(9):2523–9, 1992.

M. Orecchioni, Y. Ghosheh, A. B. Pramod, and K. Ley. Macrophage polarization: Different gene signatures in m1(lps+) vs. classically and m2(lps-) vs. alternatively activated macrophages. *Front Immunol*, 10:1084, 2019. doi: 10.3389/fimmu.2019.01084.

D. M. O'Rourke, M. P. Nasrallah, A. Desai, J. J. Melenhorst, K. Mansfield, J. J. D. Morrissette, M. Martinez-Lage, S. Brem, E. Maloney, A. Shen, R. Isaacs, S. Mohan, G. Plesa, S. F. Lacey, J. M. Navenot, Z. Zheng, B. L. Levine, H. Okada, C. H. June, J. L. Brogdon, and M. V. Maus. A single dose of peripherally infused egfrviii-directed car t cells mediates antigen loss and induces adaptive resistance in patients with recurrent glioblastoma. *Sci Transl Med*, 9(399), 2017. doi: 10.1126/scitranslmed.aaa0984.

M. Osswald, E. Jung, F. Sahm, G. Solecki, V. Venkataramani, J. Blaes, S. Weil, H. Horstmann, B. Wiestler, M. Syed, L. Huang, M. Ratliff, K. Karimian Jazi, F. T. Kurz, T. Schmenger, D. Lemke, M. Gommel, M. Pauli, Y. Liao, P. Haring, S. Pusch, V. Herl, C. Steinhauser, D. Krunic, M. Jarahian, H. Miletic, A. S. Berghoff, O. Griesbeck, G. Kalamakis, O. Garaschuk, M. Preusser, S. Weiss, H. Liu, S. Heiland, M. Platten, P. E. Huber, T. Kuner, A. von Deimling, W. Wick, and F. Winkler. Brain tumour cells interconnect to a functional and resistant network. *Nature*, 528(7580):93–8, 2015. doi: 10.1038/nature16071.

K. Pelka, M. Hofree, J. H. Chen, S. Sarkizova, J. D. Pirl, V. Jorgji, A. Bejnood, D. Dionne, W. H. Ge, K. H. Xu, S. X. Chao, D. R. Zollinger, D. J. Lieb, J. W. Reeves, C. A. Fuhrman, M. L. Hoang, T. Delorey, L. T. Nguyen, J. Waldman, M. Klapholz, I. Wakiro, O. Cohen, J. Albers, C. S. Smillie, M. S. Cuoco, J. Wu, M. J. Su, J. Yeung, B. Vijaykumar, A. M. Magnuson, N. Asinovski, T. Moll, M. N. Goder-Reiser, A. S. Applebaum, L. K. Brais, L. K. DelloStritto, S. L. Denning, S. T. Phillips, E. K. Hill, J. K. Meehan, D. T. Frederick, T. Sharova, A. Kanodia, E. Z. Todres, J. Jane-Valbuena, M. Biton, B. Izar, C. D. Lambden, T. E. Clancy, R. Bleday, N. Melnitchouk, J. Irani, H. Kunitake, D. L. Berger, A. Srivastava, J. L. Hornick, S. Ogino, A. Rotem, S. Vigneau, B. E. Johnson, R. B. Corcoran, A. H. Sharpe, V. K. Kuchroo, K. Ng, M. Giannakis, L. T. Nieman, G. M. Boland, A. J. Aguirre, A. C. Anderson, O. Rozenblatt-Rosen, A. Regev, and N. Hacohen. Spatially organized multicellular immune hubs in human colorectal cancer. *Cell*, 184(18):4734–4752 e20, 2021. doi: 10.1016/j.cell.2021.08.003.

M. Platten, L. Bunse, A. Wick, T. Bunse, L. Le Cornet, I. Harting, F. Sahm, K. Sanghvi, C. L. Tan, I. Poschke, E. Green, S. Justesen, G. A. Behrens, M. O. Breckwoldt, A. Freitag, L. M. Rother, A. Schmitt, O. Schnell, J. Hense, M. Misch, D. Krex, S. Stevanovic, G. Tabatabai, J. P. Steinbach, M. Bendszus, A. von Deimling, M. Schmitt, and W. Wick. A vaccine targeting mutant idh1 in newly diagnosed glioma. *Nature*, 592(7854):463–468, 2021. doi: 10.1038/s41586-021-03363-z.

J. Ponten and E. H. Macintyre. Long term culture of normal and neoplastic human glia. *Acta Pathol Microbiol Scand*, 74(4):465–86, 1968. doi: 10.1111/j.1699-0463.1968.tb03502.x.

T. Powles, J. P. Eder, G. D. Fine, F. S. Braiteh, Y. Loriot, C. Cruz, J. Bellmunt, H. A. Burris, D. P. Petrylak, S. L. Teng, X. Shen, Z. Boyd, P. S. Hegde, D. S. Chen, and N. J. Vogelzang. Mpdl3280a (anti-pd-l1) treatment leads to clinical activity in metastatic bladder cancer. *Nature*, 515(7528):558–62, 2014. doi: 10.1038/nature13904.

D. F. Quail and J. A. Joyce. The microenvironmental landscape of brain tumors. *Cancer Cell*, 31(3):326–341, 2017. doi: 10.1016/j.ccell.2017.02.009.

K. B. Quattrocchi, C. H. Miller, S. Cush, S. A. Bernard, S. T. Dull, M. Smith, S. Gudeman, and M. A. Varia. Pilot study of local autologous tumor infiltrating lymphocytes for the treatment of recurrent malignant gliomas. *J Neurooncol*, 45(2): 141–57, 1999. doi: 10.1023/a:1006293606710.

R. M. Ransohoff and A. E. Cardona. The myeloid cells of the central nervous system parenchyma. *Nature*, 468(7321):253–62, 2010. doi: 10.1038/nature09615.

D. A. Reardon, A. A. Brandes, A. Omuro, P. Mulholland, M. Lim, A. Wick, J. Baehring, M. S. Ahluwalia, P. Roth, O. Bahr, S. Phuphanich, J. M. Sepulveda, P. De Souza, S. Sahebjam, M. Carleton, K. Tatsuoka, C. Taitt, R. Zwirtes, J. Sampson, and M. Weller. Effect of nivolumab vs bevacizumab in patients with recurrent glioblastoma: The checkmate 143 phase 3 randomized clinical trial. *JAMA Oncol*, 6(7):1003–1010, 2020. doi: 10.1001/jamaoncol.2020.1024.

G. Reifenberger, H. G. Wirsching, C. B. Knobbe-Thomsen, and M. Weller. Advances in the molecular genetics of gliomas - implications for classification and therapy. *Nat Rev Clin Oncol*, 14(7):434–452, 2017. doi: 10.1038/nrclinonc.2016.204.

S. A. Rosenberg and N. P. Restifo. Adoptive cell transfer as personalized immunotherapy for human cancer. *Science*, 348(6230):62–8, 2015. doi: 10.1126/science.aaa4967.

C. Ryckman, K. Vandal, P. Rouleau, M. Talbot, and P. A. Tessier. Proinflammatory activities of s100: proteins s100a8, s100a9, and s100a8/a9 induce neutrophil chemotaxis and adhesion. *J Immunol*, 170(6):3233–42, 2003. doi: 10.4049/jimmunol.170.6.3233.

P. Scheiffele, J. Fan, J. Choih, R. Fetter, and T. Serafini. Neuroligin expressed in nonneuronal cells triggers presynaptic development in contacting axons. *Cell*, 101(6): 657–69, 2000. doi: 10.1016/s0092-8674(00)80877-6.

M. Schmitt. Treatment of patients with relapsed or refractory cd19+ lymphoid disease with t cells expressing a third-generation car, 2018. URL `https://clinicaltrials.gov/ct2/show/NCT03676504`.

S. P. Schoenberger, R. E. Toes, E. I. van der Voort, R. Offringa, and C. J. Melief. T-cell help for cytotoxic t lymphocytes is mediated by cd40-cd40l interactions. *Nature*, 393 (6684):480–3, 1998. doi: 10.1038/31002.

A. Schroll, K. Eller, C. Feistritzer, M. Nairz, T. Sonnweber, P. A. Moser, A. R. Rosenkranz, I. Theurl, and G. Weiss. Lipocalin-2 ameliorates granulocyte functionality. *Eur J Immunol*, 42(12):3346–57, 2012. doi: 10.1002/eji.201142351.

T. Schumacher, L. Bunse, S. Pusch, F. Sahm, B. Wiestler, J. Quandt, O. Menn, M. Osswald, I. Oezen, M. Ott, M. Keil, J. Balss, K. Rauschenbach, A. K. Grabowska, I. Vogler, J. Diekmann, N. Trautwein, S. B. Eichmuller, J. Okun, S. Stevanovic, A. B. Riemer, U. Sahin, M. A. Friese, P. Beckhove, A. von Deimling, W. Wick, and M. Platten. A vaccine targeting mutant idh1 induces antitumour immunity. *Nature*, 512 (7514):324–7, 2014. doi: 10.1038/nature13387.

J. Schuster, R. K. Lai, L. D. Recht, D. A. Reardon, N. A. Paleologos, M. D. Groves, M. M. Mrugala, R. Jensen, J. M. Baehring, A. Sloan, G. E. Archer, D. D. Bigner, S. Cruickshank, J. A. Green, T. Keler, T. A. Davis, A. B. Heimberger, and J. H. Sampson. A phase ii, multicenter trial of rindopepimut (cdx-110) in newly diagnosed

glioblastoma: the act iii study. *Neuro Oncol*, 17(6):854–61, 2015. doi: 10.1093/neuonc/nou348.

A. C. Scott, F. Dundar, P. Zumbo, S. S. Chandran, C. A. Klebanoff, M. Shakiba, P. Trivedi, L. Menocal, H. Appleby, S. Camara, D. Zamarin, T. Walther, A. Snyder, M. R. Femia, E. A. Comen, H. Y. Wen, M. D. Hellmann, N. Anandasabapathy, Y. Liu, N. K. Altorki, P. Lauer, O. Levy, M. S. Glickman, J. Kaye, D. Betel, M. Philip, and A. Schietinger. Tox is a critical regulator of tumour-specific t cell differentiation. *Nature*, 571(7764):270–274, 2019. doi: 10.1038/s41586-019-1324-y.

E. Sebzda, Z. Zou, J. S. Lee, T. Wang, and M. L. Kahn. Transcription factor klf2 regulates the migration of naive t cells by restricting chemokine receptor expression patterns. *Nat Immunol*, 9(3):292–300, 2008. doi: 10.1038/ni1565.

W. Seo, K. Shimizu, S. Kojo, A. Okeke, T. Kohwi-Shigematsu, S. I. Fujii, and I. Taniuchi. Runx-mediated regulation of ccl5 via antagonizing two enhancers influences immune cell function and anti-tumor immunity. *Nat Commun*, 11(1):1562, 2020. doi: 10.1038/s41467-020-15375-w.

P. Shrikant, I. Y. Chung, M. E. Ballestas, and E. N. Benveniste. Regulation of intercellular adhesion molecule-1 gene expression by tumor necrosis factor-alpha, interleukin-1 beta, and interferon-gamma in astrocytes. *J Neuroimmunol*, 51(2):209–20, 1994. doi: 10.1016/0165-5728(94)90083-3.

I. Siddiqui, K. Schaeuble, V. Chennupati, S. A. Fuertes Marraco, S. Calderon-Copete, D. Pais Ferreira, S. J. Carmona, L. Scarpellino, D. Gfeller, S. Pradervand, S. A. Luther, D. E. Speiser, and W. Held. Intratumoral tcf1(+)pd-1(+)cd8(+) t cells with stem-like properties promote tumor control in response to vaccination and checkpoint blockade immunotherapy. *Immunity*, 50(1):195–211 e10, 2019. doi: 10.1016/j.immuni.2018.12.021.

E. Song, T. Mao, H. Dong, L. S. B. Boisserand, S. Antila, M. Bosenberg, K. Alitalo, J. L. Thomas, and A. Iwasaki. Vegf-c-driven lymphatic drainage enables immunosurveillance of brain tumours. *Nature*, 577(7792):689–694, 2020. doi: 10.1038/s41586-019-1912-x.

J. Stanke, C. Hoffmann, U. Erben, H. von Keyserling, S. Stevanovic, G. Cichon, A. Schneider, and A. M. Kaufmann. A flow cytometry-based assay to assess minute frequencies of cd8+ t cells by their cytolytic function. *J Immunol Methods*, 360(1-2): 56–65, 2010. doi: 10.1016/j.jim.2010.06.005.

T. C. Sudhof. Neuroligins and neurexins link synaptic function to cognitive disease. *Nature*, 455(7215):903–11, 2008. doi: 10.1038/nature07456.

P. A. Szabo, H. M. Levitin, M. Miron, M. E. Snyder, T. Senda, J. Yuan, Y. L. Cheng, E. C. Bush, P. Dogra, P. Thapa, D. L. Farber, and P. A. Sims. Single-cell transcriptomics of human t cells reveals tissue and activation signatures in health and disease. *Nat Commun*, 10(1):4706, 2019. doi: 10.1038/s41467-019-12464-3.

T. Szatmari, K. Lumniczky, S. Desaknai, S. Trajcevski, E. J. Hidvegi, H. Hamada, and G. Safrany. Detailed characterization of the mouse glioma 261 tumor model for experimental glioblastoma therapy. *Cancer Sci*, 97(6):546–53, 2006. doi: 10.1111/j.1349-7006.2006.00208.x.

J. Theruvath, E. Sotillo, C. W. Mount, C. M. Graef, A. Delaidelli, S. Heitzeneder, L. Labanieh, S. Dhingra, A. Leruste, R. G. Majzner, P. Xu, S. Mueller, D. W. Yecies, M. A. Finetti, D. Williamson, P. D. Johann, M. Kool, S. Pfister, M. Hasselblatt, M. C. Fruhwald, O. Delattre, D. Surdez, F. Bourdeaut, S. Puget, S. Zaidi, S. S. Mitra, S. Cheshier, P. H. Sorensen, M. Monje, and C. L. Mackall. Locoregionally administered b7-h3-targeted car t cells for treatment of atypical teratoid/rhabdoid tumors. *Nat Med*, 26(5):712–719, 2020. doi: 10.1038/s41591-020-0821-8.

D. S. Thommen, V. H. Koelzer, P. Herzig, A. Roller, M. Trefny, S. Dimeloe, A. Kiialainen, J. Hanhart, C. Schill, C. Hess, S. Savic Prince, M. Wiese, D. Lardinois, P. C. Ho, C. Klein, V. Karanikas, K. D. Mertz, T. N. Schumacher, and A. Zippelius. A transcriptionally and functionally distinct pd-1(+) cd8(+) t cell pool with predictive potential in non-small-cell lung cancer treated with pd-1 blockade. *Nat Med*, 24(7): 994–1004, 2018. doi: 10.1038/s41591-018-0057-z.

S. L. Topalian, F. S. Hodi, J. R. Brahmer, S. N. Gettinger, D. C. Smith, D. F. McDermott, J. D. Powderly, R. D. Carvajal, J. A. Sosman, M. B. Atkins, P. D. Leming, D. R. Spigel, S. J. Antonia, L. Horn, C. G. Drake, D. M. Pardoll, L. Chen, W. H. Sharfman, R. A. Anders, J. M. Taube, T. L. McMiller, H. Xu, A. J. Korman, M. Jure-Kunkel, S. Agrawal, D. McDonald, G. D. Kollia, A. Gupta, J. M. Wigginton, and M. Sznol. Safety, activity, and immune correlates of anti-pd-1 antibody in cancer. *N Engl J Med*, 366(26):2443–54, 2012. doi: 10.1056/NEJMoa1200690.

M. Touat, Y. Y. Li, A. N. Boynton, L. F. Spurr, J. B. Iorgulescu, C. L. Bohrson, I. Cortes-Ciriano, C. Birzu, J. E. Geduldig, K. Pelton, M. J. Lim-Fat, S. Pal, R. Ferrer-Luna, S. H. Ramkissoon, F. Dubois, C. Bellamy, N. Currimjee, J. Bonardi, K. Qian, P. Ho, S. Malinowski, L. Taquet, R. E. Jones, A. Shetty, K. H. Chow, R. Sharaf, D. Pavlick, L. A. Albacker, N. Younan, C. Baldini, M. Verreault, M. Giry, E. Guillerm, S. Ammari, F. Beuvon, K. Mokhtari, A. Alentorn, C. Dehais, C. Houillier, F. Laigle-Donadey, D. Psimaras, E. Q. Lee, L. Nayak, J. R. McFaline-Figueroa, A. Carpentier, P. Cornu, L. Capelle, B. Mathon, J. S. Barnholtz-Sloan, A. Chakravarti, W. L. Bi, E. A. Chiocca, K. P. Fehnel, S. Alexandrescu, S. N. Chi, D. Haas-Kogan, T. T. Batchelor, G. M. Frampton, B. M. Alexander, R. Y. Huang, A. H. Ligon, F. Coulet, J. Y. Delattre, K. Hoang-Xuan, D. M. Meredith, S. Santagata, A. Duval, M. Sanson, A. D. Cherniack, P. Y. Wen, D. A. Reardon, A. Marabelle, P. J. Park, A. Idbaih, R. Beroukhim, P. Bandopadhayay, F. Bielle, and K. L. Ligon. Mechanisms and therapeutic implications of hypermutation in gliomas. *Nature*, 580(7804):517–523, 2020. doi: 10.1038/s41586-020-2209-9.

C. J. Turtle, L. A. Hanafi, C. Berger, T. A. Gooley, S. Cherian, M. Hudecek, D. Sommermeyer, K. Melville, B. Pender, T. M. Budiarto, E. Robinson, N. N. Steevens,

C. Chaney, L. Soma, X. Chen, C. Yeung, B. Wood, D. Li, J. Cao, S. Heimfeld, M. C. Jensen, S. R. Riddell, and D. G. Maloney. Cd19 car-t cells of defined cd4+:cd8+ composition in adult b cell all patients. *J Clin Invest*, 126(6):2123–38, 2016. doi: 10.1172/JCI85309.

E. J. van Bodegraven, J. V. van Asperen, P. A. J. Robe, and E. M. Hol. Importance of gfap isoform-specific analyses in astrocytoma. *Glia*, 67(8):1417–1433, 2019. doi: 10.1002/glia.23594.

F. Varoqueaux, G. Aramuni, R. L. Rawson, R. Mohrmann, M. Missler, K. Gottmann, W. Zhang, T. C. Sudhof, and N. Brose. Neuroligins determine synapse maturation and function. *Neuron*, 51(6):741–54, 2006. doi: 10.1016/j.neuron.2006.09.003.

V. Venkataramani, D. I. Tanev, C. Strahle, A. Studier-Fischer, L. Fankhauser, T. Kessler, C. Korber, M. Kardorff, M. Ratliff, R. Xie, H. Horstmann, M. Messer, S. P. Paik, J. Knabbe, F. Sahm, F. T. Kurz, A. A. Acikgoz, F. Herrmannsdorfer, A. Agarwal, D. E. Bergles, A. Chalmers, H. Miletic, S. Turcan, C. Mawrin, D. Hanggi, H. K. Liu, W. Wick, F. Winkler, and T. Kuner. Glutamatergic synaptic input to glioma cells drives brain tumour progression. *Nature*, 573(7775):532–538, 2019. doi: 10.1038/s41586-019-1564-x.

H. S. Venkatesh, L. T. Tam, P. J. Woo, J. Lennon, S. Nagaraja, S. M. Gillespie, J. Ni, D. Y. Duveau, P. J. Morris, J. J. Zhao, C. J. Thomas, and M. Monje. Targeting neuronal activity-regulated neuroligin-3 dependency in high-grade glioma. *Nature*, 549 (7673):533–537, 2017. doi: 10.1038/nature24014.

N. A. Vitanza, A. J. Johnson, A. L. Wilson, C. Brown, J. K. Yokoyama, A. Kunkele, C. A. Chang, S. Rawlings-Rhea, W. Huang, K. Seidel, C. M. Albert, N. Pinto, J. Gust, L. S. Finn, J. G. Ojemann, J. Wright, R. J. Orentas, M. Baldwin, R. A. Gardner, M. C. Jensen, and J. R. Park. Locoregional infusion of her2-specific car t cells in children and young adults with recurrent or refractory cns tumors: an interim analysis. *Nat Med*, 27 (9):1544–1552, 2021. doi: 10.1038/s41591-021-01404-8.

C. F. Ware. The tnf receptor super family in immune regulation. *Immunol Rev*, 244(1):5–8, 2011. doi: 10.1111/j.1600-065X.2011.01065.x.

K. Watano, K. Iwabuchi, S. Fujii, N. Ishimori, S. Mitsuhashi, M. Ato, A. Kitabatake, and K. Onoe. Allograft inflammatory factor-1 augments production of interleukin-6, -10 and -12 by a mouse macrophage line. *Immunology*, 104(3):307–16, 2001. doi: 10.1046/j.1365-2567.2001.01301.x.

G. F. Weber, G. S. Lett, and N. C. Haubein. Osteopontin is a marker for cancer aggressiveness and patient survival. *Br J Cancer*, 103(6):861–9, 2010. doi: 10.1038/sj.bjc.6605834.

S. C. Wei, J. H. Levine, A. P. Cogdill, Y. Zhao, N. A. S. Anang, M. C. Andrews, P. Sharma, J. Wang, J. A. Wargo, D. Pe'er, and J. P. Allison. Distinct cellular mechanisms underlie anti-ctla-4 and anti-pd-1 checkpoint blockade. *Cell*, 170(6): 1120–1133 e17, 2017. doi: 10.1016/j.cell.2017.07.024.

S. C. Wei, C. R. Duffy, and J. P. Allison. Fundamental mechanisms of immune checkpoint blockade therapy. *Cancer Discov*, 8(9):1069–1086, 2018. doi: 10.1158/2159-8290.CD-18-0367.

Y. Wolf, A. Shemer, L. Levy-Efrati, M. Gross, J. S. Kim, A. Engel, E. David, L. Chappell-Maor, J. Grozovski, R. Rotkopf, I. Biton, R. Eilam-Altstadter, and S. Jung. Microglial mhc class ii is dispensable for experimental autoimmune encephalomyelitis and cuprizone-induced demyelination. *Eur J Immunol*, 48(8):1308–1318, 2018. doi: 10.1002/eji.201847540.

M. Wu, Q. Huang, Y. Xie, X. Wu, H. Ma, Y. Zhang, and Y. Xia. Improvement of the anticancer efficacy of pd-1/pd-l1 blockade via combination therapy and pd-l1 regulation. *J Hematol Oncol*, 15(1):24, 2022. doi: 10.1186/s13045-022-01242-2.

S. Yip, J. Miao, D. P. Cahill, A. J. Iafrate, K. Aldape, C. L. Nutt, and D. N. Louis. Msh6 mutations arise in glioblastomas during temozolomide therapy and mediate temozolomide resistance. *Clin Cancer Res*, 15(14):4622–9, 2009. doi: 10.1158/1078-0432.CCR-08-3012.

B. Youngblood, K. J. Oestreich, S. J. Ha, J. Duraiswamy, R. S. Akondy, E. E. West, Z. Wei, P. Lu, J. W. Austin, J. L. Riley, J. M. Boss, and R. Ahmed. Chronic virus infection enforces demethylation of the locus that encodes pd-1 in antigen-specific cd8(+) t cells. *Immunity*, 35(3):400–12, 2011. doi: 10.1016/j.immuni.2011.06.015.

R. Zander, D. Schauder, G. Xin, C. Nguyen, X. Wu, A. Zajac, and W. Cui. Cd4(+) t cell help is required for the formation of a cytolytic cd8(+) t cell subset that protects against chronic infection and cancer. *Immunity*, 51(6):1028–1042 e4, 2019. doi: 10.1016/j.immuni.2019.10.009.

F. Zhang, H. Wang, X. Wang, G. Jiang, H. Liu, G. Zhang, H. Wang, R. Fang, X. Bu, S. Cai, and J. Du. Tgf-beta induces m2-like macrophage polarization via snail-mediated suppression of a pro-inflammatory phenotype. *Oncotarget*, 7(32):52294–52306, 2016. doi: 10.18632/oncotarget.10561.

Christopher Krämer
Hölderlinweg 1 – Heidelberg, Baden-Württemberg 69120 –
E-Mail: christopher.kraemer@icloud.com

Personal information

Date and place of birth	09.04.1997, Mainz, Rhineland-Palatine

School education

March 2016	General university entrance qualification, Episcopal Willigis secondary school Mainz, mark 1,0

University education

Oct 2019 - now	Medical doctoral student at the clinical cooperation unit neuroimmunology and brain tumor immunology, German Cancer Research Centre Heidelberg and university medicine Mannheim
Oct 2018 - now	Medical school, clinical studies, Ruprecht-Karls-University Heidelberg
07.09.2018	First state exam, medicine, mark: 1,0
Oct 2016 - Sep 2018	Medical school, preclinical studies, Ruprecht-Karls-University Heidelberg

Scholarships

Oct 2019 - Sep 2020	Mildred-Scheel doctoral scholarship, German Cancer Aid
Oct 2016 - now	Scholarship of the Protestant student union Villigst

Publications and conferences

Jan 2022	Kilian M, Friedrich M, Sanghvi K, Green E, Pusch S, Kawauchi D, Löwer M, Sonner JK, **Krämer C**, Zaman J, Jung S, Breckwoldt MO, Willimsky G, Eichmüller SB, von Deimling A, Wick W, Sahm F, Platten M, Bunse L. **T-cell Receptor Therapy Targeting Mutant Capicua Transcriptional Repressor in Experimental Gliomas**. Clin Cancer Res. 2022 Jan 15;28(2):378-389. doi: 10.1158/1078-0432.CCR-21-1881. Epub 2021 Nov 15. PMID: 34782365.
Nov 2021	**C. Krämer** et al., EXTH-28. **NLGN4X TCR transgenic T cell targeting experimental gliomas**. Neuro-Oncology 23, @ 1522-8517 (2021) 2021 Society for Neuro-Oncology Annual Scientific Meeting
Oct 2021	Poster and oral presentation **C. Krämer** et al. **NLGN4X TZR-transgene T-Zelltherapie im experimentellen Gliom** 2021 meeting of the neuro-oncological working group (NOA)
23.1.-24.1.2020	Poster presentation **C. Krämer** et al. **CSF leak in endoscopic pituitary surgery is associated with increased risk of diabetes insipidus** BSBS (British Skull Base Society) Meeting 2020

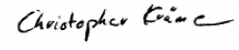

Heidelberg, 16.07.2022

9 Acknowledgements

First of all I want to thank Michael Platten for giving me the opportunity to work in his team. Thank you for all the advice in scientific and medical career related questions and for the unique opportunity to follow all my interests and ideas.
Thanks to all the people from the german cancer research centre who helped performing the experiments, described in this thesis, Stefan Pusch for helping with all the cloning questions and a special thanks to Rainer Will, who provided numerous advices for optimizations of the transduction protocol and was involved in the manufacturing of the T cell products for many experiments and also to the Centre for Preclinical Studies, for always supporting me during the experiments.
Thanks a lot, to all the current and former members of D170. Thanks for helping in all types of experiments, answering a lots of questions and especially for open scientific discussions, that often changed thinking on different problems. Thanks to Ed and Theresa for the scientific support. Thanks to the all other students in the lab, esspecially Khwab and Mirco for many fruitful discussions and help in big experiments, Katharina Lindner for support with PBMCs and cell lines, a big thanks to Yu-Chan and Alex for endless discussions and mutual experiments that pushed forward the platform for T cell manufacturing and testing. Thanks to the technicians Kristine, Steffi and Michele, who helped a lot during the past years and kept calm despite my sometimes chaotic experiments.
A special thanks goes to Lukas, for the great support from the start of my MD thesis, the detailed and very constructive discussions and esspecially for your neverending motivation and positive attitude. A huge thanks is for Michael (Miki if you don't know the proper name) who basically taught me everything that I've learned during this thesis, always answered even the stupid questions and provided an incredible help and support. It was a real pleasure to work with you. Furthermore, I want to thank my parents and family who always supported and encouraged me on my way and to Clara, who was always a great support to me.